Title
Chemical Engineering of Graphene and Single-Walled Carbon Nanotubes for Electronic Applications

Author
Chen, Mingguang

Publication Date
2017

UNIVERSITY OF CALIFORNIA
RIVERSIDE

Chemical Engineering of Graphene and Single-Walled Carbon Nanotubes for Electronic Applications

A Dissertation submitted in partial satisfaction
of the requirements for the degree of

Doctor of Philosophy

in

Chemical and Environmental Engineering

by

Mingguang Chen

September 2017

Dissertation Committee:
  Dr. Robert C. Haddon, Co-Chairperson
  Dr. Ruoxue Yan, Co-Chairperson
  Dr. Elena Bekyarova, Co-Chairperson
  Dr. Juchen Guo

The Dissertation of Mingguang Chen is approved:

Committee Co-Chairperson

Committee Co-Chairperson

Committee Co-Chairperson

University of California, Riverside

ACKNOWLEDGEMENTS

It has been a great honor and pleasure to have been cultured in the Haddon Research Group, where I not only had a chance to take part in the pioneering research in the field of carbon nanotechnology, but also learned how to tackle tough problems systematically from my advisors and lab mates with multidisciplinary backgrounds.

First and foremost, I would like to thank my advisor Professor Robert C. Haddon for providing me a precious opportunity and a great platform to do research in the fascinating field of carbon nanomaterials. As a mentor, he was always very supportive, friendly, thoughtful and encouraging. He was always available and glad to discuss the experimental results with me, followed by valuable guidance. As a scientist, he was extremely diligent, knowledgeable, talented and insightful. He was able to give analysis and explanation of research results from the perspective of chemistry, physics, material science and engineering. Without his mentoring and help, I would not have been able to bring this dissertation into existence.

Also, I want to express my sincere thanks to Elena for her continuous help and support since I entered this group. Especially after Dr. Haddon’s untimely passing, even though still in huge grief, she pulled herself up and served as my research advisor to continue the unfinished projects started by Professor Haddon.

I am also very grateful to Dr. Ruoxue Yan for her willingness to serve as my faculty advisor and chair of my committee, for providing me timely help and support whenever I needed. Many thanks to Dr. Juchen Guo for serving on my committee and reviewing my work.

Special thanks to Dr. Aron Pekker for teaching me many skills in instrument operation and device fabrications, Dr. Xiaojuan Tian for helpful support and precious advices, Dr. Santanu Sarkar and Dr. Pradip Bag for training me in the Diels Alder reactions, Dr. Walt A de Heer for providing epitaxial graphene for my work. Also, I thank other group members Dr. Mikhail Itkis, Dr. Matthew Moser, Dr. Sushanta Pal, Wangxiang, Dejan, Bassim, Guanghui, and Thais for their help and valuable discussions, and the staff from the Center for Nanoscale Science and Nanotechnology - Nancy, Eva, Andy, and Nadine for administrative help. I am also grateful to the staff in the cleanroom Mark, Dong and Dexter for all the help.

Many thanks to my friends, Dr. Xiuheng Wang and Dr. Long Chen. Dr. Xiuheng Wang has always been encouraging and helpful during my Ph.D. study. Dr. Long Chen has been my friend for 4 years; our friendship begun when we started our Ph.D. careers, he has always been very generous, provided me with help in time and shared his impressive insights assisting me in dealing with tough problems.

Last but not least, I want to express my deepest gratitude to my parents, Mrs. Jiying Niu and Mr. Xianhua Chen, and my sister Ms. Xiaodan Chen for their permanent support and unconditional love. I am sincerely grateful for their sacrifices and the care they have given me, always and forever.

This work was supported by the National Science Foundation under contract DMR-1305724 (organometallic chemistry) and PPG Industries Inc (studies of PPG GNP material).

Portions of the dissertation are adapted with permission from the following references:

Chapter 2:

1. Chen, M.; Li, G.; Li, W.; Stekovic, D.; Arkook, B.; Itkis, M. E.; Pekker, A.; Bekyarova, E.; Haddon, R. C., Large-Scale Cellulose-Assisted Transfer of Graphene toward Industrial Applications. *Carbon* **2016,** 110, 286-291.
2. Chen, M.; Stekovic, D.; Li, W.; Arkook, B.; Haddon, R.; Bekyarova, E., Sublimation-Assisted Graphene Transfer Technique Based on Small Polyaromatic Hydrocarbons. *Nanotechnology* **2017**.

Chapter 3:

3. Chen, M.; Tian, X.; Li, W.; Bekyarova, E.; Li, G.; Moser, M.; Haddon, R. C., Application of Organometallic Chemistry to the Electrical Interconnection of Graphene Nanoplatelets. *Chem. Mater.* **2016,** 28, 2260-2266.

ABSTRACT OF THE DISSERTATION

Chemical Engineering of Graphene and Single-Walled Carbon Nanotubes for Electronic Applications

by

Mingguang Chen

Doctor of Philosophy, Graduate Program in Chemical and Environmental Engineering
University of California, Riverside, September 2017
Dr. Robert C. Haddon, Dr. Ruoxue Yan, Dr. Elena Bekyarova, Co-Chairpersons

Carbon nanomaterials have received a great deal of attention and investment in recent years, not only because of their excellent properties, but also driven by the fact that conventional Si-based electronics is pushed to its limits, and when the size of a Si based transistor is miniaturized to several nanometers, the cost increases dramatically. Chapter 1 reviews the synthesis, properties and application of carbon nanotubes and graphene. Chemical functionalization is an efficient way to manipulate and tune the properties of carbon nanomaterials and to broaden their applications in different fields.

Transfer of CVD transfer without degrading its quality is essential to the wide applications of this carbon material in electronics. In Chapter 2, two novel graphene transfer methods are reported. The availability of clean graphene is critical for the chemical modification of graphene and its application in flexible electronics.

The interaction between carbon surfaces and transition metals, discussed in Chapter 3, has long been an interesting topic. Graphene half sandwich complexes and graphene sandwich complexes were successfully synthesized and the electrical conductivity was used to characterize the synthetic process. Besides, the fascinating electrical properties of individual carbon nanotubes were extended toward macroscale by aligning individual tubes on a large scale and applying organometallic chemistry to constructively interconnect the sidewalls of parallel tubes and two ends of nanotubes in series with transition metals, which greatly improved the electrical performance of aligned carbon nanotube devices and paves the way for the fabrication of carbon nanotube-based high performance microprocessors.

The absence of a bandgap in graphene inhibits its application to transistors, meanwhile from a chemical standpoint the unique band structure of graphene dictates the chemical reactivity of graphene as exemplified in the Diels Alder (DA) reaction discussed in Chapter 4. The effect of a facile room temperature DA

reaction on the magnetoresistance of epitaxial graphene (Epigraphene) was studied in a temperature range from 300 K to 2 K. The transition from the positive magnetoresistance in pristine Epigraphene to a large negative magnetoresistance in naphthazarin-Epigrahene adduct provides an alternative way to develop graphene based magneto-electronic devices.

Contents

List of Figures

Figure 2.12. Characterization of the transferred graphene. (a) AFM and (b) SEM images after transfer of graphene on SiO_2/Si substrate; (c) Raman spectrum of a single layer CVD graphene transferred by NAT method. (d-f) Raman intensity maps of 10 μm x 10 μm areas of D, G, and 2D peaks, respectively.

Figure 2.13. Electrical properties of a NAT-graphene FET on 300 nm SiO2/Si. (a) Optical image of a typical FET graphene device. (b) Conductivity versus gate voltage recorded at drain-source voltage of 0.01 Volt.

Figure 3.1. UV-vis of (a) Cr(η^6-benzene)$_2$, (b) Cr(η^6-benzene)$(CO)_3$, (c) Cr(CO)6, (d) $Mo(CO)_6$ and (e) $W(CO)_6$ dissolved in acetonitrile and the wavelength of light used in the photochemical experiments described in this chapter.

Figure 3.2. (a) Schematic of the photochemical reaction on SLG inside a glovebox. (b) Evolution of conductivity of SLG films on photochemical reaction with 3 different chromium reagents. (c) Conductivity enhancement of graphene half sandwich complexes formed with each chromium reagent.

Figure 3.3 Conductivity enhancement of SLG reacted with $Cr(CO)_6$ under different gate voltage.

Figure 3.4. Schematic of the formation of a graphene-metal-graphene sandwich complexe.

Figure 3.5. (a) Three views of a typical Gr-SWNT-Gr device employed in this study. (b) Evolution of on the in-plane conductivity of the device with e-beam deposition of Cr atoms between two graphene layers.

Figure 3.6 (a) Device configurations, carbon films were transferred to evenly-spaced pre-patterned electrodes on glass substrates. A Kapton thin film with a hole (d=80 um) in zone1 was used as a shadow mask for chromium deposition. The edges of the film were sealed with a Kapton tape. (b) SEM image of an 8 nm Sc-SWNT random network. (c) Conductivity evolution for the Sc-SWNT thin film only (top) upon chromium evaporation. (d) Conductivity evolution for a device of SLG (bottom) + Sc-SWNT thin film (top) upon chromium evaporation.

Figure 3.7 Device configurations of (a) SLG+Sc-SWNT (b) Sc-SWNT (c) SLG. (d) Evolution of conductivity for corresponding devices upon Cr evaporation.

Chapter 1. Introduction of carbon nanomaterials

Carbon is an essential element of life, which is reflected in its ability to form a vast number of organic compounds, from DNA to protein, fat and carbohydrates. Furthermore, it is the constituent of important inorganic materials, including diamond - the hardest natural material, and graphite - one of the softest inorganic substances. For a very long time, the well-known pure carbon allotropes were graphite, diamond and amorphous carbon, which are all 3-dimensional materials. A nanomaterial usually refers to a material with a size smaller than 100 nm in at least one dimension. Nanomaterials tend to show unique optical, electronic, thermal and mechanical properties due to quantum confinement effect. For example, when the thickness of graphite decreases until only one layer of carbon atoms remains, it turns into graphene, which exhibits remarkable properties different from graphite. The properties of carbon nanomaterials can be tuned by chemical functionalization in order to fit the needs of different applications.

1.1 Graphene

Graphene is a 2-dimensional form of carbon with honeycomb like structure, which is only one atom thick. Graphene can be viewed as the building block of all graphitic materials as illustrated in Figure 1.1. Graphene can be transformed into 0 D fullerene (experimentally done with the help of the high energy of the e-beam),[5] rolled into 1D carbon nanotube and stacked into 3D graphite.[6]

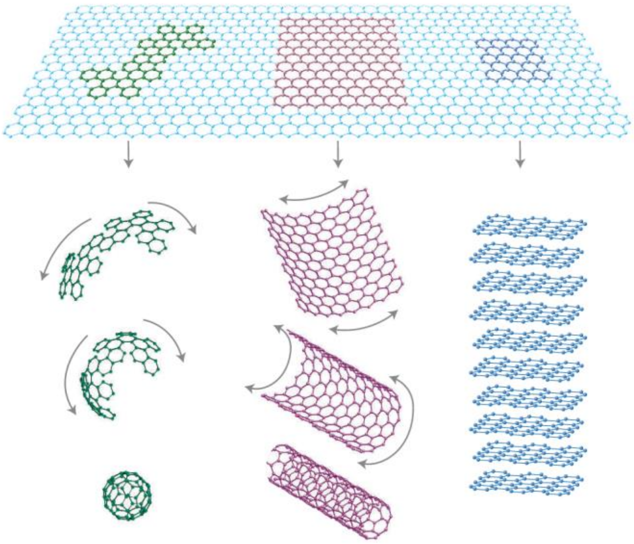

Figure 1.1 Schematics of transformation of graphene to fullerene, carbon nanotube and graphite, respectively. Reprinted with permission from ref.[6] (Copyright © 2007 Nature Publishing Group).

Discovery of Graphene

The term "graphene" was introduced in 1997 by IUPAC and it was described as "A single carbon layer of the graphite structure, describing its nature by analogy to a polycyclic aromatic hydrocarbon of quasi infinite size".[7, 8]

In 2004, Andre Geim and Konstantin Novoselov at the University of Manchester, UK reported the unusual electronic properties of few layer graphene obtained by scotch tape exfoliation of graphite.[9] At nearly the same time, Walt A. de Heer at

Georgia Institute of Technology reported 2D electron gas behavior from few layer epitaxial graphene.[10] Geim and Novoselov argue that metastable state and interatomic bonds protect graphene from dislocations or defects caused by thermal fluctuations. Also, 3D warping helps to suppress thermal vibrations.[6]. Graphene has kept attracting intense attention from scientists and engineers since its discovery. Its exceptional mechanical, optical, magnetic, thermal and electronic properties are under intense study and engineers are seeking routes to synthesize or transfer high quality large scale graphene economically in order to pave the way for graphene's commercialization. In 2010, Geim and Novoselov won the Nobel Prize in Physics for their groundbreaking experiments regarding graphene.

1.1.1 Electronic structure and properties of graphene

Graphene consists of two types of carbon atoms, which are chemically equivalent, but crystallographically different as shown in Figure 1.2. The crystal structure can be described as a triangular lattice comprised of two atoms A and B.

The distance between neighboring carbon atoms is denoted by a, then in the Bravais lattice formed by all the A (B) atoms, the lattice spacing is $\sqrt{3}\mathrm{a}$. The primitive lattice vectors are $\mathrm{a}_1 = \sqrt{3}a\ (1{,}0); a_2 = a(\frac{\sqrt{3}}{2}, \frac{3}{2})$, and the corresponding reciprocal lattice vectors are denoted as b1 and b2 as shown in Figure 1.2 (b).

$\mathrm{b} \cdot \mathrm{a}_j = 2\pi\delta_{ij}$, thus $\boldsymbol{b_1} = \frac{2\pi}{3}\frac{1}{a}\left(\sqrt{3}, -1\right), \boldsymbol{b_2} = \frac{4\pi}{3}\frac{1}{a}\ (0{,}1)$.

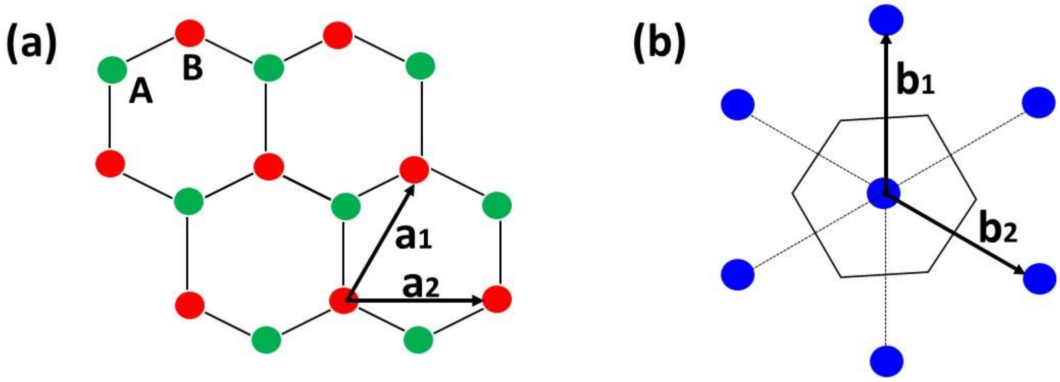

Figure 1.2 (a) Honeycomb lattice structure of graphene - the unit cell has two atoms A (green) and B (red), $\mathbf{a_1}$ and $\mathbf{a_2}$ denote unit vectors. (b) The reciprocal lattice of graphene; the hexagon is the boundary of the first Brillouin zone; $\mathbf{b_1}$ and $\mathbf{b_2}$ are the unit vectors in the reciprocal lattice.

The unusual properties of graphene such as anomalous integer quantum Hall effect [11] root in its unique electronic band structure. There are four valence electrons in carbon atoms, however, in the form of graphene, only three valence electrons are involved in the σ bonding. Therefore one remaining electron would be considered for calculation of the band structure of graphene. In this case, a simple tight binding model can be applied. By solving the corresponding eigenfunctions, two eigenvalues representing two bands can be obtained. The band with positive energy and band with negative energy touch each other at the Dirac points located at the corners of the Brillouin zone as shown in Figure 1.3 [1].

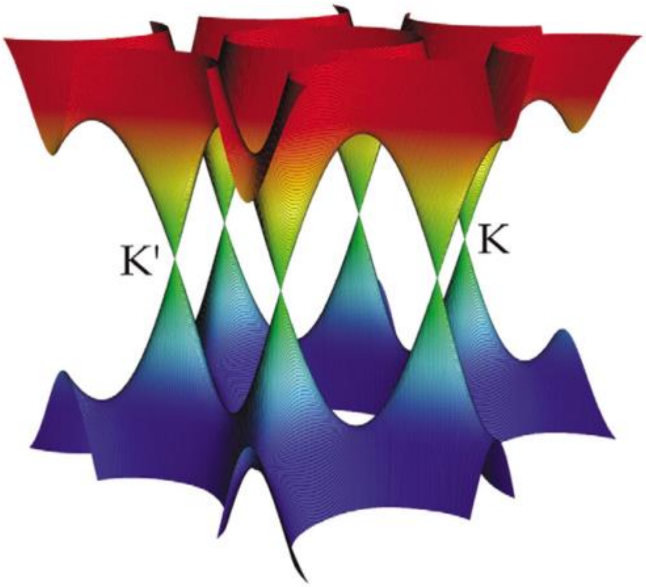

Figure 1.3 Band structure of graphene. The conductance band (top) and the valence band (bottom) touch each other at the K and K’ points. Reprinted with permission from ref.1 (Copyright © 2007 Elsevier Inc.).

1.1.2 Forms and production of graphene

There are a variety of ways to produce graphene. Based on the routes of production, graphene can be categorized mainly into Scotch Tape Exfoliated Graphene, Solvent Exfoliated Graphene, Epitaxial Graphene and Chemical Vapor Deposition (CVD) Graphene as shown in Figure 1.4.

As the production methods are different, the features and properties of different kind of graphene vary. Technically, scotch tape exfoliated graphene has higher quality, but is restricted by its small size (maximum tens of microns). Solvent exfoliated graphene is favored by the industry due to its large scale production and

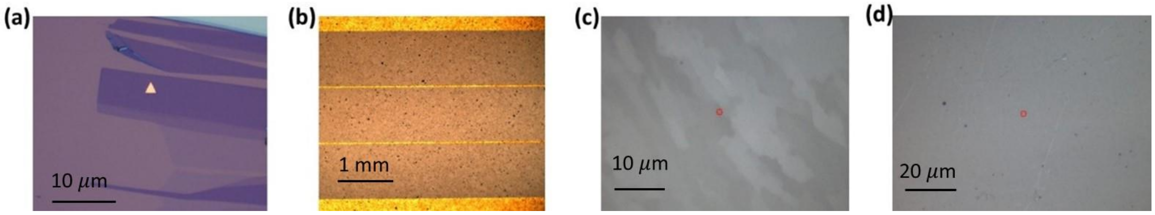

Figure 1.4 Forms of graphene: (a) Scotch tape exfoliated single layer, bilayer and multilayer graphene on a 300 nm SiO_2/Si substrate. (b) Solution exfoliated graphene sprayed on top of a glass substrate with pre-patterned electrodes. (c) Epitaxial few layer graphene grown on SiC substrate. (d) CVD graphene transferred on a quartz substrate.

availability of simple routes to solution-based and film-based material forms. Epitaxial graphene has high quality and large size, which makes it a competitive candidate for graphene based electronic applications, but the cost of SiC substrate needs to be reduced before wide commercialization. CVD graphene is one of the most promising forms of graphene due to its macro-size, continuity and high quality. As CVD graphene films are often grown on copper and nickel foils, transfer of graphene to insulating substrates is necessary for electronic based applications. Fortunately, a large number of graphene transfer methods suitable for different purposes have been developed as discussed in detail in Chapter 2.

1.1.3 Chemical reactivity of graphene

The work function of graphene is about 4.6 eV, which is obtained by the crossing of the valence and conduction bands at the Dirac point. The maximum of the valence band in inorganic semiconductors correspond to the HOMO of organic semiconductors; likewise, the minimum of the conduction band correspond to the LUMO (Huckel Molecular Orbital theory, HMO). At the Dirac point, the high lying HOMO and low lying LUMO plus the orbital symmetries facilitate the chemical engineering of graphene (Figure 1.5). Graphene can be regarded as the third wave of carbon allotropes and expected to be the building block for the next generation electronics and spintronics due to its intriguing properties. In order to explore and realize the graphene's potential for a wide range of applications, chemical engineering of its properties is necessary.

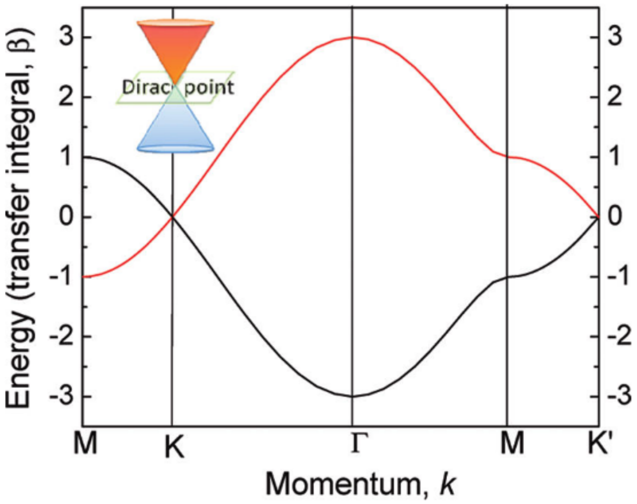

Figure 1.5 Band dispersion of graphene within Huckel Molecular Orbital (HMO) theory. Reprinted with permission from ref.2 (Copyright © 2012 American Chemical Soceity).

1.1.4 Applications of graphene

While opaque metals are traditionally good conductors, transparent polymer films are good insulators. However, a transparent graphene film conducts electricity much better than copper due to its conjugated π electrons, which facilitates its applications in solar cells,[12] optical modulators,[13] photodetectors,[14] light-emitting diodes (LEDs),[15] touch screens,[16], smart windows, flexible electronics,[17] and wearable devices.[18]

Moreover, graphene power holds great promise for applications such as coatings,[19] water desalination,[20] supercapacitors,[21] photovoltaic cells,[22] and energy storage.[23, 24] As the strongest material in nature, graphene can also be used for advanced composites,[25] aerospace,[26] body armor,[27] and space elevator.[28]

1.2 Carbon nanotubes

Carbon nanotube (CNT) is a 1-dimensional (1D) allotrope of carbon with a cylindrical structure and a diameter on the nanoscale. Similar to graphene, quantum confinement effects gift carbon nanotube many extraordinary properties, which are essential for applications in electronics, optics, and many other fields of nanotechnology. Furthermore, CNT has an unprecedented length-to-diameter ratio of ~130,000,000:1. [29]

There are three types of carbon nanotubes: multi-walled carbon nanotubes (MWNTs), comprised of concentric piles of graphite cylinders,[30] double-walled carbon nanotubes (DWNTs) and single-walled carbon nanotubes (SWNTs), which consist of a single graphene sheet seamlessly wrapped into a cylindrical tube (Figure 1.6).[31, 32]

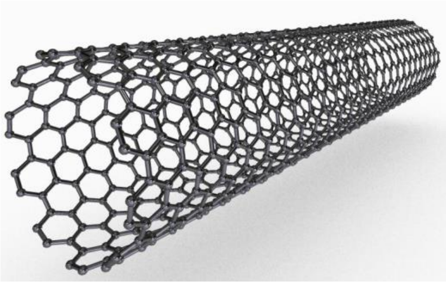

Figure 1.6. Schematic of a single walled carbon nanotube.

1.2.1 Structure and properties of carbon nanotubes

A pair of integers (n, m) is used to index the nanotube structure, which also identifies the diameter and chirality of a single carbon nanotube (Figure 1.7). The diameter (nm) of a SWNT can be given by the following equation:

$$\mathrm{d} = 0.0783\sqrt{n^2 + m^2 + nm} \qquad (1)$$

and the chiral angel can be calculated by the equation:

$$\alpha = \arctan\frac{\sqrt{3}m}{2n+m} \qquad (2)$$

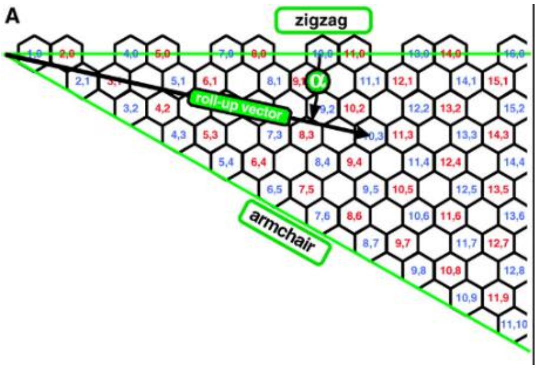

Figure 1.7 (a) Graphene sheet segment showing indexed lattice points. Nanotubes designated (n,m) are obtained by rolling the sheet from (0,0) to (n,m) along a roll-up vector. The chiral angle (from 0 to 30°) is measured between that vector and the zigzag axis; the tube circumference is the vector's length. Reprinted with permission from ref.3 (Copyright © 2002, The American Association for the Advancement of Science).

Depending on the diameter and chiral angle, the SWNTs are classified as armchair (*n* =m), zigzag (*n*= 0 o*r* *m* = 0), or chiral (any other *n* and m) nanotubes, where m and n are integers. All armchair SWNTs are metallic; zigzag and chiral SWNTs are metallic when *n-m=3k (k is an integer)* and semiconducting when *n-m≠3k* with a band gap that inversely depends on the nanotube diameter.[33, 34] Typically about one third of the SWNTs are metallic and two third are semiconducting.[33].

Metallic SWNT has a graphene like band structure, and thus can be treated as a metal, while a semiconducting SWNT has a bandgap related to its chirality. The bandgap can be calculated by the following equation:

$$E_g = \frac{2\vec{h}v_F}{d} = \frac{25.54\vec{h}v_F}{\sqrt{n^2+m^2+nm}} \qquad (3)$$

where $\vec{h}$ is reduced Plank constant and v_F is the magnitude of the velocity of a wave packet around K points for SWNT. From Equation (3), we can obtain a reverse relation between the diameter and bandgap of semiconducting SWNT. In other words, the smaller the diameter, the larger the bandgap.

The electronic density of states (DOS) of semiconducting and metallic SWNTs is illustrated in the inset of Figure 1.8. The interband electronic transitions of the SWNTs give rise to characteristic spectral features in the near-IR (NIR)/Vis spectral region. Because SWNTs are a mixture of metallic and semiconducting tubes, interband transitions from both materials can be seen. Furthermore, the presence of a wide distribution of nanotube diameters results in broadening of the resultant peaks. In the optical spectra of SWNTs shown in Figure 1.8 the distance between each pair of peaks represents the energy of the band gap of SWNTs. S_{11} and S_{22} are the energy separations of the first and second pairs of singularities in the DOS of semiconducting SWNTs, respectively. M_{11} is the energy separation of the first pair of singularities in the DOS of metallic SWNTs.

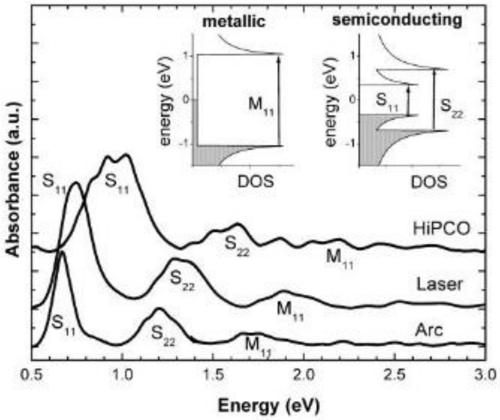

Figure 1.8 Absorption spectra of SWNT films and density of states (inset) of metallic and semiconducting. Reprinted with permission from ref.4 (Copyright © 2002, American Chemical Soceity).

Originating from its special structure, SWNT has extraordinary mechanical, optical, thermal and electronic properties. Small diameter SWNT bundles have an elastic modulus of ~ 1 TPa and a shear modulus of ~ 1GPa,[35] which make them excellent low-density high modulus fibers. Semiconducting SWNTs have photoluminescence, and the band gap can be modulated by doping or chemical functionalization, which extends their applications in photonics and optoelectronics.[36] SWNT has ballistic conduction along the tube axis due to its 1D structure, with a room-temperature thermal conductivity of ~ 3500 $\mathrm{W} \cdot m^{-1}K^{-1}$, [37] which is about 10 times higher than that of copper. SWNTs also have remarkable electronic properties, such as a carrier mobility of ~ 10,000 $cm^2V^{-1}S^{-1}$ [38] and a current density of ~ $4 \times 10^9\ A\, cm^{-2}$, [39] which make them ideal candidates for ultrafast next generation flexible electronics.

1.2.2 Production methods of carbon nanotubes

A number of techniques have been successfully applied for production of CNTs, including electric arc (EA) method,[31, 40] laser ablation (LO),[40, 41] chemical vapor deposition (CVD),[42-44] tubular fluidized bed method [45] and ball milling.

The SWNTs synthesized by different techniques have different diameter and length distributions. All techniques produce soot, which consists of SWNTs and impurities. The impurities are considered as amorphous carbon, nanoparticles comprised of metal catalyst and graphite.

Arc discharge method

In this method, carbon atoms are vaporized at the high temperatures generated by the current passed between the two electrodes. The process is usually carried out in an inert gas atmosphere such as He or Ar. The method can be used to produce both SWNTs and MWNTs. For the growth of SWNTs, the anode is made from a mixture of graphite powder and metal catalysts and the cathode consists only of graphite.

Laser ablation method

In this technique a graphite target containing metal catalysts (usually less than 1 wt% of Ni, Co, or Fe) is ablated with a strong laser pulse under inert gas atmosphere. Laser ablation can produce both multi-walled and single-walled carbon nanotubes[41] of very high quality.

Chemical Vapor Deposition (CVD) method

CVD is a classical way to produce carbon materials. The nanotubes are produced by vapor phase pyrolysis of a carbon-containing gas (C_2H_2, CO, hexane, CH_4) with metal nanoparticles or volatile organometallic compounds such as iron phthalocyanine, nickel phthalocyanine or ferritin. These organometallic compounds act as both catalyst and carbon source. Usually the pyrolysis of the metal nanoparticles or organometallic compounds is performed in an Ar/H_2 environment at high temperature in a quartz tube. The main advantage of CVD is the large-scale continuous production. The CVD method has been widely used to produce SWNTs[42, 46-51] DWNT [52, 53] and MWNTs [54-57]. Also aligned single-walled carbon nanotubes can be produced using this method.[58, 59]

Ball Milling method

Graphite powders are put into a steel container filled with steel balls. The ball milling method can mainly produce short multiwall carbon nanotubes.[60]

Other methods

Plasma torch[61] and direct organic synthesis[62] are also other available routes for synthesis of carbon nanotubes.

1.2.3 Chemical reactivity of carbon nanotubes

The chemical reactivity of fullerene is high due to curvature induced strain, which tends to be reduced by fullerene addition chemistry. Likewise, the pyramidalization and misalignment of the π orbitals make the carbon nanotubes more reactive than graphene (Figure 1.9). From the perspective of reactivity, the covalent chemistry of individual SWNT can be classified into two categories - end caps and side wall chemistry. The carbon atoms in the end caps have a pyramidalization angle of $\theta_p \approx 11.6^{\circ}$, which is much larger than $\theta_p \approx 6.0^{\circ}$ in the side wall. Thus carbon atoms in the end caps are more reactive in order to release the higher strain.

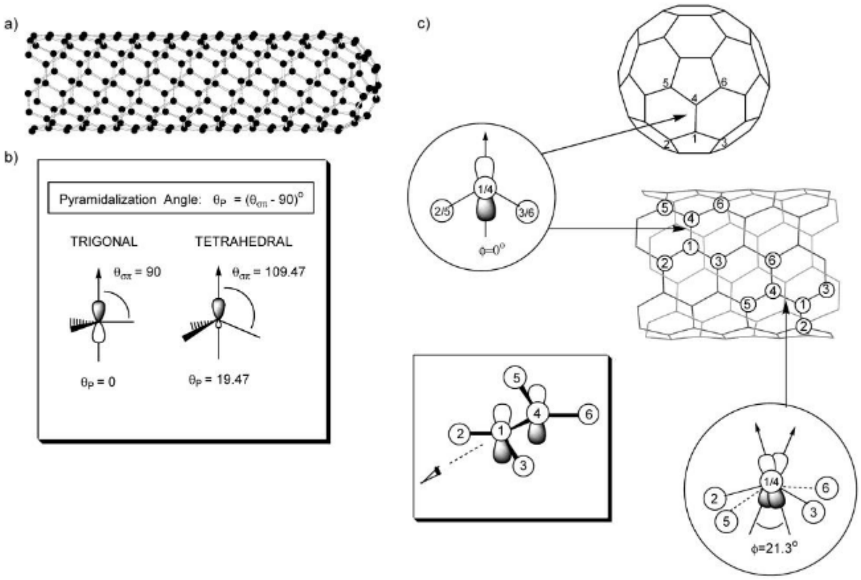

Figure 1.9 Diagrams of (a) metallic (5,5) SWNT (b) pyramidalization angle (θ_p), and (c) the π orbital misalignment angle (∅) along the C1-C4 in the (5,5) SWNT and its capping fullerene, C_{60}. Reprinted with permission from ref.4 (Copyright © 2002, American Chemical Soceity).

However, in contrast to fullerenes, the carbon atoms in SWNT have some misalignment angles ∅ when forming the bond at an angle to the circumference. It is believed that misalignment in π orbital introduces the main strain in SWNT.[4] It is very attractive while challenging to functionalize SWNTs and maintain their extraordinary electronic structure or improve transport properties at the same time. Fortunately, organometallic chemistry provides facile routes to realize this goal and broaden the SWNT applications in the next generation electronics and spintronics.

1.2.4 Applications of carbon nanotubes and their derivatives

Due to special optical, mechanical, electronic and thermal properties, carbon nanotubes have demonstrated potential in a number of fields such as electronics,[63, 64] sensors,[65, 66] composites,[67, 68] energy storage.[69-72]

Electronics

Individual metallic SWNTs have higher electrical conductivity and current density than any metals, while individual semiconducting (Sc-) SWNTs have higher mobility and transconductance than any semiconductor,[73] which makes them competitive candidates for future electronics. SWNT-based transistors and integrated circuits have been demonstrated, which paves the ways to the fabrication of logic gate for future computer technology.[74] Besides, the direct band-gap of Sc-SWNTs provide an opportunity to create both light emitters and light detectors, and SWNT-based lighter emitters and photodetectors have been demonstrated in recent publications.[36, 75-78] Due to the high transparency and excellent flexibility of the CNT thin films, CNT based solar cells, [79-81] touch screens,[82] smart windows,[83] and OLEDs[84] have shown superior performance compared to conventional devices and attractive properties.

Sensors

The resistance of CNTs can be easily tuned by dopants, which make them suitable for the fabrication of highly sensitive nanoscale chemical or biological sensors.[85-91] Importantly, the modification of the electronic structure of CNTs by chemical functionalization can further improve the performance of CNT based sensors.[92]

Composites

Due to the exceptional strength, highly modulus, excellent electrical conductivity of individual carbon nanotubes, they are widely used as an idea filler of various composites with improved strength, thermal and electrical conductivity.[93-98] Functionalization of CNTs can further broaden the application of CNTs in composites with unique properties.[99]

Energy storage

Carbon nanotubes have demonstrated encouraging potential in improving the performance of Li batteries[72, 100-102] and supercapacitors. [103-106]

References

1. Katsnelson, M. I., Graphene: Carbon in Two Dimensions. *Mater. Today* **2007,** 10, 20-27.

2. Sarkar, S.; Bekyarova, E.; Haddon, R. C., Chemistry at the Dirac Point: Diels-Alder Reactivity of Graphene. *Acc. Chem. Res.* **2012,** 45, 673-682.

3. Bachilo, S. M.; Strano, M. S.; Kittrell, C.; Hauge, R. H.; Smalley, R. E.; Weisman, R. B., Structure-Assigned Optical Spectra of Single-Walled Carbon Nanotubes. *Science* **2002,** 298, 2361-2366.

4. Niyogi, S.; Hamon, M. A.; Hu, H.; Zhao, B.; Bhowmik, P.; Sen, R.; Itkis, M. E.; Haddon, R. C., Chemistry of Single-Walled Carbon Nanotubes. *Acc. Chem. Res.* **2002,** 35, 1105-1113.

5. Chuvilin, A.; Kaiser, U.; Bichoutskaia, E.; Besley, N. A.; Khlobystov, A. N., Direct Transformation of Graphene to Fullerene. *Nat. Chem.* **2010,** 2, 450-453.

6. Geim, A. K.; Novoselov, K. S., The Rise of Graphene. *Nat. Mater.* **2007,** 6, 183-191.

7. IUPAC, *In Compendium of Chemical Terminology*. 2nd ed. ed.; Blackwell Scientific, Oxford, 1997.

8. Boehm, H. P., Graphene-How a Laboratory Curiosity Suddenly Became Extremely Interesting. *Angew. Chem. Int. Ed.* **2010,** 49, 9332-9335.

9. Novoselov, K. S.; Geim, A. K.; Morozov, S. V.; Jiang, D.; Zhang, Y.; Dubonos, S. V.; Grigorieva, I. V.; Firsov, A. A., Electric Field Effect in Atomically Thin Carbon Films. *Science* **2004,** 306, 666-669.

10. Berger, C.; Song, Z.; Li, T.; Li, X.; Ogbazghi, A. Y.; Feng, R.; Dai, Z.; Marchenkov, A. N.; Conrad, E. H.; First, P. N.; de Heer, W. A., Ultrathin Epitaxial Graphite: 2d Electron Gas Properties and a Route toward Graphene-Based Nanoelectronics. *J. Phys. Chem. B* **2004,** 108, 19912-19916.

11. Novoselov, K. S.; Geim, A. K.; Morozov, S. V.; Jiang, D.; Katsnelson, M. I.; Grigorieva, I. V.; Dubonos, S. V.; Firsov, A. A., Two-Dimensional Gas of Massless Dirac Fermions in Graphene. *Nature* **2005,** 438, 197-200.

12. Lee, Y.; Tu, K.; Yu, C.; Li, S.; Hwang, J.; Lin, C.; Chen, K.; Chen, L.; Chen, H.; Chen, C., Top Laminated Graphene Electrode in a Semitransparent Polymer

Solar Cell by Simultaneous Thermal Annealing/Releasing Method. *ACS Nano* **2011,** 5, 6564-6570.

13. Liu, M.; Yin, X.; Ulin-Avila, E.; Geng, B.; Zentgraf, T.; Ju, L.; Wang, F.; Zhang, X., A Graphene-Based Broadband Optical Modulator. *Nature* **2011,** 474, 64-67.

14. Liu, C.-H.; Chang, Y.-C.; Norris, T. E.; Zhong, Z., Graphene Photodetectors with Ultra-Broadband and High Responsivity at Room Temperature. *Nature Nanotech.* **2014,** 9, 273-278.

15. Han, T. H.; Lee, Y.; Choi, M. R.; Woo, S. H.; Bae, S. H.; Hong, B. H.; Ahn, J. H.; Lee, T. W., Extremely Efficient Flexible Organic Light-Emitting Diodes with Modified Graphene Anode. *Nat. Photon* **2012,** 6, 105-110.

16. Bae, S.; Kim, H.; Lee, Y.; Xu, X. F.; Park, J. S.; Zheng, Y.; Balakrishnan, J.; Lei, T.; Kim, H. R.; Song, Y. I.; Kim, Y. J.; Kim, K. S.; Ozyilmaz, B.; Ahn, J. H.; Hong, B. H.; Iijima, S., Roll-to-Roll Production of 30-Inch Graphene Films for Transparent Electrodes. *Nat. Nanotech.* **2010,** 5, 574-578.

17. Bonaccorso, F.; Sun, Z.; Hasan, T.; Ferrari, A. C., Graphene Photonics and Optoelectronics. *Nat. Photonics* **2010,** 4, 611-622.

18. Wang, Y.; Wang, L.; Yang, T.; Li, X.; Zang, X.; Zhu, M.; Wang, K.; Wu, D.; Zhu, H., Wearable and Highly Sensitive Graphene Strain Sensors for Human Motion Monitoring. *Adv. Funct. Mater.* **2014,** 24, 4666-4670.

19. Bhunia, S. K.; Jana, N. R., Peptide-Functionalized Colloidal Graphene Via Interdigited Bilayer Coating and Fluorescence Turn-on Detection of Enzyme. *ACS Appl. Mater. Interfaces* **2011,** 3, 3335–3341.

20. Surwade, S. P.; Smirnov, S. N.; Vlassiouk, I. V.; Unocic, R. R.; Veith, G. M.; Dai, S.; Mahurin, S. M., Water Desalination Using Nanoporous Single-Layer Graphene. *Nat. Nanotechnol.* **2015,** 10, 459-464.

21. Liu, C. G.; Yu, Z. N.; Neff, D.; Zhamu, A.; Jang, B. Z., Graphene-Based Supercapacitor with an Ultrahigh Energy Density. *Nano Lett.* **2010,** 10, 4863-4868.

22. Park, H.; Brown, P. R.; Bulovic, V.; Kong, J., Graphene as Transparent Conducting Electrodes in Organic Photovoltaics: Studies in Graphene Morphology, Hole Transporting Layers, and Counter Electrodes. *Nano Lett.* **2012,** 12, 133-140.

23. Yang, Z. B.; Ren, J.; Zhang, Z. T.; Chen, X. L.; Guan, G. Z.; Qin, L. B.; Zhang, Y.; Peng, H. S., Recent Advancement of Nanostructured Carbon for Energy Applications. *Chem. Rev.* **2015,** 115, 5159-5223.

24. Huang, Y.; Liang, J. J.; Chen, Y. S., An Overview of the Applications of Graphene-Based Materials in Supercapacitors. *Small* **2012,** 8, 1805-1834.

25. Hou, Z., -L.; Song, W.-L.; Wang, P.; Meziani, M. J.; Kong, C. Y.; Anderson, A.; Maimaiti, H.; LeCroy, G. E.; Qian, H.; Sun, Y.-P., Flexible Graphene-Graphene Composites of Superior Thermal and Electrical Transport Properties. *ACS Appl. Mater. Interfaces* **2014,** 6, 15026-15032.

26. Zhang, T.; Chang, H.; Wu, Y.; Xiao, P.; Yi, N.; Lu, Y.; Ma, Y.; Huang, Y.; Zhao, K.; Yan, X., Macroscopic and Direct Light Propulsion of Bulk Graphene Material. *Nat. Photonics* **2015,** 9, 471-476.

27. Wetzel, E. D.; Balu, R.; Beaudet, T. D., A Theoretical Consideration of the Ballistic Response of Continuous Graphene Membranes. *J Mech Phys Solids.* **2015,** 82, 23-31.

28. Pugno, N. M., Towards the Artsutanov's Dream of the Space Elevator: The Ultimate Design of a 35gpa Strong Tether Thanks to Graphene. *Acta Astronaut.* **2013,** 82, 221-224.

29. Wang, X.; Li, Q.; Xie, J.; Jin, Z.; Wang, J.; Li, Y.; Jiang, K.; Fan, S., Fabrication of Ultralong and Electrically Uniform Single-Walled Carbon Nanotubes on Clean Substrates. *Nano Lett.* **2009,** 9, 3137-3141.

30. Iijima, S., Helical Microtubules of Graphitic Carbon. *Nature* **1991,** 354, 56-58.

31. Iijima, S.; Ichihashi, T., Single-Shell Carbon Nanotubes of 1-Nm Diameter. *Nature* **1993,** 363, 603-605.

32. Bethune, D. S.; Kiang, C. H.; de Vries, M. S.; Gorman, G.; Savoy, R.; Vazquez, J.; Bevers, R., Cobalt-Catalized Growth of Carbon Nanotubes with Single-Atomic-Layer Walls. *Nature* **1993,** 363, 605-607.

33. Dresselhaus, M. S.; Dresselhaus, G.; Eklund, P. C., *Science of Fullerenes and Carbon Nanotubes*. Academic: San Diego, 1996.

34. Baughman, R. H.; Zakhidov, A. A.; Heer, W. A., Carbon Nanotubes-the Route toward Applications. *Science* **2002,** 297, 787-792.

35. Salvetat, J. P.; Briggs, G. A. D.; Bonard, J. M.; Basca, R. R.; Kulik, A. J.; Stockli, T.; Burnham, N. A.; Forro, L., Elastic and Shear Moduli of Single-Walled Carbon Nanotube Ropes. *Phys. Rev. Lett.* **1999,** 82, 944-947.

36. Avouris, P.; Freitag, M.; Perebeinos, V., Carbon-Nanotube Photonics and Optoelectronics. *Nature Photonics* **2008,** 2, 341-350.

37. Pop, E.; Mann, D.; Wang, Q.; Goodson, K.; Dai, H. J., Thermal Conductance of an Individual Single-Wall Carbon Nanotube above Room Temperature. *Nano Lett.* **2006,** 6, 96-100.

38. Hong, S.; Myung, S., Nanotube Electronics: A Flexible Approach to Mobility. *Nat. Nanotechnol.* **2007,** 2, 207.

39. Wei, B. Q.; Vajtai, R.; Ajayan, P. M., Reliability and Current Carrying Capacity of Carbon Nanotubes. *Appl. Phys. Lett.* **2001,** 79, 1172-1174.

40. Journet, C.; Maser, W. K.; Bernier, P.; Loiseau, A.; Lamy de la Chappelle, M.; Lefrant, S.; Deniard, P.; Lee, R.; Fischer, J. E., Large Scale Production of Single-Walled Carbon Nanotubes by the Electric-Arc Technique. *Nature* **1997,** 388, 756-758.

41. Guo, T.; Nikolaev, P.; Thess, A.; Colbert, D. T.; Smalley, R. E., Catalytic Growth of Single-Walled Nanotubes by Laser Vaporization. *Chem. Phys. Lett.* **1995,** 243, 49-54.

42. Dai, H.; Rinzler, A. G.; Nikolaev, P.; Thess, A.; Colbert, D. T.; Smalley, R. E., Single-Wall Nanotubes Produced by Metal-Catalyzed Disproportionation of Carbon Monoxide. *Chem. Phys. Lett.* **1996,** 260, 471-475.

43. Nikolaev, P.; Bronikowski, M. J.; Bradley, R. K.; Rohmund, F.; Colbert, D. T.; Smith, K. A.; Smalley, R. E., Gas-Phase Catalytic Growth of Single-Walled Carbon Nanotubes from Carbon Monoxide. *Chem. Phys. Lett.* **1999,** 313, 91-97.

44. Joselevich, E.; Lieber, C. M., Vectorial Growth of Metallic and Semiconducting Single-Wall Carbon Nanotubes. *Nano Lett.* **2002,** 2, 1137-1141.

45. Kitiyanan, B.; Alvarez, W. E.; Harwell, J. H.; Resasco, D. E., Controlled Production of Single-Wall Carbon Nanotubes by Catalytic Decomposition of Co on Bimetallic Co-Mo Catalysts. *Chem. Phys. Lett.* **2000,** 317, 497-503.

46. Cassel, A. M.; Raymakers, J. A.; Kong, J.; Dai, H., Large Scale Cvd Synthesis of Single-Walled Carbon Nanotubes. *J. Phys. Chem. B* **1999,** 103, 6484-6492.

47. Kim, W.; Choi, H. C.; Shim, M.; Li, Y.; Wang, D.; Dai, H., Synthesis of Ultralong and High Percentage of Semiconducting Single-Walled Carbon Nanotubes. *Nano Lett.* **2002,** 2, 703-708.

48. Joselevich, E.; Lieber, C. M., Vetorial Growth of Metallic and Semiconducting Single-Wall Carbon Nanotubes. *Nano Lett.* **2002,** 2, 1137-1141.

49. Zheng, B.; Lu, C.; Gu, G.; Markarovski, A.; Finkelstein, G.; Liu, J., Efficient Cvd Growth of Single-Walled Carbon Nanotubes on Surface Using Carbon Monoxide Precursor. *Nano Lett.* **2002,** 2, 895-898.

50. Wei, B.; Vajtai, R.; Choi, Y. Y.; Ajayan, P. M.; Zhu, H.; Xu, C.; Wu, D., Structural Characterizations of Long Single-Walled Carbon Nanotube Strands. *Nano Lett.* **2002,** 2, 1105-1107.

51. Zhu, H. W.; Xu, C. L.; Wu, D. H.; Wei, B. Q.; Vajtai, R.; Ajayan, P. M., Direct Synthesis of Long Single-Walled Carbon Nanotube Strands. *Science* **2002,** 296, 884-886.

52. Li, W. Z.; Wen, J. G.; Sennett, M.; Ren, Z. F., Clean Double-Walled Carbon Nanotubes Synthesized by Cvd. *Chem. Phys. Lett.* **2003,** 368, 299-306.

53. Yamada, T.; Namai, T.; Hata, K.; Futaba, D. N.; Mizuno, K.; Fan, J.; Yudasaka, M.; Yumura, M.; Iijima, S., Size-Selective Growth of Double-Walled Carbon Nanotube Forests from Engineered Iron Catalysts. *Nat. Nanotechnol.* **2006,** 1, 131-136.

54. Huang, S.; Dai, L.; Mau, A. W. H., Patterned Growth and Contact Transfer of Well-Aligned Carbon Nanotube Films. *J. Phys. Chem. B* **1999,** 103, 4223-4227.

55. Chopra, N.; Kichambare, P. D.; Andrews, R.; Hinds, B. J., Control of Multiwalled Carbon Nanotube Diameter by Selective Growth on the Exposed Edge of a Thin Film Multilayer Structure. *Nano Lett.* **2002,** 2, 1177-1181.

56. Delzeit, L.; Nguyen, C. V.; Chen, B.; Stevens, R.; Cassell, A.; Han, J.; Meyyappan, M., Multiwalled Carbon Nanotubes by Chemical Vapor Deposition Using Multilayered Metal Catalysts. *J. Phys. Chem. B* **2002,** 106, 5629-5639.

57. Lee, Y. T.; Park, J.; Choi, Y. S.; Ryu, H.; Lee, H. J., Temperature-Dependent Growth of Vertically Aligned Carbon Nanotubes in the Range. *J. Phys. Chem. B* **2002,** 106, 7614-7618.

58. Ren, Z. F.; Huang, Z. P.; Xu, J. W.; Wang, J. H.; Bush, P.; Siegal, M. P.; Provencio, P. N., Synthesis of Large Arrays of Well-Aligned Carbon Nanotubes on Glass. *Science* **1998,** 282, 1105-1107.

59. Chhowalla, M.; Teo, K. B. K.; Ducati, C.; Rupesinghe, N. L.; Amaratunga, G. A. J.; Ferrari, A. C.; Roy, D.; Robertson, J.; Milne, W. I., Growth Process Conditions of Vertically Aligned Carbon Nanotubes Using Plasma Enhanced Chemical Vapor Deposition. *J. Appl. Phys.* **2001,** 90, 5308-5316.

60. Pierard, N.; Fonseca, A.; Konya, Z.; Willems, I.; Tendeloo, G. V.; Nagy, J. B., Production of Short Carbon Nanotubes with Open Tips by Ball Milling. *Chem. Phys. Lett.* **2001,** 335, 1-8.

61. Chen, C. K.; Perry, W. L.; Xu, H.; Jiang, Y.; Phillips, J., Plasma Torch Production of Macroscopic Carbon Nanotube Structures. *Carbon* **2003,** 41, 2555-2560.

62. Scott, L. T., Methods for the Chemical Synthesis of Carbon Nanotubes: An Approach Based on Hemispherical Polyarene Templates. *Pure Appl. Chem.* **2017**.

63. Martel, R.; Schmidt, T.; Shea, H. R.; Hertel, T.; Avouris, P., Single- and Multi-Wall Carbon Nanotube Field-Effect Transistors. *Appl. Phys. Lett* **1998,** 73, 2447-9.

64. Bachtold, A.; Hadley, P.; Nakanishi, T.; Dekker, C., Logic Circuits with Carbon Nanotube Transistors. *Science* **2001,** 294, 1317-1320.

65. Wang, S. G.; Zhang, Q.; Wang, R.; Yoon, S. F., A Novel Multi-Walled Carbon Nanotube Based Biosensor for Glucose Detection. *Biochem. Biophys. Res. Commun.* **2003,** 311, 572-576.

66. Cai, H.; Cao, X. N.; Jiang, Y.; He, P. G.; Fang, Y. Z., Carbon Nanotube-Enhanced Electrochemical DNA Biosensor for DNA Hybridization Detection. *Anal. Bioanal. Chem.* **2003,** 375, 287-293.

67. Ajayan, P. M.; Schadler, L. S.; Giannaris, C.; Rubio, A., Single-Walled Carbon Nanotube-Polymer Composites: Strength and Weakness. *Adv. Mater.* **2000,** 12, 750-753.

68. Ounaies, Z.; Park, C.; Wise, K. E.; Soichi, E. J.; Harrison, J. S., Electrical Properties of Single Wall Carbon Nanotube Reinforsed Polyimide Composites. *Comp. Sci. Tech.* **2003,** 63, 1-10.

69. Frackowiak, E.; Beguin, F., Carbon Materials for the Electrochemical Storage of Energy in Capacitors. *Carbon* **2001,** 39, 937-950.

70. Futaba, D. N.; Hata, K.; Yamada, T.; Hiraoka, T.; Hayamizu, Y.; Kakudate, Y.; Tanaike, O.; Hatori, H.; Yumura, M.; Iijima, S., Shape-Engineerable and Highly Densely Packed Single-Walled Carbon Nanotubes and Their Application as Super-Capacitor Electrodes. *Nat. Mater.* **2006,** 5, 987-994.

71. Kiebele, A.; Gruner, G., Carbon Nanotube Based Battery Architecture. *Applied Physics Letters* **2007,** 91, 144104

72. Landi, B. J.; Ganter, M. J.; Cress, C. D.; DiLeo, R. A.; Raffaelle, R. P., Carbon Nanotubes for Lithium Ion Batteries. *Energy Environ. Sci.* **2009,** 2, 638-654.

73. McEuen, P. L.; Fuhrer, M. S.; Park, H., Single-Walled Carbon Nanotube Electronics. *IEEE Trans. Nanotechnol* **2002,** 99, 78-85.

74. Avouris, P.; Appenzeller, J.; Martel, R.; Wind, S. J., Carbon Nanotube Electronics. *Proc. IEEE.* **2003,** 91, 1772-1784.

75. Itkis, M. E.; Yu, A.; Haddon, R. C., Single-Walled Carbon Nanotube Thin Film Emitter-Detector Integrated Optoelectronic Device. *Nano Lett.* **2008,** 8, 2224-2228.

76. Arnold, M. S.; Zimmerman, J. D.; Renshaw, C. K.; Xu, X.; Lunt, R. R.; Austin, C. M.; Forrest, S. R., Broad Spectral Response Using Carbon Nanotube/Organic Semiconductor/C60 Photodetectors. *Nano Lett.* **2009,** 9, 3354-3358.

77. Scarselli, M.; Castrucci, P.; De Crescenzi, M., Electronic and Optoelectronic Nano-Devices Based on Carbon Nanotubes. *J. Phys.: Condens. Matter.* **2012,** 24, 313202.

78. Park, S.; Kim, S. J.; Nam, J. H.; Pitner, G.; Lee, T. H.; Anyzner, A. L.; Wang, H. L.; Fong, S. W.; Vosgueritchian, M.; Park, Y. J.; Brongersma, M. L.; Bao, Z. N., Significant Enhancement of Infrared Photodetector Sensitivity Using a Semiconducting Single-Walled Carbon Nanotube/C_{60} Phototransistor. *Adv. Mater.* **2015,** 27, 759-765.

79. Landi, B. J.; Castro, S. L.; Ruf, H. J.; Evans, C. M.; Bailey, S. G.; Raffaelle, R. P., Cdse Quantum Dot-Single Wall Carbon Nanotube Complexes for Polymeric Solar Cells. *Solar Energy Materials and Solar Cells* **2005,** 87, 733-746.

80. Wadhwa, P.; Liu, B.; McCarthy, M. A.; Wu, Z.; Rinzler, A. G., Electronic Junction Control in a Nanotube-Semiconductor Schottky Junction Solar Cell. *Nano Lett.* **2010,** 10, 5001-5005.

81. Gong, M.; Shastry, T. A.; Xie, Y.; Bernardi, M.; Jasion, D.; Luck, K. A.; Marks, T. J.; Grossman, J. C.; Ren, S. Q.; Hersam, M. C., Polychiral Semiconducting Carbon Nanotube–Fullerene Solar Cells. *Nano Lett.* **2014,** 14, 5308-5314.

82. Hecht, D. S.; Thomas, D.; Hu, L.; Ladous, C.; Lam, T.; Park, Y.; Irvin, G.; Drzaic, P., Carbon-Nanotube Film on Plastic as Transparent Electrode for Resistive Touch Screens. *J SOC INF DISPLAY* **2009,** 17, 941-946.

83. Wang, F.; Itkis, M. E.; Bekyarova, E.; Haddon, R. C., Charge Compensated, Semiconducting Single-Walled Carbon Nanotube Thin Film as an Electrically Configurable Optical Medium. *Nat. Photonics* **2013,** 7, 459-465.

84. Xu, W.; Zhao, J.; Qian, L.; Han, X.; Wu, L.; Wu, W.; Song, M.; Zhou, L.; Su, W.; Wang, C., Sorting of Large-Diameter Semiconducting Carbon Nanotube and Printed Flexible Driving Circuit for Organic Light Emitting Diode (Oled). *Nanoscale* **2014,** 6, 1589-1595.

85. Kong, J.; Franklin, N. R.; Zhou, C. W.; Chapline, M. G.; Peng, S.; Cho, K. J.; Dai, H. J., Nanotube Molecular Wires as Chemical Sensors. *Science* **2000,** 287, 622-625.

86. Varghese, O. K.; Kichambre, P. D.; Gong, D.; Ong, K. G.; Dickey, E. C.; Grimes, C. A., Gas Sensing Characteristics of Multi-Wall Carbon Nanotubes. *Sensors and Actuators B-Chemical* **2001,** 81, 32-41.

87. Chopra, S.; Pham, A.; Gaillard, J.; Parker, A.; Rao, A. M., Carbon-Nanotube-Based Resonant-Circuit Sensor for Ammonia. *Applied Physics Letters* **2002,** 80, 4632-4634.

88. Li, J.; Lu, Y.; Ye, Q.; Cinke, M.; Han, J.; Meyyappan, M., Carbon Nanotube Sensor for Gas and Organic Vapor Detection. *Nano Lett.* **2003,** 3, 929-933.

89. Wong, Y. M.; Kang, W. P.; Davidson, J. L.; Wisitsora-at, A.; Soh, K. L., A Novel Microelectronic Gas Sensor Utilizing Carbon Nanotubes for Hydrogen Gas Detection. *Sens. Actuators, B* **2003,** 93, 327-332.

90. Joshi, K. A.; Tang, J.; Haddon, R. C.; Wang, J.; Chen, W.; Mulchandani, A., A Disposable Biosensor for Organophosphorus Nerve Agents Based on Carbon Nanotubes Modified Thick Film Electrode. *Electroanalysis* **2005,** 17, 54-58.

91. Zhang, T.; Mubeen, S.; Bekyarova, E.; Yoo, B. Y.; Haddon, R. C.; Myung, N. V.; Deshusses, M. A., Poly(M-Aminobenzene Sulfonic Acid) Functionalized Single-Walled Carbon Nanotubes Based Gas Sensor. *Nanotechnol.* **2007,** 18, 165504 -6.

92. Bekyarova, E.; Davis, M.; Burch, T.; Itkis, M. E.; Zhao, B.; Sunshine, S.; Haddon, R. C., Chemically Functionalized Single-Walled Carbon Nanotubes for Ammonia Sensors. *J. Phys. Chem. B* **2004,** 108, 19717-19720.

93. Baughman, R. H.; Zakhidov, A. A.; de Heer, W. A., Carbon Nanotubes - the Route toward Applications. *Science* **2002,** 297, 787-792.

94. Dalton, A. B.; Collins, S.; Munoz, E.; Razal, J. M.; Ebron, V. H.; Ferraris, J. P.; Coleman, J. N.; Kim, B. G.; Baughman, R. H., Super-Tough Carbon-Nanotube Fibres. *Nature* **2003,** 423, 703.

95. Wanekaya, A. K.; Lei, Y.; Bekyarova, E.; Chen, W.; Haddon, R.; Mulchandani, A.; Myung, N. V., Fabrication and Properties of Conducting Polypyrrole/Swnt-Pabs Composite Films and Nanotubes. *Electroanal.* **2006,** 18, 1047-1054.

96. Yu, A.; Itkis, M. E.; Bekyarova, E.; Haddon, R. C., Effect of Single-Walled Carbon Nanotube Purity on the Thermal Conductivity of Carbon Nanotube-Based Composites. *Appl. Phys. Lett.* **2006,** 89, 133102 - 4.

97. Moisala, A.; Li, Q.; Kinloch, I. A.; Windle, A. H., Thermal and Electrical Conductivity of Single- and Multi-Walled Carbon Nanotube-Epoxy Composites. *Compos. Sci. Technol.* **2005,** 66, 1285-1288.

98. Bekyarova, E.; Thostenson, E. T.; Yu, A.; Kim, H.; Gao, J.; Tang, J.; Hahn, H. T.; Chou, T.-W.; Itkis, M. E.; Haddon, R. C., Multiscale Carbon Nanotube-Carbon Fiber Reinforcement for Advanced Epoxy Composites. *Langmuir* **2007,** 23, 3970-3974.

99. Bekyarova, E.; Thostenson, E. T.; Yu, A.; Itkis, M. E.; Fakhrutdinov, D.; Chou, T.-W.; Haddon, R. C., Functionalized Single-Walled Carbon Nanotubes for Carbon Fiber-Epoxy Composites. *J. Phys. Chem. C* **2007,** 111, 17865-17871.

100. Hu, L. B.; Wu, H.; La Mantia, F.; Yang, Y. A.; Cui, Y., Thin, Flexible Secondary Li-Ion Paper Batteries. *ACS Nano* **2010,** 4, 5843-5848.

101. Wu, Z. Z.; Han, X. G.; Zheng, J. X.; Wei, Y.; Qiao, R. M.; Shen, F.; Dai, J. Q.; Hu, L. B.; Xu, K.; Lin, Y.; Yang, W. L.; Pan, F., Depolarized and Fully Active Cathode Based on $Li(Ni_{0.5}co_{0.2}mn_{0.3})O^{-2}$ Embedded in Carbon Nanotube Network for Advanced Batteries. *Nano Lett.* **2014,** 14, 4700-4706.

102. Wang, W.; Favors, Z.; Li, C.; Liu, C.; Ye, R.; Fu, C.; Bozhilov, K.; Guo, J.; Ozkan, M.; Ozkan, C. S., Silicon and Carbon Nanocomposite Spheres with Enhanced Electrochemical Performance for Full Cell Lithium Ion Batteries. *Sci. Rep.* **2017,** 7.

103. Gao, L. J.; Peng, A. P.; Wang, Z. Y.; Zhang, H.; Shi, Z. J.; Gu, Z. N.; Cao, G. P.; Ding, B. Z., Growth of Aligned Carbon Nanotube Arrays on Metallic Substrate and Its Application to Supercapacitors. Solid State Commun. 2008, 146, 380-383.

104. Yu, D. S.; Dai, L. M., Self-Assembled Graphene/Carbon Nanotube Hybrid Films for Supercapacitors. J. Phys. Chem. Lett. 2010, 1, 467-470.

105. Bekyarova, E.; Palanisamy, R.; Itkis, M. E.; Haddon, R. C. In Carbon Nanotube Thin Films and Hybrid Structures for Supercapacitor and Fuel Cell Applications, Meeting Abstracts, 2014; The Electrochemical Society: 2014; pp 1146-1146.

106. Haddon, R. C. In Carbon Nanotube Thin Films and Hybrid Structures for Supercapacitor and Fuel Cell Applications, 225th ECS Meeting (May 11-15, 2014), 2014; ECS: 2014.

Chapter 2. Transfer methods of CVD graphene

2.1 Introduction

As we discussed in Chapter 1.1, graphene is a one atom thick two dimensional carbon material, whose valence and conduction bands touch each other at the Dirac point.[1, 2] The fascinating properties, which originate from the unique electronic structure of graphene, motivate the wide interest in the potential application of this material in many fields such as electronics,[3-8] spintronics,[9] optics,[5] environmental engineering,[10, 11] integrated circuits (IC) on a graphene wafer, [12, 13] flexible electronics,[14] transparent electrodes,[15] energy storage[16, 17] aerospace.[18]

Graphene can be categorized in two groups: graphene films and graphene powders based on the form factor as shown in Figure 2.1. Even though graphene powders can be produced in large scale, dispersed into solutions for both solution based and film-based applications, [8] it is hard to preserve the excellent electrical transport properties of single layer graphene on large scale due to the small size of the individual graphene layers and poor contact between them, which makes this material not suitable for high performance electronics. Graphene films can be further divided into epitaxial graphene on SiC, chemical vapor deposition (CVD) graphene (mainly on Cu/Ni) and scotch tape exfoliated graphene on various substrates.

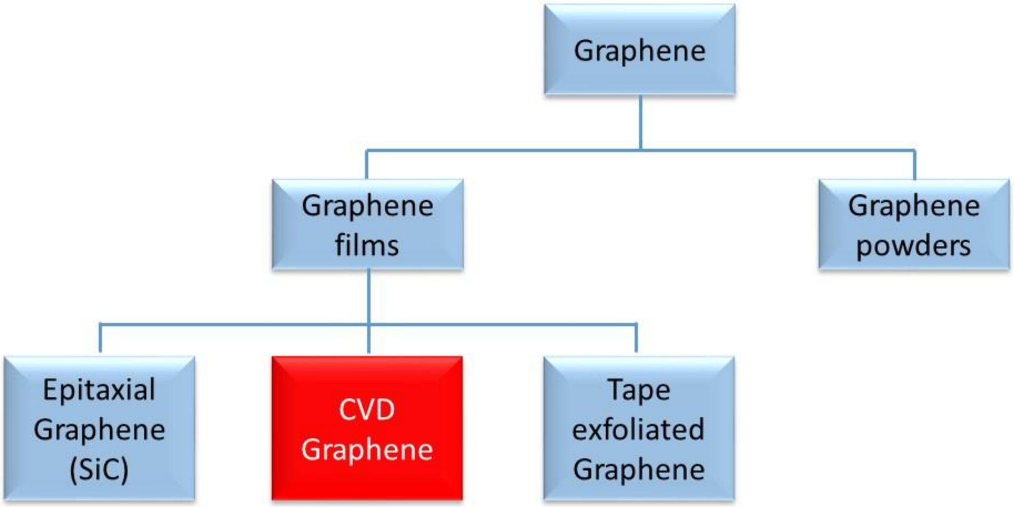

Figure 2. 1. The main forms of graphene.

Wafer scale single domain graphene is required to build uniform graphene integrated circuits compatible with current industrial fabrication processes. Chemical vapor deposition (CVD) is among the most promising methods for production of macro-size, continuous, high-quality graphene films for industrial applications.[19-22] The CVD process utilizes a metal substrate (copper or nickel) for the graphene growth, which requires transfer of the graphene film onto a desired substrate, which is usually accomplished using polymers as discussed in Section 2.3.

Recently millimeter-scale single-crystalline growth of CVD graphene has been achieved [23-26], which makes CVD graphene appealing candidate as the starting material of graphene interconnects, flexible electronics and spintronics. Currently, large domain CVD graphene is synthesized with metal catalysts, such as Cu or Ni, and it need to be transferred to appropriate substrates for electronic applications. Although a variety of synthetic and transfer methods of CVD graphene have been developed, they can be classified into three main categories as shown in Figure 2.2: (1) transfer with the help of a supporting layer onto target substrates. (2) transfer without any supporting layer onto target substrates and (3) direct growth of CVD graphene on targeted substrates from precursors inside a furnace without any post growth transfer process. Below we review representative graphene transfer methods from the perspective of mechanism, cleanness, quality, reliability and cost.

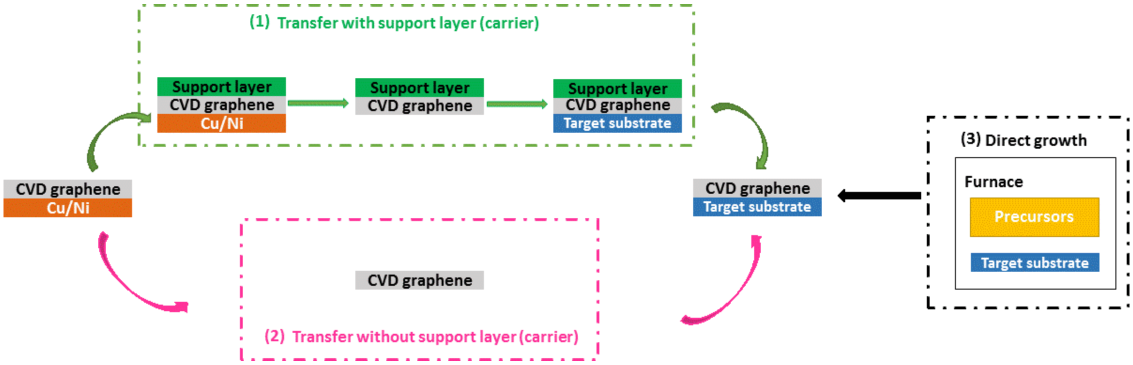

Figure 2. 2. Schematic of various routes to obtain CVD graphene on target substrates.

Nearly every CVD graphene transfer technique have to solve two problems: (1) how to separate graphene and the metal substrates (Cu/Ni) and (2) how to protect graphene after the separation.

Transfer with supporting layer

A conventional but very efficient way to protect graphene from external forces during the transfer process is to utilize a supporting layer coated on top of the graphene surfaces. As metal substrates can be easily etched away completely or peeled off after special pre-treatments, the main factor that determines the quality of the transferred graphene is the supporting layer. The supporting layer should possess the following characteristics in order to minimize the degradation of graphene's quality in the transfer process: (a) flexible, (b) mechanical strong to support the graphene films, (c) easy to remove from graphene.

Polymer based graphene transfer

PMMA -assisted graphene transfer The early stage CVD graphene transfer methods adopt PMMA as the carrier [20, 27]. In this method, usually the as-grown CVD graphene on one side of the copper foil is coated with PMMA solution in anisole or other organic solvent. After PMMA polymerizes, the graphene on the other side of the copper foil is removed by O_2 plasma etching (or by harsh chemical solutions) and the sample is placed on the surface of $FeCl_3$ solution to etch away the copper. After this step the etching solution is replaced with clean water multiple times. Finally the PMMA/Graphene is lifted off with a target substrate and placed on a hotplate for high temperature baking in order to remove water residues trapped between the graphene and the target substrate and improve their contact.

Figure 2.3. Schematic illustration of conventional PMMA-assisted graphene transfer processes.

However, researchers have been struggling with the degradation of graphene's intrinsic properties due to contamination with PMMA residue and paramagnetic Fe^{3+}. [28-30]

PDMS-assisted graphene transfer Polydimethylsiloxane (PDMS) has been extensively studied and widely used in soft lithography as a cost-effective way to fabricate micro- and nanoscale devices [31] [32]. In the early PDMS assisted transfer method, multilayer CVD graphene was attached to crosslinked solid PDMS elastomer, and transferred to targeted substrates by a simple "stamping" process after Ni was etched away.[33] Despite the large scale conformal contact between the PDMS elastomer with targeted substrates.[31] a stronger adhesion between graphene and targeted substrates is needed theoretically for intact graphene transfer, which have high requirements for the cleanliness, flatness and rigidness of the targeted substrates and often gives fragmental graphene flakes.[34] Actually, in most cases PDMS functions as a rigid holder to realize dry transfer of graphene instead of direct contact with graphene surfaces. [34, 35]

Thermal Release Tape-assisted graphene transfer Thermal release tape is a tape with specific adhesives which adhere to substrates strongly at room temperature while losing adhesion at high temperature (above ~100 ° C). A representative thermal release tape-assisted graphene transfer method is the so-called roll-to-roll (R2R) technique. [15,36] This method inherits the large-scale and high-throughput characteristics of roll to roll production.[37,38] Although R2R graphene transfer method is favorable in transferring large scale graphene to flexible substrate for the fabrication of graphene flexible electronics, it is not suitable for transferring graphene to rigid substrates such as silicon wafers and glass substrates.

Transfer without supporting layer

It is widely known that the surface tension of the etching solution could tear graphene apart, which is why a supporting layer is proposed to protect graphene during the metal etching process.[20, 27,39, 33, 40-43] Alternative way to protect graphene has been suggested which relies on the modification of the surface tension of the etching solution to a harmless level instead of strengthening graphene by a support layer. [44] Lin et. al, mixed isopropyl alcohol (IPA) with ammonium persulfate in order to reduce the surface tension of the etching solution to a harmless level to graphene.[44] The graphene on Cu is directly placed on the surface of this mixed etchant confined by a graphite holder. After Cu was completely etched away, the mixed etchant was replaced with fresh mixture of water and IPA by pumping out the etchant on one side and pumping in the fresh mixture on the other side at the same rate. Finally, graphene floating on the surface was lowered to the target substrate by pulling out the remaining solution slowly with a syringe pump. This support-free method successfully avoided contaminations from polymer and organic residues, and thus largely improved the quality of transferred graphene. However due to the lack of support after Cu was etched away, the graphene can be cracked easily by the fluctuation of the solution, and thus the integrity of the transferred graphene depends strongly on the operation conditions, which makes the reliability of the method a challenge for transferring intact graphene on a large scale.

Thus, transfer of CVD graphene to a substrate of interest remains a challenging problem and most transfer methods introduce contaminations and defects which degrade the graphene quality. Furthermore, most graphene transfer methods are typically expensive and difficult to scale up. In this chapter we demonstrate two novel transfer methods that provide high quality, clean graphene films.

The first graphene transfer method utilizes a cellulose supporting layer and we illustrate that this technique is capable of producing large area, defect-free graphene and molecularly clean surfaces. This cellulose assisted transfer (CAT) method is based on scalable and reliable processes and it largely reduces the cost, time and contaminations of the obtained graphene layer and can be expanded to industrial scale applications.

In the second transfer method we employ a small molecule polyaromatic hydrocarbon – naphathalene, which can be readily removed by sublimation at room temperature making this method very attractive for plastic substrates.

The transferred graphene samples were thoroughly characterized with Raman spectroscopy, Atomic Force Microscopy, Scanning Electron Microscopy and X-ray photoelectron spectroscopy. The transferred graphene films were utilized in the study of the organometallic chemistry of graphitic surfaces discussed in Chapter 3.

2.2 Cellulose-assisted large scale graphene transfer method

In this section, we discuss the development of a novel technique for the transfer of graphene on various substrates. The method utilizes cellulose acetate as the coating layer, which protects graphene from unfavourable forces and contaminations during the transfer process by forming a soft flexible thin film on top of graphene. The etching of Cu foil, used in the CVD graphene growth, is accomplished with a hydrogen peroxide – hydrogen chloride solution, which decreases the possibility for magnetic contaminations of the graphene. This cellulose assisted transfer (CAT) method largely reduces the cost, time and contaminations of the obtained graphene and can be expanded to industrial scale applications. The transferred grapene films were characterized with Raman spectroscopy, atomic force microscopy (AFM) and X-ray photoelectron spectroscopy (XPS) to evaluate the quality of the obtained films. The fabricated field effect transistor (FET) devices showed high mobility and on-off ratio.

2.2.1 Experimental Section

CAT graphene transfer

As-grown monolayer CVD graphene (Graphene Supermarket) was first spin coated with a cellulose acetate solution (Average Mn ~ 50,000 by GPC, Sigma Aldrich, 4.5 mg/mL dissolved in acetone) at 2000 rpm. The spin-coated thin film dries immediately as the acetone evaporates. The graphene on the uncoated side was etched away by oxygen plasma (Oxford Plasmalab 100/180 model; forward power -30 W; ICP power – 300 W, etch time 30 s). An aqueous solution of H2O2 and HCl was prepared by mixing equal volumes of 2 M HCl and 1 M H_2O_2; the solution etches away the Cu substrate (25 μm) underneath the CVD graphene within 10 minutes. The graphene sample was thoroughly cleaned by replacing the etching solution with distilled water. The substrate with the transferred graphene was placed on a hot plate and kept at 35 °C for 10 min, followed by baking at 200

°C for 20 min. After the substrate with the graphene was cooled down to ~60 °C, it was submerged into a hot acetone bath overnight to remove the cellulose acetate.

PMMA graphene transfer

As-grown monolayer CVD graphene was first spin coated with a PMMA solution (950 PMMA A4, MicroChem, 10% by volume dissolved in chlorobenzene) at 2000 rpm. The spin-coated thin film was kept at room temperature overnight inside a clean petri dish. The graphene on the uncoated side was etched away by oxygen plasma as described in above. Then the PMMA/Graphene/Cu sample was placed on the surface of $FeCl_3$ solution (0.5 M) to etch away the Cu substrate (thickness - 25 μm; typical etching time - 60 minutes). After the Cu was removed, the etching solution was replaced with clean water by repeatedly flowing out the waste solution and flowing in clean water until neutral pH was reached. The substrate with the graphene was transferred to a hot plate and kept at 35 °C for 10 min, after this step the temperature was increased and maintained at 200 °C for 20 minutes. After the substrate with the graphene was cooled down to ~60 ^{o}C, it was submerged into a hot acetone bath overnight to remove the PMMA.

Raman spectroscopy and mapping

Raman spectra and mapping of CVD graphene were recorded with a Nicolet Almega XR Dispersive Raman microscope using 532 nm laser excitation and 25%

power source. The laser spot size is around 1 µm with a 50 x objective lens. Raman mapping area for all samples is 20 µm x 18 µm, with a step size of 1 µm in both x and y directions.

Atomic Force Microscopy (AFM)

AFM images were collected in a tapping mode with Digital Instruments, MMAFM-2.

X-ray photoelectron spectroscopy (XPS)

XPS of transferred CVD graphene on 300 nm SiO_2/Si substrates was carried out with a Kratos AXIS ULTRADLD XPS system equipped with Al Kα monochromated X-ray source and a 165 mm mean radius electron energy hemispherical analyzer. Vacuum pressure was kept below 3×10^{-9} torr during the acquisition. The high-resolution scans were run using a power of 300 watts, 20 pass energy and a step size of 0.05 eV. A low-energy electron flood from a filament was used for charge neutralization. The size slot for the XPS is 300 µm x 700 µm. The spectra are shown without energy-scale correction and the peak fits consist of Lorentzian and Gaussian distributions.

Fabrication of field effect transistors (FETs)

Drain and source electrodes (10 nm Cr/100 nm Au) were evaporated by an e-beam Evaporator onto 300 nm SiO_2/Si substrates with a shadow mask. After that, as-grown monolayer CVD graphene was transferred onto the pre-patterned substrates by conventional PMMA transfer and CAT methods, respectively. The channel dimensions of all graphene devices are 0.25 mm (length) x 1 mm (width). No photolithography was employed to exclude the effect of photoresist residues on the electronic properties of the transferred graphene samples. Thermal annealing at 200 ℃ in vacuum (5 x 10^{-7} torr) was performed to remove atmospheric dopants and bring the Dirac point in the vicinity of 0 volts.

2.2.2 Results and Discussion

Description of the graphene transfer method In this work, we employed cellulose acetate as a holding layer to protect graphene during the transfer process because of its low cost, excellent draping qualities and environmentally friendly properties. Cellulose acetate, an acetylated derivative of the naturally abundant and sustainable polymer cellulose, can be dissolved in acetone and, when spin-coated on a flat surface, it gives a continuous thin and flexible film (Figure 2.4). Cellulose acetate has a long history of application in a number of industrial fields. It has been used as the film base in photographs,[45] as a substrate for magnetic tape,[46] and as a component in household fabrics[47] among other applications. Thus, a mature and comprehensive system to produce, transport and stock cellulose acetate has already been built.

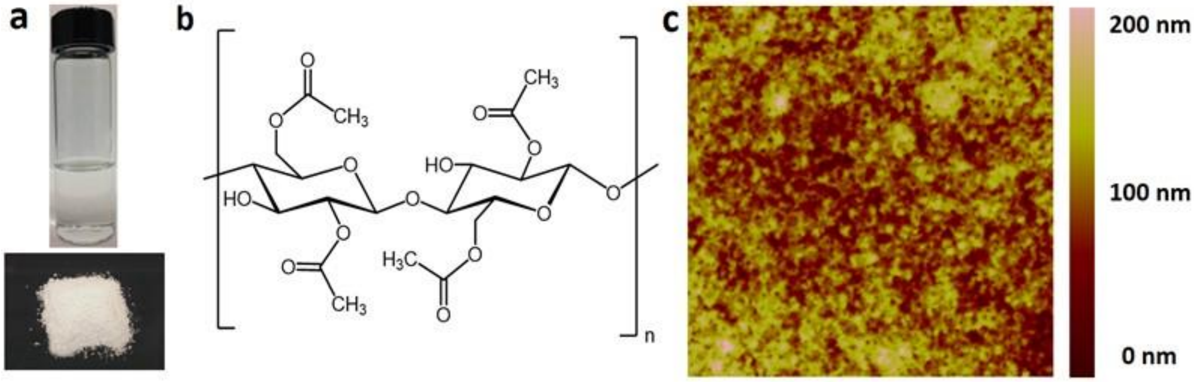

Figure 2.4 (a) Photographs of a cellulose acetate powder (lower) and a cellulose acetate solution in acetone (upper). (b) The structure of cellulose acetate. (c) AFM image of a spin-coated cellulose acetate thin film on top of as-grown CVD graphene. Reprinted with permission from ref.40 (Copyright © 2016 Elsevier Ltd.).

For the graphene transfer, a thin layer of cellulose acetate film is first spin-coated on top of the graphene film grown on Cu or Ni, as shown in Figure 2.5a. The cellulose acetate film adheres strongly to the graphene surface and protects the graphene from the surface tension of the etching solution after the Cu or Ni are etched away. The metal substrate (Cu) is etched with an $H_2O_2/HCl/H_2O$ solution. For the etching the central batch reactor (Figure 2.5) is filled with a fresh $H_2O_2/HCl/H_2O$ solution and the cellulose acetate/graphene/copper sample is placed on the surface of the etching solution. The etching occurs through the following chemical reaction:

$$\mathrm{H_2O_2 + 2HCl + Cu \rightarrow CuCl_2 + 2H_2O}$$

After the copper is completely etched away, fresh water is introduced into the central reactor from the inlet tank and the waste solution is extracted from the outlet tank at the same rate using peristaltic pumps, thus converting the system into a continuous tank reactor. After the pH of the solution inside the reactor approaches that of pure water, the target substrate is positioned onto the bottom of the central reactor through a slit designed between the inlet tank and the central reactor. In the next step, the water is drained out from the outlet tank at a slow rate allowing the cellulose acetate/graphene to lower down onto the substrate. Alternatively, the floating cellulose acetate coated graphene can be lifted out from the pure water bath with the target substrate. Next, the cellulose acetate/graphene/target substrate is transferred to a hot plate and kept at 35 °C for 10 min to remove large water droplets trapped between the graphene film and the substrate. The temperature is then increased to 200 °C and maintained for 20 minutes to enhance the contact between graphene and the substrate. The final

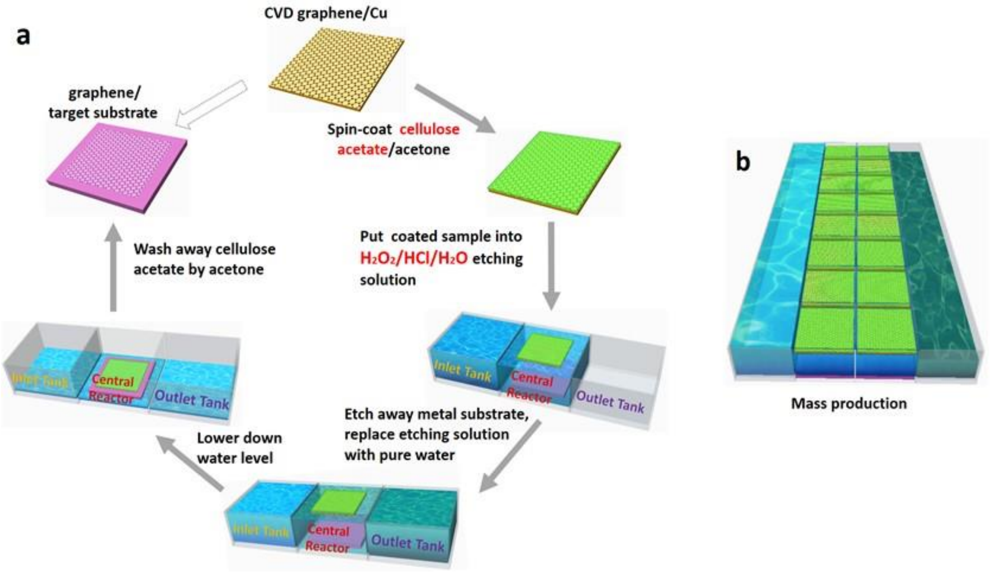

Figure 2.5 Schematic illustration of (a) the CAT method and (b) the reactor for simultaneous transferring graphene onto multiple substrates for industrial applications. Reprinted with permission from ref.40 (Copyright © 2016 Elsevier Ltd.).

step of the transfer process is removing the cellulose film, which is dissolved in hot acetone vapors for 5 minutes. The substrate with the graphene is then submerged into hot acetone to completely remove the cellulose acetate. The process can be easily scaled to simultaneously conduct the graphene transfer on multiple substrates as illustrated in Figure 2.5b.

Characterization of the transferred graphene In order to systematically investigate the quality of the CAT graphene and compare it with the conventional wet transfer method, various characterization tools were employed. Raman spectroscopy is a powerful and sensitive technique to characterize the quality of carbon materials, specifically graphene.[48, 49] The appearance of a D peak in the vicinity of 1340 cm^{-1} generally indicates presence of defects in the sp^2 carbon network of graphene.[48, 50] Other important metrics are the amplitude and spectral shape of the G and 2D peaks, observed in the vicinity of 1580 cm^{-1} and 2700 cm^{-1}, respectively, which can be utilized to characterize the quality of graphene and the number of graphene layers. [49] For example, because the 2D peak is sensitive to long range order, higher intensity of the 2D peak is an indication of higher crystalline quality of the single layer graphene. [49] Figure 2.6a compares representative Raman spectra of graphene samples transferred by the CAT and PMMA-assisted methods. The CAT graphene typically gives a Raman spectrum with little or no D-peak as compared to the obvious D peak present in the Raman spectrum of graphene after the PMMA transfer. This is an indication of a much smaller concentration of defects in the CAT-graphene.

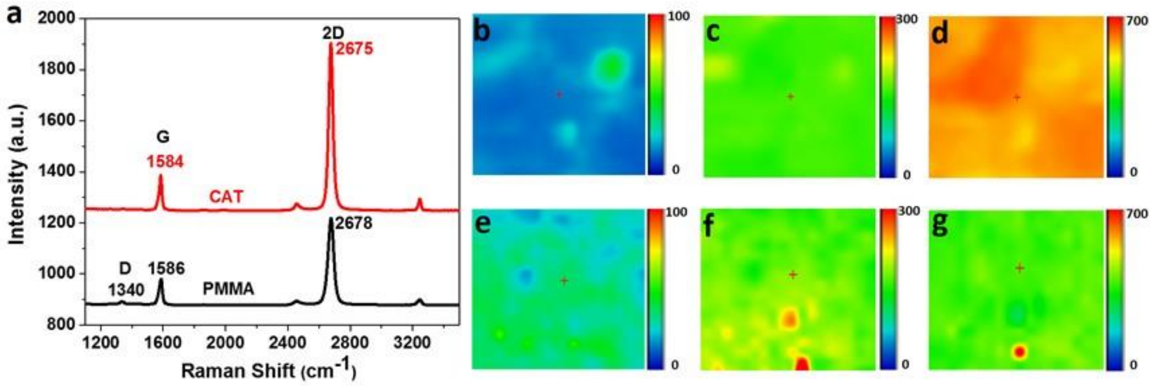

Figure 2.6 (a) Raman spectra of single layer CVD graphene transferred by the CAT and PMMA methods. (b-d) Raman intensity maps of D-, G- and 2D peaks, respectively, for CAT-graphene on a SiO_2/Si substrate. (e-g) Raman intensity maps of D-, G- and 2D peaks, respectively, for PMMA-graphene on a SiO_2/Si substrate. Reprinted with permission from ref.40 (Copyright © 2016 Elsevier Ltd.).

G and 2D peaks are well pronounced in both samples, but the 2D to G peak ratio is approximately 2 times higher for the CAT graphene film confirming its higher quality as compared to the conventional wet transfer method. Moreover, the slight blue shift of the position of G peak and 2D peak of PMMA-graphene compared to CAT-graphene indicates that p type dopants were introduced,[51, 52] most likely due to PMMA residues.[53] In addition to the evaluation of the individual spectra (Figure 2.6a) we conducted a statistical comparison of the quality of the graphene films by collecting Raman maps of 20 µm x 18 µm areas. The D, G and 2D peak maps are shown in Figure 2.6b-2.6d for the CAT-graphene and Figure 2.6e-2.6g for the PMMA transferred graphene, respectively. Comparison of the D-maps (Figure 2.6b and 2.6e) shows that most of the area in the case of CAT-graphene is defect free and less than 10% of the area displays a relatively small D peak, which confirms that the CAT method yields graphene with significantly lower defect density as compared to the conventional wet transfer method. Figure 2.6c and 2.6f show similar amplitudes of the G peak across both graphene samples, while the average amplitude of 2D peak in CAT-graphene sample is about 2 times higher than that in PMMA-graphene, which indicates that the CAT method preserves the quality of single layer CVD graphene. Overall, Raman spectroscopy shows that the CAT-graphene is almost defect free (Figure 2.6b), displaying a relatively uniform large intensity 2D peak (Figure 2.6d), while the PMMA-transferred graphene displays a prominent D peak throughout the mapped surface (Figure 2.6e) accompanied with a lower intensity 2D peak (Figure 2.6g).

Atomic force microscopy (AFM) was employed to characterize the surface cleanliness and morphology of the graphene transferred by both methods. As shown in Figure 2.7a, graphene transferred by the CAT method shows a very clean and relatively uniform surface with an average roughness (Ra) of 0.4 nm. The AFM images revealed the presence of wrinkles with an average height of ~ 1 nm (Figure 2.7b). The majority of the wrinkles presumably originate from the growth process of CVD graphene (formed during the cool down step).[19] Some wrinkles may be introduced during the transfer process by mechanical manipulation or thermal expansion due to temperature change. We note that even scotch tape exfoliated graphene may have wrinkles. [54] In contrast, the surface of the PMMA-assisted graphene is covered with a polymer residue (Figure 2.7d) with a typical height of the impurities being > 5 nm and an average roughness of 1 nm, 2.5 times higher than in CAT-graphene (Figure 2.7e). The cleanness of the CAT-graphene is further confirmed by XPS spectroscopy. Figure 2.7g,h displays typical C1s core spectra of graphene samples transferred by the CAT and PMMA methods. The CAT-graphene gives rise to a narrow C1s peak with a major contribution from sp^2 hybridized C atoms (284.4 eV) and a shoulder at 285.3 eV associated with sp^3 carbon presumably due to edges and defects.[28] The C1s spectrum of the PMMA transferred graphene is broad and it can be deconvoluted to five peaks. In addition to the sp^2 hybridized (284.4 eV) and sp^3 hybridized (285.1 eV) carbon peaks, there is a significant contribution from C-O species associated with the PMMA residue (C-O at 286.5 eV, C=O at 287.5 eV and C-C=O at 289 eV).[28]

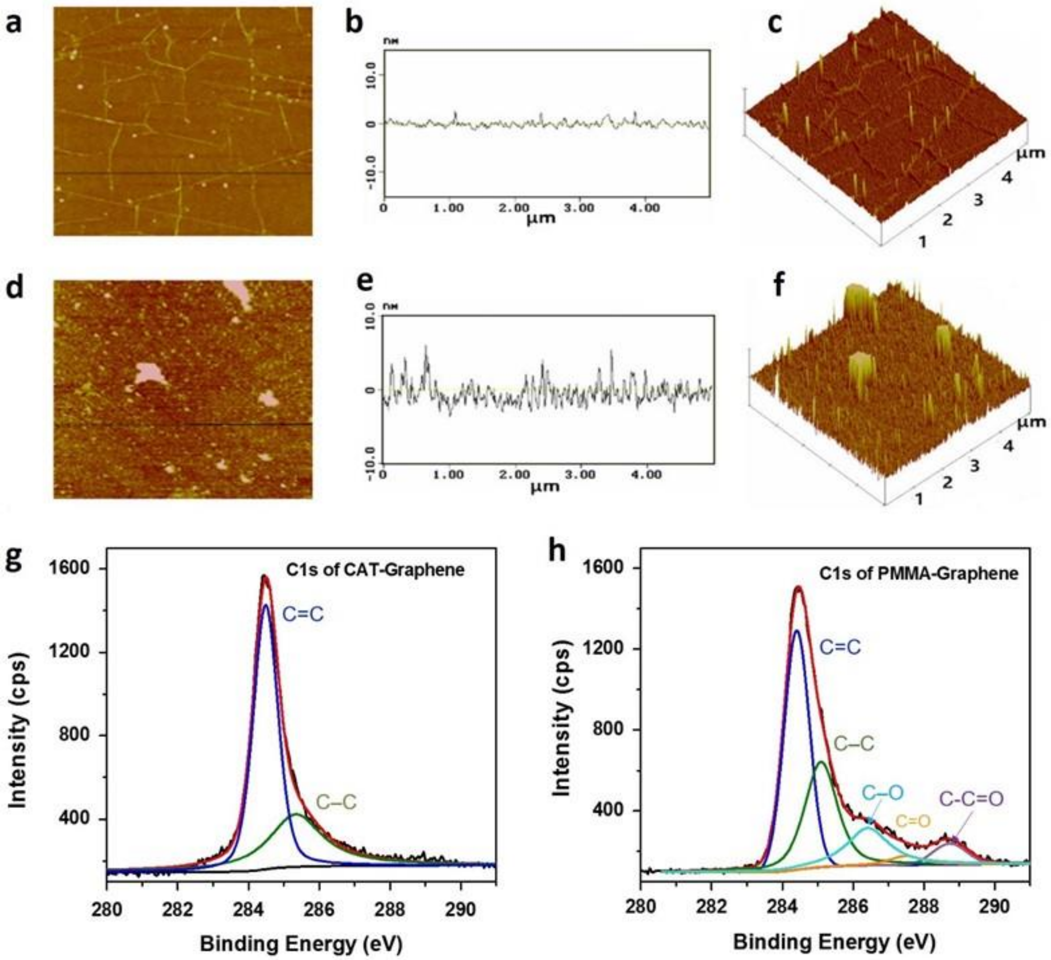

Figure 2.7 AFM images (amplitude, height profile and 3D-morphology) of single layer CVD graphene on 300 nm SiO_2/Si transferred by a-c) CAT method d-f) PMMA method. C1s core spectra of single layer graphene transferred by g) CAT and h) PMMA method. The peak fits consist of Lorentzian and Gaussian distributions. Reprinted with permission from ref.40 (Copyright © 2016 Elsevier Ltd.).

In order to compare the electronic transport properties of the CVD graphene prepared by CAT and PMMA transfer, graphene-based back gated field effect transistors (FETs) were fabricated on 300 nm SiO_2/Si substrates with pre-patterned Cr/Au electrodes. Relatively large dimensions of graphene devices with a channel length of 0.25 mm and channel width of 1 mm were fabricated in order to avoid contamination with resist residues during the photolithography or the e-beam lithography processes. After the transfer, the devices were annealed for 2 hours at 200 ℃ in vacuum prior to measurements. Figure 2.8a shows the transport characteristics of the corresponding FET devices. The FET fabricated with the CAT-graphene shows sharper and more symmetric transport characteristics in comparison with the PMMA-transferred graphene device. The hole and electron mobilities extracted from the linear range for CAT transferred graphene are 1695 $cm^2V^{-1}s^{-1}$ and 1675 $cm^2V^{-1}s^{-1}$, respectively, significantly higher than those obtained for the PMMA transferred graphene (450 $cm^2V^{-1}s^{-1}$ for holes and 380 $cm^2V^{-1}s^{-1}$ for electrons).

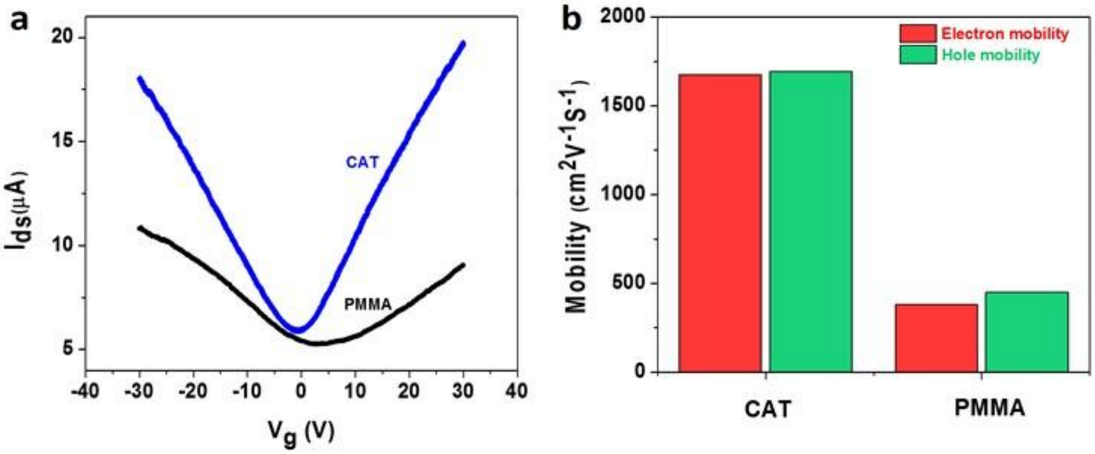

Figure 2.8. FET characterization of graphene transferred onto 300 nm SiO_2/Si substrates. (a) Drain-source current vs gate voltage of the FET devices. (b) Comparison of the mobilities of the large size CAT-graphene and PMMA-graphene. Reprinted with permission from ref.40 (Copyright © 2016 Elsevier Ltd.).

The larger difference between the hole and electron mobilities for the PMMA transferred graphene device indicates an asymmetry of scattering for the two types of carriers, which may be caused by the residual contaminants (Fe^{3+} and PMMA). In principle, higher mobility values were reported in literature for some CVD graphene samples,[19,55] but those reports typically utilize graphene channels of microscopic (<10 μm) dimensions, while the current study was conducted with millimeter scale devices in which high mobility is much more difficult to achieve.

Nevertheless, compared with the PMMA transferred method, cellulose assisted transfer introduces much fewer residues, and magnetic impurities, which helps to largely conserve the transport properties of the original CVD graphene and thus obtain higher mobility devices.

2.3 Sublimation-assisted graphene transfer method

In this section we discuss a method for transfer of ultraclean graphene based on the small polycyclic hydrocarbon naphthalene in place of much larger polymers. In section 2.3, we discussed a graphene transfer method based on cellulose acetate, which produces ultraclean graphene, however, it cannot be applied to plastic substrates because the processes involve organic solvents. By replacing the large polymers with a small molecule, such as naphthalene, we were able to accomplish the graphene transfer without the necessity of washing with organic solvents.

An ideal carrier would satisfy three conditions: (1) easy to apply onto the Cu/Ni-graphene substrate (2) has strong adhesion to graphene (3) easy to remove under mild conditions once the graphene has been placed on the target substrate. Generally, polymer materials satisfy the first two conditions, but condition 3 remains a challenge.

We demonstrate that the naphthalene-assisted transfer (NAT) of graphene is a simple and facile technique, which produces high quality clean graphene that can be transferred onto arbitrary substrates. The naphthalene is easy to remove by sublimation and it does not affect the electronic properties of graphene, making this technique suitable for preparation of electronic devices. The transferred graphene is characterized with Raman spectroscopy, atomic force microscopy (AFM) and scanning electron microscopy (SEM). The transfered graphene was also used for the fabrication of field effect transistors with carrier mobilities above 700 $cm^2V^{-1}s^{-1}$ at 300 K.

2.3.1 Experimental Section

Naphthalene Assisted Transfer of Graphene

CVD graphene grown on copper foil was purchased from Nanjing Mknano Tech. Because CVD growth produces graphene on both sides of the copper foil, one side of as-grown monolayer CVD graphene was first removed by oxygen plasma (Oxford Plasmalab 100/180 model; forward power 30 W; ICP power 300 W, etch time 30 s). Naphthalene crystals (Sigma Aldrich) were placed into a small beaker and melted on a preheated hotplate at 100 °C. The melted liquid naphthalene was drop cast onto the surface of graphene on copper, followed by immediate pressing with a glass slide to squeeze out extra naphthalene and leave a thin film on top of the graphene. To prevent adhesion of the naphthalene to the glass surface, the slide was covered with a Kapton tape (McMaster, model #7361811). The pressing slide is then removed after the naphthalene has cooled (5-10 seconds). To remove the copper, an aqueous solution of H_2O_2 and HCl was prepared by mixing equal volumes of 2 M HCl and 1 M H_2O_2; the solution etched away the Cu substrate (25 μm) underneath the CVD graphene within 10 minutes. The graphene sample supported by the naphthalene film was thoroughly cleaned by replacing the etching solution with distilled water multiple times. The graphene was then lifted with the target substrate, placed in a vacuum oven and kept at 60 °C for 1 hour to sublime the naphthalene supporting layer. The graphene can be further cleaned by immersing it into hot (60 °C) ethanol for 15 minutes to remove any remaining adsorbed naphthalene molecules on the surface of graphene; this step however is not required for successful transfer of clean graphene.

Thermogravimetic analysis (TGA)

The TGA measurements were performed at a heating rate of 1 °C/min in air with a Pyris 1 thermo-gravimetric analyzer (Perkin Elmer).

Raman Spectroscopy and Mapping

Raman spectra and mapping were recorded with a Nicolet Almega XR Dispersive Raman microscope using 532 nm laser excitation and 25% power source. The laser spot size is around 1 µm with a 50x objective lens. The Raman mapping area for all samples is 10 µm x 10 µm, with a step size of 1 µm in both *x* and *y* directions.

Atomic Force Microscopy (AFM)

AFM images of graphene films transferred on SiO_2/Si substrate were collected in a tapping mode with Digital Instruments Nanoscope IIIA. High resolution silicon AFM Probes NSG01 (cantilever length 125 um, cantilever width 30 um, cantilever thickness 1.5-2.5 um, resonant frequency 87-230 kHz, force constant 1.45-15.1N/m, NT-MDT Spectrum Instruments NT-MDT Spectrum Instruments) were used.

Scanning Electron Microscopy (SEM)

SEM images were collected with a Leo XB1540 Focused Ion Beam Milling system in the cleanroom of the University of California, Riverside.

Fabrication of Field Effect Transistors (FETs)

For the fabrication of field effect transistors, the drain and source electrodes (10 nm Cr/100 nm Au) were evaporated by e-beam (Temescal BJD 1800) onto 300 nm SiO_2/Si substrates following photolithography processes. Next the as-grown monolayer CVD graphene was transferred onto the pre-patterned substrates. The channel dimensions of the FET graphene device are 6 μm (length) and 2 μm (width). The devices were thermally annealed at 200 ℃ in vacuum (5×10^{-7} torr) prior to measurements to remove atmospheric dopants and bring the Dirac point in the vicinity of 0 V.

2.3.2 Results and Discussion

In this work we replace high molecular weight polymers with the small molecule naphthalene as the holding layer in graphene transfer. Naphthalene is the smallest polycyclic aromatic hydrocarbon (PAH) and it is essentially a dimer of benzene.[56] Much like graphene, naphthalene shares the same building block - the benzenoid aromatic ring (Figure 2.9), and this structural similarity has stimulated theoretical and experimental interest in the adsorption of naphthalene on pristine graphene.

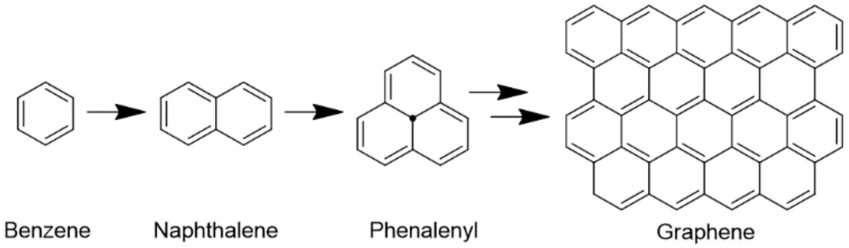

Figure 2.9. Schematic illustration of the structural similarity between naphthalene and graphene: from left to right benzene (monomer), naphthalene (dimer), phenalenyl (trimer) and graphene (polymer). Reprinted with permission from ref.43 (Copyright © 2017 IOP Publishing Ltd).

Calculations have predicted a strong adsorption of the small PAH molecule on the honeycomb lattice of graphene due to $\pi-\pi$ interactions with a binding energy of 763 meV,[57] which is comparable to the experimental values obtained for graphite.[58] The adsorbed naphthalene molecule adapts an approximately planar geometry with a preferential AB stacking configuration [59] making this small PAH a good candidate for a graphene supporting layer during transfer. Furthermore, band structure calculations suggest that the adsorbed naphthalene molecule does not induce a charge transfer preserving the electronic structure of graphene,[59] which is important for applications in electronics and optoelectronics. Other attractive features of naphthalene as a supporting layer are its good casting properties and sublimation at room temperature under atmospheric pressure. [60] In fact, naphthalene is most known as being used in moth balls as it repels unwanted pests upon sublimation. Naphthalene is soluble in most organic solvents and it can be easily spin-coated on top of graphene. Most transfer technique utilize spin-coating for the formation of a carrier layer and in our first Experiments we spin-coated an ethanol solution of naphthalene on top of the CVD graphene. However, we also found that the process can be further simplified by coating the graphene films with molten naphthalene, because this small PAH melts at relatively low temperature (melting point 80 ^{o}C). This step allows the formation of a supporting film without the use of any solvent. Figure 2.10 illustrates pictures of naphthalene in crystalline and melted form, and a TGA graph showing the weight loss of the material at low temperature (from room temperature to 100 ^{o}C).

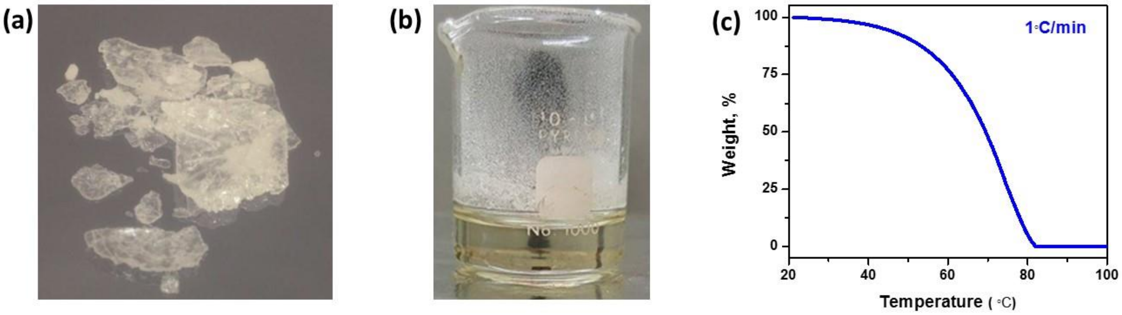

Figure 2.10 Crystalline (a) and melted (b) naphthalene. (c) Thermogravimetric analysis of naphthalene crystals in air at a heating rate of 1 ^{o}C/min; the weight is normalized to the initial material weight. Reprinted with permission from ref.43 (Copyright © 2017 IOP Publishing Ltd).

In a typical experiment the naphthalene is melted in a beaker and drop cast onto the surface of the CVD-grown graphene, then pressed with a glass slide to ensure good continuous contact. Once the naphthalene cools into a wax-like solid, the substrate is placed into the water-based etching solution until the copper foil, supporting the graphene, is dissolved. The naphthalene film provides a good mechanical support for the graphene through this step because of the naphthalene's low solubility in water, due to its nonpolar character. In the next step, the naphthalene-supported graphene is placed onto the target substrate and it is sublimed in air (or vacuum) leaving a clean graphene film. The transfer process is schematically illustrated in Figure 2.11.

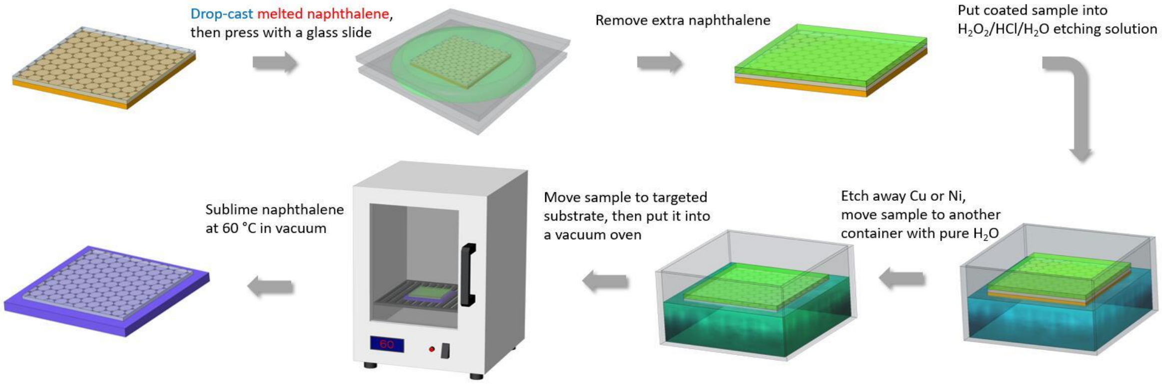

Figure 2.11. Schematic illustration of the naphthalene assisted transfer of graphene. Reprinted with permission from ref.43 (Copyright © 2017 IOP Publishing Ltd).

The cleanliness of the transferred graphene was evaluated by AFM and SEM and representative images of the transferred graphene are shown in Figure 2.12. Both characterization techniques reveal a very clean graphene surface which is associated with the clean removal of the supporting naphthalene layer by sublimation. This is an important advantage of the sublimation-assisted transfer method over the conventional polymer-assisted transfer techniques, which require tedious cleaning steps to remove the polymer and obtaining residue-free graphene remains problematic.

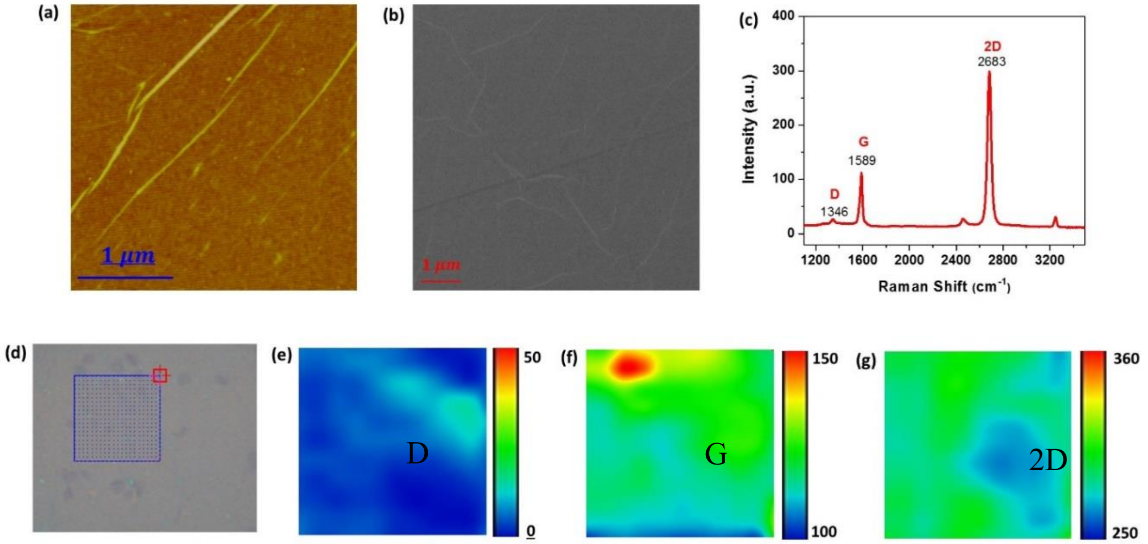

Figure 2.12. Characterization of the transferred graphene. (a) AFM and (b) SEM images after transfer of graphene on SiO_2/Si substrate; (c) Raman spectrum of a single layer CVD graphene transferred by NAT method. (d-f) Raman intensity maps of 10 μm x 10 μm areas of D, G, and 2D peaks, respectively. Reprinted with permission from ref.43 (Copyright © 2017 IOP Publishing Ltd).

The solvent free and low temperature removal of the supporting layer makes the naphthalene-assisted graphene transfer technique suitable for transfer on virtually any substrate, especially flexible plastic films that are widely used as substrates for transparent electrodes or flexible electronics. The transferred graphene was further characterized with Raman spectroscopy. This analytical technique is routinely used for evaluation of graphene quality.[49 61] The characterization typically involves analysis of several distinct peaks: the G peak corresponding to the high-frequency E2g phonon at the Brillouin zone center, the D peak related to the breathing modes of the six-atom rings which becomes Raman active in the presence of defects, and the 2D peak (overtone of D-peak) that appears as a single sharp peak with much higher intensity than the G peak and does not require defects for activation. Doping of graphene is known to shift the position of G and 2D peaks and to significantly decrease the ratio of 2D to G peak intensities. [61] Typical Raman spectrum and Raman maps of the D, G and 2D peaks are shown in Figure 2.12 (e-g). The Raman spectra showed a small or no D peak, which confirms the good quality of the transferred graphene film. The G peak was observed at 1589 cm^{-1}, indicating absence of doping. Because charge transfer or doping changes the Fermi level of graphene, doping results in shift of the G band position and it has been reported to upshift the peak for both electron and hole doping.[51] The fact that naphthalene preserves the pristine state of graphene is also manifested in the strong 2D peak at 2683 cm^{-1} observed in the Raman maps of 10 µm x 10 µm areas (Figure 2.12f). It is known that both the intensity and the position of the 2D peak are downshift for high electron doping. [52] [62]

To determine the electronic properties of the NAT graphene, field effect transistors were fabricated and tested. The optical image of a typical NAT-graphene FET device with dimensions of 6 µm (length) and 2 µm (width) is shown in Figure 2.13a.

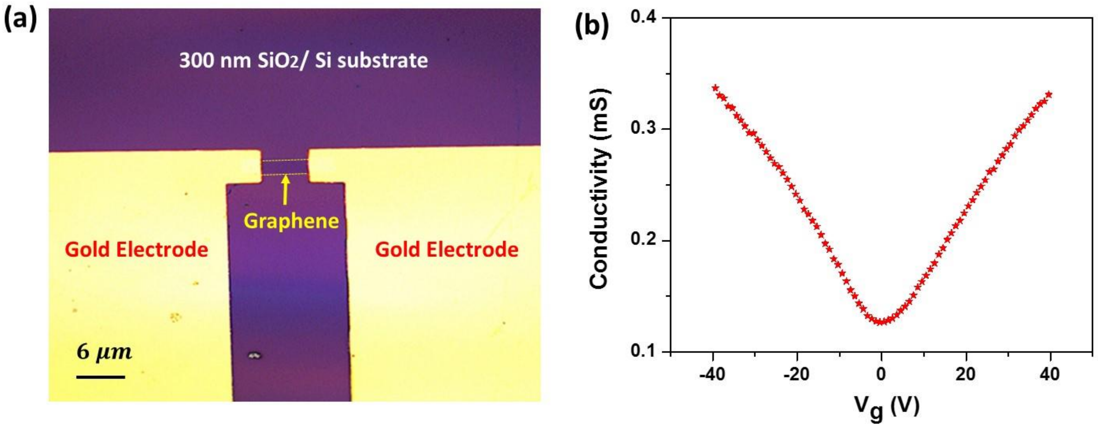

Figure 2.13. Electrical properties of a NAT-graphene FET on 300 nm SiO2/Si. (a) Optical image of a typical FET graphene device. (b) Conductivity versus gate voltage recorded at drain-source voltage of 0.01 Volt. Reprinted with permission from ref.43 (Copyright © 2017 IOP Publishing Ltd).

Figure 2.13b illustrates the corresponding conductivity versus gate voltage after thermal annealing. Figure 2.13 shows a representative I (Vg) curve of a graphene FET device. The curve shows symmetric transport characteristics with the Dirac point at 0V. The extracted values of hole and electron mobilities are in the range of 700 $cm^2V^{-1}s^{-1}$ with an on-off ratio of 2.3 at 30 Volt.

In summary, we have developed a new single molecule-based transfer method for graphene. This new method is simple and avoids the use of difficult to remove polymers. By replacing high molecular weight polymers with low molecular weight small molecules, high quality graphene films can be easily obtained. The ability of naphthalene to sublime at room temperature is one of the most attractive features for transfer of graphene on substrates that have chemical incompatibility with organic solvents or thermal restrictions. The availability of clean graphene films will facilitate the progress in understanding the formation of organometallic interconnects in extended pi-conjugated carbon systems. [8,7,63]

2.4 Conclusions

Because graphene is one atom thick material, its electronic properties are sensitive to interference from contaminations. Furthermore, chemists and chemical engineers, need access to ultraclean graphene in order to study the chemical reactivity of the material and develop advanced structures and devices. However, PMMA residues are notoriously hard to remove as in conventional PMMA wet transfer method, which restricts the applications of CVD graphene in chemistry and chemical engineering. In section 2.3, we reported a superior cellulose assisted (CAT) graphene transfer method, which gives much cleaner transferred graphene films, improves the efficiency of the transfer processes and reduces the cost dramatically.

Although the CAT method exhibits numerous advantages compared to conventional transfer methods, it is still difficult to apply to plastic thin film (such as PET) substrates for the fabrication of graphene based flexible electronics. Therefore, a graphene transfer that utilizes mild conditions for removal of the supporting layer is developed as described in section 2.4. The naphthalene assisted graphene transfer technique provides a reliable route to residue-free transfer of large area graphene to both hard and flexible substrates. The ability of naphthalene to sublime at room temperature is one of the most attractive features for transfer of graphene on substrates that have chemical incompatibility with organic solvents or have thermal restrictions. The NAT method can broaden the application of CVD graphene in flexible electronics, spintronics, and fields where ultraclean graphene and mild graphene transfer conditions are required.

The main advantages of the CAT and NAT methods in comparison with other graphene transfer techniques are summarized in Table 2.1.

Table 2.1 Comparison of several parameters of different graphene transfer methods.

Graphene Transfer Method	Approximate time for one transfer	Cost	On/ Off ratio on SiO_2/Si substrate (30V)	Magnetic contamination	Comments	Reference
Conventional wet transfer (PMMA/Fe^{3+})	1~2 days	High	2.2	Yes	Light sensitive, many residues /contamination	[27]
CLT transfer (Static charge/Fe^{3+})	2 hours	High	2.4	Yes	High voltage	[21]
Polymer free transfer (IPA/$(NH_4)_2S_2O_8$)	4 hours	Medium	N/A	No	Low yield	[44]
CAT transfer (Cellulose/H_2O_2/HCl)	1 hour	Low	3.5	No	Few residues	[40]
NAT transfer (Naphthalene/H_2O_2/HCl)	1 hour	Low	2.2	No	Ultraclean, mild transfer condition	[43]

In summary, just as no solvent can dissolve universally all substances, there is no unique graphene transfer method that can fulfill all purposes. The future development of graphene transfer methods need to move towards low cost, ultraclean graphene surface, scalability, and simplification until ultimately CVD graphene can be grown on various insulating substrates that will eliminate the need for transfer.

References

1. Wallace, P. R., The Band Theory of Graphite. *Phys. Rev.* **1947,** 71, 622-634.

2. Novoselov, K. S.; Geim, A. K.; Morozov, S. V.; Jiang, D.; Zhang, Y.; Dubonos, S. V.; Grigorieva, I. V.; Firsov, A. A., Electric Field Effect in Atomically Thin Carbon Films. *Science* **2004,** 306, 666-669.

3. Berger, C.; Song, Z.; Li, T.; Li, X.; Ogbazghi, A. Y.; Feng, R.; Dai, Z.; Marchenkov, A. N.; Conrad, E. H.; First, P. N.; de Heer, W. A., Ultrathin Epitaxial Graphite: 2d Electron Gas Properties and a Route toward Graphene-Based Nanoelectronics. *J. Phys. Chem. B* **2004,** 108, 19912-19916.

4. Chen, Z. H.; Lin, Y. M.; Rooks, M. J.; Avouris, P., Graphene Nano-Ribbon Electronics. *Physica E* **2007,** 40, 228-232.

5. Liu, C.-H.; Chang, Y.-C.; Norris, T. E.; Zhong, Z., Graphene Photodetectors with Ultra-Broadband and High Responsivity at Room Temperature. *Nature Nanotech.* **2014,** 9, 273-278.

6. Torrisi, F.; Hasan, T.; Wu, W. P.; Sun, Z. P.; Lombardo, A.; Kulmala, T. S.; Hsieh, G. W.; Jung, S. J.; Bonaccorso, F.; Paul, P. J.; Chu, D. P.; Ferrari, A. C., Inkjet-Printed Graphene Electronics. *ACS Nano* **2012,** 6, 2992-3006.

7. Bekyarova, E.; Niyogi, S.; Sarkar, S.; Tian, X.; Chen, M.; Moser, M. L.; Ayub, K.; Mitchell, R. H.; Haddon, R. C., Stereochemical Effect of Covalent Chemistry on the Electronic Structure and Properties of the Carbon Allotropes and Graphene Surfaces. *Synth. Met.* **2015,** 210, 80-84.

8. Chen, M.; Tian, X.; Li, W.; Bekyarova, E.; Li, G.; Moser, M.; Haddon, R. C., Application of Organometallic Chemistry to the Electrical Interconnection of Graphene Nanoplatelets. *Chem. Mater.* **2016,** 28, 2260-2266.

9. Nair, R. R.; Sepioni, M.; Tsai, I.-L.; Lehtinen, P. O.; Keinonen, J.; Krasheninnikov, A. V.; Thomson, T.; Geim, A. K.; Grigorieva, I. V., Spin-Half Paramagnetism in Graphene Induced by Point Defects. *Nature Phys.* **2012,** 8, 199-202.

10. Li, Y.; Yuan, H.; von dem Bussche, A.; Creighton, M.; Hurt, R. H.; Kane, A. B.; Gao, H., Graphene Microsheets Enter Cells through Spontaneous Membrane Penetration at Edge Asperities and Corner Sites. *Proc. Natl. Acad. Sci. U.S.A.* **2013,** 110, 12295-12300.

11. Guo, F.; Silverberg, G.; Bowers, S.; Kim, S.; Datta, D.; Shenoy, V.; Hurt, R. H., Graphene-Based Environmental Barriers. *Environ. Sci. Technol.* **2012,** 46, 7717-7724.

12. Areshkin, D. A.; White, C. T., Building Blocks for Integrated Graphene Circuits. *Nano Lett.* **2007,** 7, 3253-3259.

13. Lin, Y.; Valdes-Garcia, A.; Han, S.; Farmer, D. B.; Meric, I.; Sun, Y.; Wu, Y.; Dimitrakopoulos, C.; Grill, A.; Avouris, P., Wafer-Scale Graphene Integrated Circuit. *Science* **2011,** 332, 1294-1297.

14. El-Kady, M. F.; Strong, V.; Dubin, S.; Kaner, R. B., Laser Scribing of High-Performance and Flexible Graphene-Based Electrochemical Capacitors. *Science* **2012,** 335, 1326-1330.

15. Bae, S.; Kim, H.; Lee, Y.; Xu, X. F.; Park, J. S.; Zheng, Y.; Balakrishnan, J.; Lei, T.; Kim, H. R.; Song, Y. I.; Kim, Y. J.; Kim, K. S.; Ozyilmaz, B.; Ahn, J. H.; Hong, B. H.; Iijima, S., Roll-to-Roll Production of 30-Inch Graphene Films for Transparent Electrodes. *Nat. Nanotech.* **2010,** 5, 574-578.

16. Wang, Y.; Shi, Z. Q.; Huang, Y.; Ma, Y. F.; Wang, C. Y.; Chen, M. M.; Chen, Y. S., Supercapacitor Devices Based on Graphene Materials. *J. Phys. Chem. C* **2009,** 113, 13103-13107.

17. Huang, Y.; Liang, J. J.; Chen, Y. S., An Overview of the Applications of Graphene-Based Materials in Supercapacitors. *Small* **2012,** 8, 1805-1834.

18. Zhang, T.; Chang, H.; Wu, Y.; Xiao, P.; Yi, N.; Lu, Y.; Ma, Y.; Huang, Y.; Zhao, K.; Yan, X., Macroscopic and Direct Light Propulsion of Bulk Graphene Material. *Nat. Photonics* **2015,** 9, 471-476.

19. Li, X. S.; Cai, W. W.; An, J. H.; Kim, S.; Nah, J.; Yang, D. X.; Piner, R.; Velamakanni, A.; Jung, I.; Tutuc, E.; Banerjee, S. K.; Colombo, L.; Ruoff, R. S., Large-Area Synthesis of High-Quality and Uniform Graphene Films on Copper Foils. *Science* **2009,** 324, 1312-1314.

20. Liang, X.; Sperling, B. A.; Calizo, I.; Cheng, G.; Hacker, C. A.; Zhang, Q.; Obeng, Y.; Yan, K.; Peng, H. L.; Li, Q.; Zhu, X.; Yuan, H.; Walker, A. R. H.; Liu, Z.; Peng, L.; Richter, C., Toward Clean and Crackless Transfer of Graphene. *ACS Nano* **2011,** 5, 9144-9153.

21. Wang, D.; Huang, I.; Ho, P.; Li, S.; Yeh, Y.; Wang, D.; Chen, W.; Lee, Y.; Chang, Y.; Chen, C.; Liang, C.; Chen, C., Clean-Lifting Transfer of Large-Area Residual-Free Graphene Films. *Adv. Mater.* **2013,** 25, 4521-4526.

22. Kobayashi, T.; Bando, M.; Kimura, N.; Shimizu, K.; Kadono, K.; Umezu, N.; Miyahara, K.; Hayazaki, S.; Nagai, S.; Mizuguchi, Y., Production of a 100-M-Long High-Quality Graphene Transparent Conductive Film by Roll-to-Roll Chemical Vapor Deposition and Transfer Process. *Appl. Phys. Lett.* **2013,** 102, 023112.

23. Yan, Z.; Lin, J.; Peng, Z.; Sun, Z.; Zhu, Y.; Li, L.; Xiang, C.; Samuel, E. L.; Kittrell, C.; Tour, J. M., Toward the Synthesis of Wafer-Scale Single-Crystal Graphene on Copper Foils. *ACS Nano* **2012,** 6, 9110-9117.

24. Zhou, H.; Yu, W. J.; Liu, L.; Cheng, R.; Chen, Y.; Huang, X.; Liu, Y.; Wang, Y.; Huang, Y.; Duan, X., Chemical Vapour Deposition Growth of Large Single Crystals of Monolayer and Bilayer Graphene. *Nat. Commun.* **2013,** 4.

25. Hao, Y.; Bharathi, M. S.; Wang, L.; Liu, Y.; Chen, H.; Nie, S.; Wang, X.; Chou, H.; Tan, C.; Fallahazad, B., The Role of Surface Oxygen in the Growth of Large Single-Crystal Graphene on Copper. *Science* **2013,** 342, 720-723.

26. Wang, S.; Hibino, H.; Suzuki, S.; Yamamoto, H., Atmospheric Pressure Chemical Vapor Deposition Growth of Millimeter-Scale Single-Crystalline Graphene on the Copper Surface with a Native Oxide Layer. *Chem. Mater.* **2016,** 28, 4893-4900.

27. Li, X. S.; Zhu, Y. W.; Cai, W. W.; Borysiak, M.; Han, B. Y.; Chen, D.; Piner, R. D.; Colombo, L.; Ruoff, R. S., Transfer of Large-Area Graphene Films for High-Performance Transparent Conductive Electrodes. *Nano Lett.* **2009,** 9, 4359-4363.

28. Lin, Y.; Lu, C.; Yeh, C.; Jin, C.; Suenaga, K.; Chiu, P., Graphene Annealing: How Clean Can It Be? *Nano Lett.* **2011,** 12, 414-419.

29. Park, H.; Brown, P. R.; Bulovic, V.; Kong, J., Graphene as Transparent Conducting Electrodes in Organic Photovoltaics: Studies in Graphene Morphology, Hole Transporting Layers, and Counter Electrodes. *Nano Lett.* **2012,** 12, 133-140.

30. Ambrosi, A.; Pumera, M., The Cvd Graphene Transfer Procedure Introduces Metallic Impurities Which Alter the Graphene Electrochemical Properties. *Nanoscale* **2014,** 6, 472-476.

31. Xia, Y.; Whitesides, G. M., Soft Lithography. *Annu. Rev. Mater. Sci.* **1998,** 28, 153-184.

32. Ko, S. H.; Park, I.; Pan, H.; Grigoropoulos, C. P.; Pisano, A. P.; Luscombe, C. K.; Frechet, J. M. J., Direct Nanoimprinting of Metal Nanoparticles for Nanoscale Electronics Fabrication. *Nano Lett.* **2007,** 7, 1869-1877.

33. Kim, K. S.; Zhao, Y.; Jang, H.; Lee, S. Y.; Kim, J. M.; Kim, K. S.; Ahn, J. H.; Kim, P.; Choi, J. Y.; Hong, B. H., Large-Scale Pattern Growth of Graphene Films for Stretchable Transparent Electrodes. *Nature* **2009,** 457, 706-710.

34. Song, J.; Kam, F.; Png, R.; Seah, W.; Zhuo, J.; Lim, G.; Ho, P. K. H.; Chua, L., A General Method for Transferring Graphene onto Soft Surfaces. *Nat. Nanotechnol.* **2013,** 8, 356-362.

35. Suk, J. W.; Kitt, A.; Magnuson, C. W.; Hao, Y.; Ahmed, S.; An, J.; Swan, A. K.; Goldberg, B. B.; Ruoff, R. S., Transfer of Cvd-Grown Monolayer Graphene onto Arbitrary Substrates. *ACS Nano* **2011,** 5, 6916-6924.

36. Kang, J.; Hwang, S.; Kim, J. H.; Kim, M. H.; Ryu, J.; Seo, S. J.; Hong, B. H.; Kim, M. K.; Choi, J. B., Efficient Transfer of Large-Area Graphene Films onto Rigid Substrates by Hot Pressing. *ACS nano* **2012,** 6, 5360-5365.

37. Ahn, S. H.; Guo, L. J., High-Speed Roll-to-Roll Nanoimprint Lithography on Flexible Plastic Substrates. *Adv. Mater.* **2008,** 20, 2044-2049.

38. Søndergaard, R. R.; Hösel, M.; Krebs, F. C., Roll-to-Roll Fabrication of Large Area Functional Organic Materials. *J. Polym. Sci. Part B Polym. Phys.* **2012,** 51, 16-34.

39. Kim, H. H.; Lee, S. K.; Lee, S. G.; Lee, E.; Cho, K., Wetting-Assisted Crack- and Wrinkle-Free Transfer of Wafer-Scale Graphene onto Arbitrary Substrates over a Wide Range of Surface Energies. *Adv. Funct. Mater.* **2016**.

40. Chen, M.; Li, G.; Li, W.; Stekovic, D.; Arkook, B.; Itkis, M. E.; Pekker, A.; Bekyarova, E.; Haddon, R. C., Large-Scale Cellulose-Assisted Transfer of Graphene toward Industrial Applications. *Carbon* **2016,** 110, 286-291.

41. Matruglio, A.; Nappini, S.; Naumenko, D.; Magnano, E.; Bondino, F.; Lazzarino, M.; Dal Zilio, S., Contamination-Free Suspended Graphene Structures by a Ti-Based Transfer Method. *Carbon* **2016,** 103, 305-310.

42. Lee, J.; Kim, Y.; Shin, H.; Lee, C.; Lee, D.; Moon, C.; Lim, J.; Chan Jun, S., Clean Transfer of Graphene and Its Effect on Contact Resistance. *Appl. Phys. Lett.* **2013,** 103, 103104.

43. Chen, M.; Stekovic, D.; Li, W.; Arkook, B.; Haddon, R.; Bekyarova, E., Sublimation-Assisted Graphene Transfer Technique Based on Small Polyaromatic Hydrocarbons. *Nanotechnology* **2017**.

44. Lin, W. H.; Chen, T. H.; Chang, J. K.; Taur, J. I.; Lo, Y. Y.; Lee, W. L.; Chang, C. S.; Su, W. B.; Wu, C. I., A Direct and Polymer-Free Method for Transferring Graphene Grown by Chemical Vapor Deposition to Any Substrate. *ACS Nano* **2014,** 8, 1784-1791.

45. Machell, J. S.; Sand, I. D. Light Sensitive Silver Halide Element with Cellulose Ester Film Base. US5288715 A, 1994.

46. Von, B. R. A. Magnetic Recording Tape and Method of Making Same. US 2711901 A, 1955.

47. Chen, J. C.; Soden, K. J. Anti-Adhesion Cellulose Acetate Wound Dressing. US 6500539 B1, 2002.

48. Dresselhaus, M. S.; Jorio, A.; Hofmann, M.; Dresselhaus, G.; Saito, R., Perspectives on Carbon Nanotubes and Graphene Raman Spectroscopy. *Nano Lett.* **2010,** 10, 751-758.

49. Ferrari, A. C.; Basko, D. M., Raman Spectroscopy as a Versatile Tool for Studying the Properties of Graphene. *Nature Nanotech.* **2013,** 8, 235-246.

50. Ferrari, A. C.; Meyer, J. C.; Scardaci, V.; Casiraghi, C.; Lazzeri, M.; Mauri, F.; Piscanec, S.; Jiang, D.; Novoselov, K. S.; Roth, S.; Geim, A. K., Raman Spectrum of Graphene and Graphene Layers. *Phys. Rev. Lett.* **2006,** 97, 187401-4.

51. Pisana, S.; Lazzeri, M.; Casiraghi, C.; Novoselov, K. S.; Geim, A. K.; Ferrari, A. C.; Mauri, F., Breakdown of the Adiabatic Born-Oppenheimer Approximation in Graphene. *Nature Mater.* **2007,** 6, 198-201.

52. Das, A.; Pisana, S.; Chakraborty, B.; Piscanec, S.; Saha, S. K.; Waghmare, U. V.; Novoselov, K. S.; Krishnamurthy, H. R.; Geim, A. K.; Ferrari, A. C.; Sood, A. K., Monitoring Dopants by Raman Scattering in an Electrochemically Top-Gated Graphene Transistor. *Nature Nanotech.* **2008,** 3, 210-215.

53. Pirkle, A.; Chan, J.; Venugopal, A.; Hinojos, D.; Magnuson, C. W.; McDonnell, S.; Colombo, L.; Vogel, E. M.; Ruoff, R. S.; Wallace, R. M., The Effect of Chemical Residues on the Physical and Electrical Properties of Chemical Vapor Deposited Graphene Transferred to Sio2. *Appl. Phys. Lett.* **2011,** 99, 122108.

54. Morozov, S. V.; Novoselov, K. S.; Katsnelson, M. I.; Schedin, F.; Ponomarenko, L. A.; Jiang, D.; Geim, A. K., Strong Suppression of Weak Localization in Graphene. *Phys. Rev. Lett.* **2006,** 97, 016801.

55. Gao, L.; Ni, G. X.; Liu, Y. P.; Liu, B.; Castro Neto, A. H.; Loh, K. P., Face-to-Face Transfer of Wafer-Scale Graphene Films. *Nature* **2014,** 505, 190-194.

56. Abrahams, S. C.; Robertson, J. M.; White, J. G., The Crystal and Molecular Structure of Naphthalene .1. X-Ray Measurements. *Acta Crys.* **1949,** 2, 233-238.

57. Chakarova-Kack, S. D.; Schroder, E.; Lundqvist, B. I.; Langreth, D. C., Application of Van Der Waals Density Functional to an Extended System: Adsorption of Benzene and Naphthalene on Graphite. *Phys. Rev. Lett.* **2006,** 96.

58. Zacharia, R.; Ulbricht, H.; Hertel, T., Interlayer Cohesive Energy of Graphite from Thermal Desorption of Polyaromatic Hydrocarbons. *Phys. Rev. B* **2004,** 69, 155406.

59. AlZahrani, A. Z., First-Principles Study on the Structural and Electronic Properties of Graphene Upon Benzene and Naphthalene Adsorption. *Appl. Surf. Sci.* **2010,** 257, 807-810.

60. Lipsett, F. R., On the Production of Single Crystals of Naphthalene and Anthracene. *Can. J. Phys.* **1957,** 35, 284-298.

61. Ferrari, A. C., Raman Spectroscopy of Graphene and Graphite: Disorder, Electron-Phonon Coupling, Doping and Nonadiabatic Effects. *Solid State Commun.* **2007,** 143, 47-57.

62. Wang, Q. H.; Jin, Z.; Kim, K. K.; Hilmer, A. J.; Paulus, G. L. C.; Shih, C. J.; Ham, M. H.; Sanchez-Yamagishi, J. D.; Watanabe, K.; Taniguchi, T.; Kong, J.; Jarillo-Herrero, P.; Strano, M. S., Understanding and Controlling the Substrate Effect on Graphene Electron-Transfer Chemistry Via Reactivity Imprint Lithography. *Nat. Chem.* **2012,** 4, 724-732.

63. Wang, F.; Itkis, M. E.; Bekyarova, E.; Sarkar, S.; Tian, X.; Haddon, R. C., Solid-State Bis-Hexahapto-Metal Complexation of Single-Walled Carbon Nanotubes. *J. Phys. Org. Chem.* **2012,** 25, 607-610.

Chapter 3. Organometallic Chemistry of Carbon Nanomaterials

Organometallic complexes of carbon materials are potentially useful for interconnecting the graphitic surfaces and therefore increasing the dimensionality of graphene and carbon nanotubes, and this potentially leads to increased electrical conductivity.[1, 2]

When it comes to the interaction between metals and graphitic surfaces, there are three different mechanisms: (a) physisorption, in which the fundamental force is van der Waals interaction; (b) ionic chemisorptions (doping), in which a large amount of charge transfer occurs between the metal and the graphitic surface; the main feature of this interaction is that the carbon band structure is well preserved; and (c) covalent chemisorption, in which the original band structure of the carbon material is largely affected by rehydridization of the carbon atoms from sp^2 to sp^3. We regard (c) as destructive rehybridization because it results in decreased conductivity and reduced carrier mobility. Recently the Haddon research group has demonstrated a fourth mechanism: (d) chemisorption, with the formation of bis-hexahapto bonds between the metal and graphene surface and we refer to this mechanism as constructive rehybridization.

The motivation of this research is to make use of the organometallic chemistry of graphene and aligned single walled carbon nanotubes (SWNTs) to design new materials and pave the way to their commercial applications in advanced electronics and spintronics.

3.1 Organometallic Chemistry of Graphene

3.1.1 Introduction

Graphene has received a great deal of attention in recent years,[3] with anticipated applications in material science[4], biotechnology[5], electronics[6, 7 8, 9] and spintronics.[10] Furthermore the interaction between metals and graphene surfaces has long been a popular topic.[11-16] In fact, bulk materials composed of single-layer graphene (SLG) sheets have been known for many years as exemplified by the stage 1 graphite intercalation compounds (GICs) such as KC_8, similarly the stage 2 GICs contain bilayer graphene and this continues up to at least the stage 4 compounds.[17] The Haddon research group pioneered the organometallic chemistry of the tricoordinate conjugated carbon allotropes.[18-20] Previous work has explored particularly carbon nanotubes and it was shown that the formation of covalent bis(η^6-SWNT)M bonds (where M = metal) is an effective way to interconnect the junctions of the SWNTs in thin films leading to an enhanced electrical conductivity in the case of the some of the first row transition metals (Ti, V, Cr, Mn, Fe),[1] the group 6 metals (Cr, Mo, W),[21] and the lanthanides (La, Nd, Sm, Eu, Gd, Dy, Ho, Yb).[22, 23] It would be expected that the same chemistry could be applied to the insertion of transition metals between pairs of parallel graphene surfaces to generate compounds analogous to the GICs in which the ionic bonds characteristic of the GICs are replaced by covalent bis-hexahapto bonds,[20] and there is strong theoretical evidence for this mode of bonding.[24-28] But the compounds cannot be prepared by the routes usually employed for the synthesis of GICs because of the absence of charge transfer in the transition metal complexes.[2]

In this work, we have pursued the hexahapto-graphene half sandwich compounds by photochemistry (Chapter 3.1.2) and graphene sandwich compounds by both photochemistry and metal vapor synthesis. (Chapter 3.1.3)

3.1.2 Graphene Half Sandwich Complexes

Introduction

The electronic structure of graphene makes this material an ideal substrate for hexahapto complexation reactions; because the valence and conduction bands of graphene touch at the Dirac point, both the degenerate bonding (e_{1g}) and anti-bonding (e_{2u}) benzene π-orbitals are readily available for hybridization with the transition metal d-orbitals. Importantly, this induces structural rehybridization or perturbation of the graphene electronic structure. Recently, a number of high level calculations have been published which confirm the viability of the hexahapto organometallic bond to the benzenoid rings in carbon nanotubes and graphene.[24-28] We have also reported a facile photochemical route for introducing organometallic interconnects to SWNT junctions. Here we investigate the interaction of the group 6 transition metal reagents with the surface of a single layer graphene based on similar methods.

Experimental Section

Preparation of graphene device on glass substrates

As-grown single layer CVD graphene (Graphene Supermarket, USA) was transferred to pre-patterned electrodes by the CAT method as described in Chapter 2.3. Briefly, CVD graphene on copper was spin-coated with cellulose acetate dissolved in acetone, followed by etching the Cu foil in an H_2O_2/HCl etching solution. After transfer the sample (graphene/cellulose acetate film) onto a glass substrate with pre-patterned electrodes, the cellulose acetate was washed away with acetone. The samples were annealed in vacuum at 200 ℃ for 2 hours inside a glass tube and immediately transferred into a glove box for conducting the photochemical reactions.

Fabrication of graphene field effect transistor

We use the methods described in Chapter 2.3.1 for the fabrication of graphene FET devices. Technically, drain and source electrodes (10 nm Cr/100 nm Au) were evaporated by e-beam onto 300 nm SiO_2/Si substrates with a shadow mask. Then as-grown monolayer CVD graphene was transferred onto the pre-patterned substrates by the CAT method, described in Chapter 2.3.1. The channel dimensions of all graphene devices are 0.25 mm (length) x 1 mm (width). No photolithography patterning was employed to exclude the effect of photoresist residues on the electronic properties of the transferred graphene samples. Thermal annealing at 200 ℃ in vacuum (5 x 10^{-7} torr) was performed before the photochemical reaction to remove atmospheric dopants and bring the Dirac point in the vicinity of 0 volts.

Photochemical reaction conditions

Solutions of $Mo(CO)_6$ (Sigma Aldrich 98%) and $W(CO)_6$ (Alfa Aesar 97%) were prepared in degassed acetonitrile inside a glovebox at a concentration of 1×10^{-3} M. A drop (~0.1 mL) of solution was cast onto the graphene samples inside the glovebox, followed by irridation with light sources. We employed the following light sources for different reagents: $Cr(CO)_6$, $Mo(CO)_6$ and $W(CO)_6$ [UVC, 254 nm], $Cr(\eta^6\text{-benzene})(CO)_3$ [UVA, 365 nm], $Cr(\eta^6\text{-benzene})_2$ [room light].

Characterization

The resistance was recorded with a Keithley 236 source measure unit controlled by a Labview program, and FET data was measured with a Keithley 236 source measure (gate voltage) and Keithley 6517A electrometer (drain-source voltage) driven by Labview programs. The resistance was converted to conductivity based on the dimensions shown in Figure 3.2a providing the thickness of SLG is 0.35 nm. UV-vis spectroscopy of the transitional metal hexacarbonyle reagents was obtained with a Varian Cary 5000 spectrophotometer.

Results and discussion

As chromium reagents are vulnerable to oxidation and clean graphene surfaces are very sensitive to dopants from air, the experiments were conducted in a glovebox under argon atmosphere conditions. The UV-vis spectra of three chromium reagents $Cr(CO)_6$, $Cr(\eta^6\text{-benzene})(CO)_3$, and $Cr(\eta^6\text{-benzene})_2$[29] and Group VI transition metal carbonyles in aceonitrile are shown in Figure 3.1; the wavelength of light used to initialize the reaction of those carbonyles with single layer grahene is indicated by a dash line.

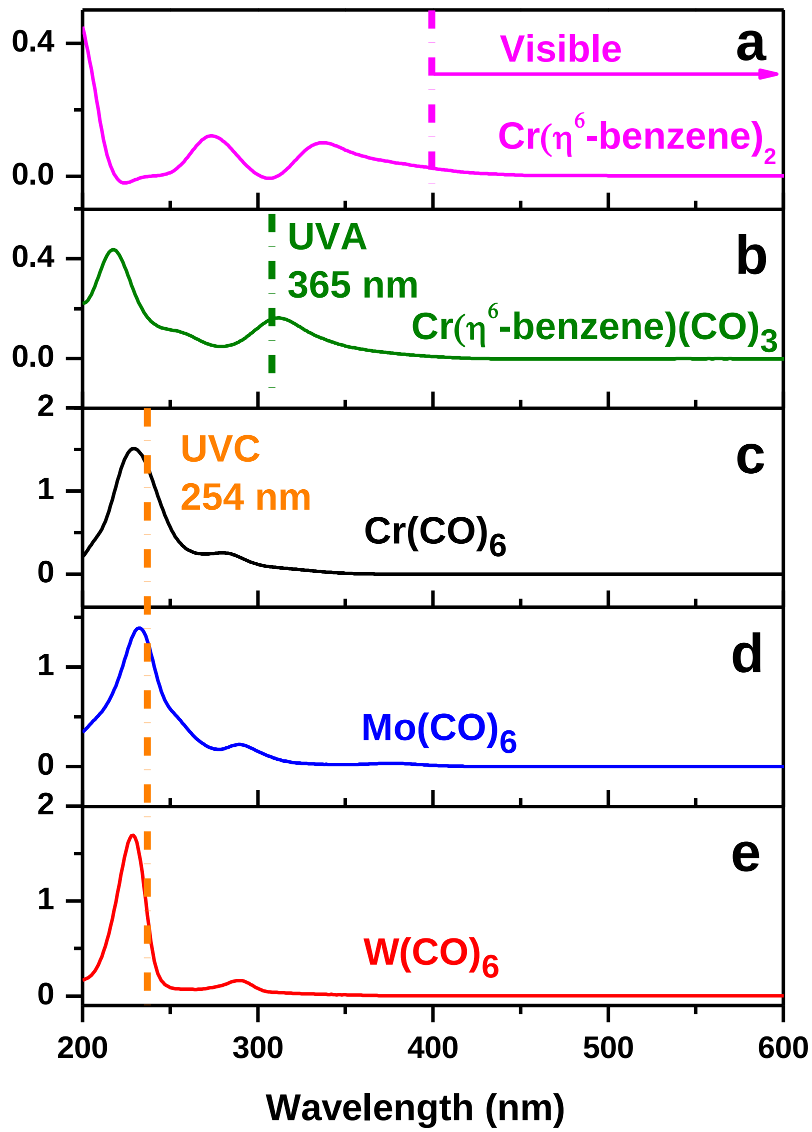

Figure 3.1. UV-vis of (a) Cr(η^6-benzene)$_2$, (b) Cr(η^6-benzene)(CO)$_3$, (c) Cr(CO)6, (d) Mo(CO)$_6$ and (e) W(CO)$_6$ dissolved in acetonitrile and the wavelength of light used in the photochemical experiments described in this chapter.

For hexacarbonyles (Figure 3.1c-e), UVC (254 nm) was used, while for Cr(η^6-benzene)(CO)$_3$ (Figure 3.1b), UVA (365 nm) was employed, visible light is enough for reaction with Cr(η^6-benzene)$_2$ (Figure 3.1a). The schematic of the photochemical reaction performed on SLG is shown in Figure 3.2a.

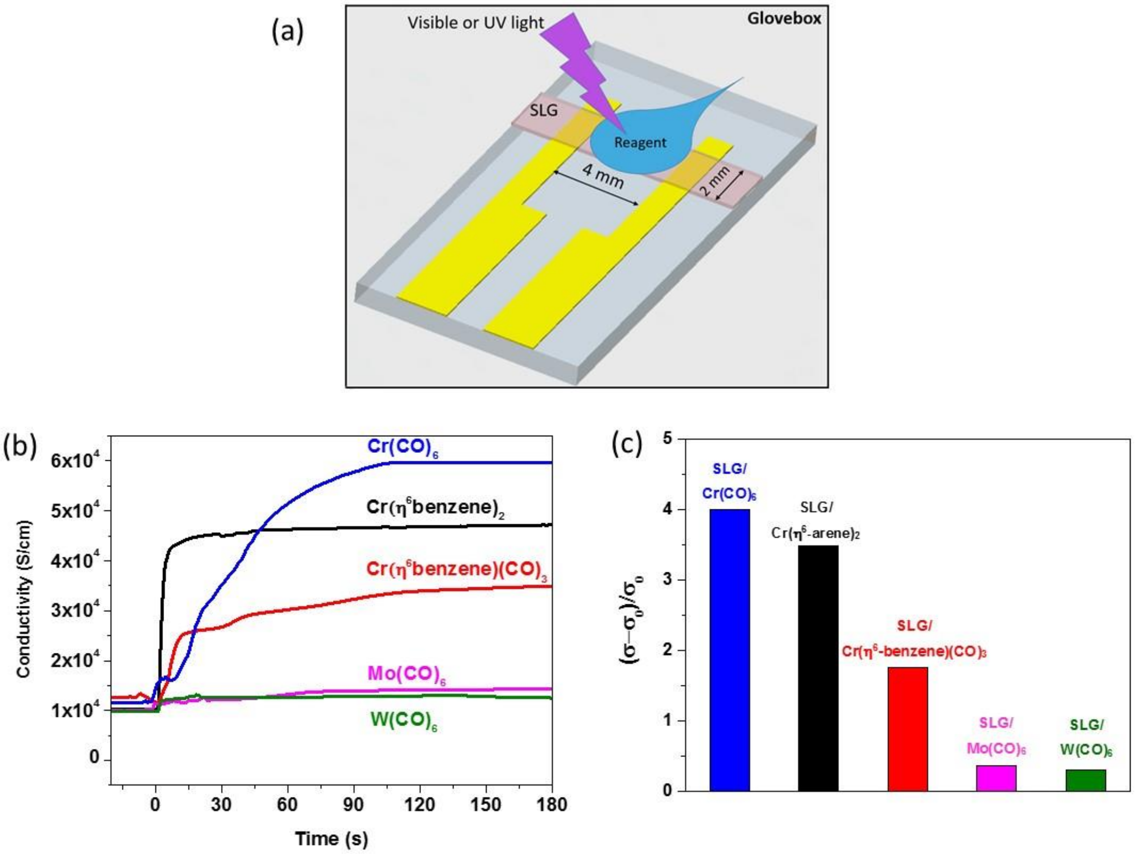

Figure 3.2. (a) Schematic of the photochemical reaction on SLG inside a glovebox. (b) Evolution of conductivity of SLG films on photochemical reaction with 3 different chromium reagents. (c) Conductivity enhancement of graphene half sandwich complexes formed with each chromium reagent.

After annealing, the graphene devices were transferred into a glovebox and electrically connected to outside measure unit Keithley 236 through feed throughs on the back of the glovebox. The reaction of Cr(η^6-benzene)$_2$ with SLG occurs as soon as we cast a drop of the reagent on the graphene surface in the presence of room light. However, for reagents $Cr(CO)_6$, $Mo(CO)_6$ and $W(CO)_6$ UV light of 254 nm is necessary to initiate the reaction, and for Cr(η^6-benzene)$(CO)_3$ exposure to UV light of 365 nm gives higher enhancement of the SLG conductivity. As reported in the literature, $Cr(CO)_6$ will lose the CO ligands successively upon exposure to UV light,[30, 31] the highly reactive intermediates will complex with inert ligands, in this case, acetonirtile to form a complex $Cr(CO)_3(CH_3CN)_3$; as we have shown in our previous work this complex reacts with the graphene surface of SWNTs immediately, and the results in Figure 3.2b show that the conductivity of SLG increased abruptly ~ 4 times. It is reasonable to postulate that CH_3CN in $Cr(CO)_3(CH_3CN)_3$ was replaced readily by graphene to form Cr(η^6-graphene)$(CO)_3$, which preserves the delocalized band structure of graphene due to the constructive rehybridization of the graphene π-system with the vacant chromium d_π orbital. The proposed reaction pathways for $M(CO)_6$ (M=Cr, Mo and W) are shown in Sheme 3.1. Theoretical calculations predict that significant coverage of the graophene surface with $Cr(CO)_3$ ligands increases the density of states near the Fermy level, which will thus increase the conductivity of a single layer graphene.[28] However, as the diameter of the transition metal increases, the interaction between the metal complex with the graphene surface decreases, which is reflected less enhancement of the conductivity for Mo(η^6-graphene)$(CO)_3$ and W(η^6-graphene)$(CO)_3$ complexes as evidenced in Figure 3.2b.

The photochemistry of Cr(η^6-benzene)(CO)$_3$ is complicated, as both arene exchange and CO loss can occur during exposure to UV light. From the slope of the curves in Figure 3.2b, we estimate that the reaction rate of the chromium reagents with graphene follow the sequence: Cr(η^6-benzene)$_2$ > Cr(η^6-benzene)(CO)$_3$ > Cr(CO)$_6$. This indicates that both arene exchange and CO loss take place in the case of Cr(η^6-benzene)(CO)$_{3,}$. However, the coverage of organometallic groups on the surface of graphene is low, as Cr(η^6-benzene)(CO)$_3$ gives the least enhancement of conductivity among all three chromium reagents.

The proposed mechanisms of photochemical raction of Cr(η^6-benzene)$_2$ with SLG is shown in Scheme 3.1, electron transfer processes from Cr(η^6-benzene)$_2$ to graphene are responsible for the accelerated exchange of the arene ligand.

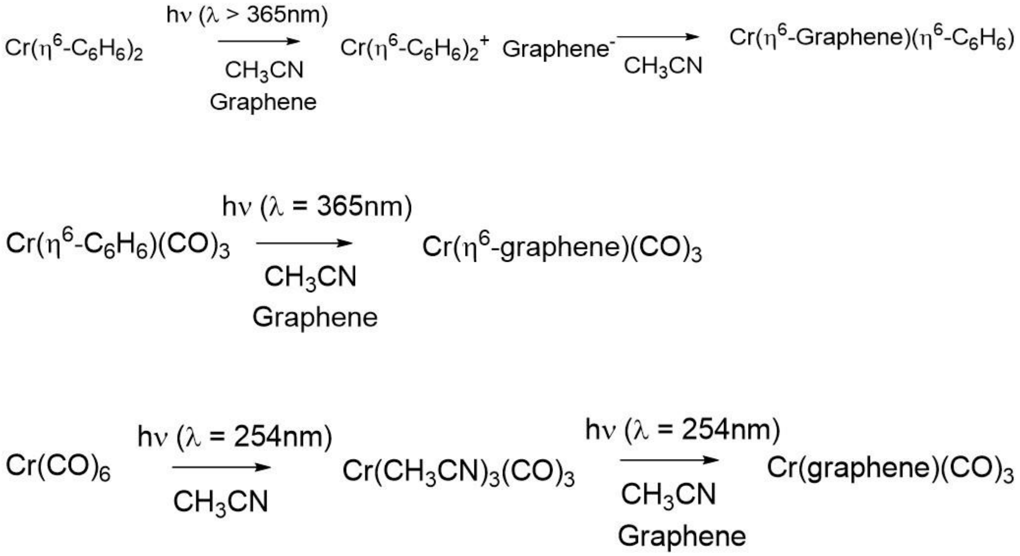

$$\mathrm{Cr}(\eta^6\text{-}\mathrm{C_6H_6})_2 \xrightarrow[\substack{\mathrm{CH_3CN} \\ \text{Graphene}}]{h\nu\ (\lambda > 365\text{nm})} \mathrm{Cr}(\eta^6\text{-}\mathrm{C_6H_6})_2^{+}\ \text{Graphene}^{-} \xrightarrow[\mathrm{CH_3CN}]{} \mathrm{Cr}(\eta^6\text{-Graphene})(\eta^6\text{-}\mathrm{C_6H_6})$$

$$\mathrm{Cr}(\eta^6\text{-}\mathrm{C_6H_6})(\mathrm{CO})_3 \xrightarrow[\substack{\mathrm{CH_3CN} \\ \text{Graphene}}]{h\nu\ (\lambda = 365\text{nm})} \mathrm{Cr}(\eta^6\text{-graphene})(\mathrm{CO})_3$$

$$\mathrm{Cr(CO)_6} \xrightarrow[\mathrm{CH_3CN}]{h\nu\ (\lambda = 254\text{nm})} \mathrm{Cr(CH_3CN)_3(CO)_3} \xrightarrow[\substack{\mathrm{CH_3CN} \\ \text{Graphene}}]{h\nu\ (\lambda = 254\text{nm})} \mathrm{Cr(graphene)(CO)_3}$$

Scheme 3.1 Photochemical reaction schemes for single layer graphene (SLG) with (a) Cr(η^6-benzene)$_2$ (b) Cr(η^6-benzene)(CO)$_3$ and (c) Cr(CO)$_6$

As we mentioned above, theoretically the twofold degeneracy at the Dirac point facilitates the hybridization of both the degenerate bonding (e_{1g}) and anti-bonding (e_{2u}) benzene π-orbitals with the d-orbitals of the transition metals. In order to explore the effect of Dirac point on the graphene's reactivity, we fabricated graphene field effect transistors and conducted the photochemical reactions with $Cr(CO)_6$. For these experiments the graphene devices were gated at different voltages to shift the Fermi level away from the Dirac point. Thus, three experimental conditions were selected and the reactions were conducted at the Dirac point, typical for pristine graphene, at negative gate voltage to shift the Fermi level into the graphene valance band and at positive gate voltage to shift the Fermi level into the graphene conduction band. The results are shown in Figure 3.3.

When the reaction was conducted at the Dirac point, there was maximum enhancement of the graphene conductivity, which indicates strong reaction and it is presumably associated with a largest coverage of chromium carbonyl ligands. While when the reaction was performed at negative gate voltage [Dirac point – 10 volts], the conductivity enhancement was about 70% of that achieved at the Dirac point. When we increased the gate voltage to positive values [Dirac point + 60 volts] there was only small change of conductivity (~ 5%). In summary, we demonstrated that the special electronic structure of graphene at the Dirac point expedites its organometallic chemistry.

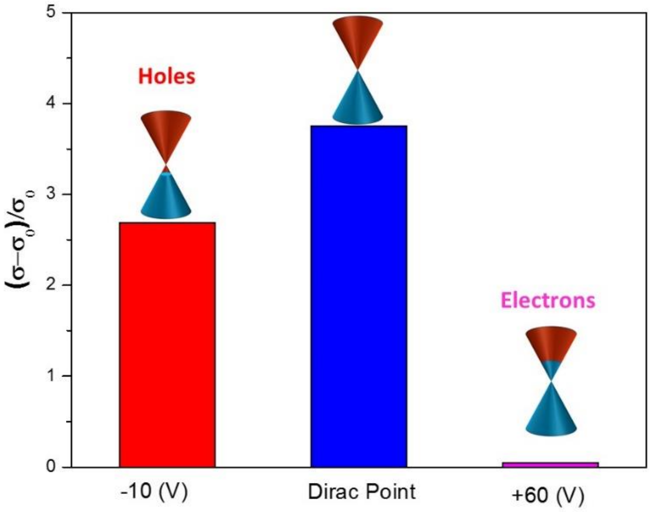

Figure 3.3 Conductivity enhancement of SLG reacted with $Cr(CO)_6$ under different gate voltage.

Conclusion

In conclusion, we successfully synthesized graphene-transition metal half sandwich structures by a facile photochemical route and demonstrated that the new materials have enhanced conductivity as compared to pristine graphene. Based on the conductivity enhancement we estimate the following reactivity order of the transition metal reagents towards graphene: $Cr(\eta^6\text{-benzene})_2$ > $Cr(\eta^6\text{-benzene})(CO)_3$ > $Cr(CO)_6$ > $Mo(CO)_6$ > $W(CO)_6$. Furthermore, we demonstrated that the reactivity of graphene reaches its maximum at the Dirac point, while away from the Dirac point the reaction is suppressed. This work may have potential applications in graphene based electronics, spintronics and catalysis.

3.1.3 Graphene Sandwich Complexes

Introduction

The interaction between metals and graphene surfaces has fascinated researchers for a long time. For example, graphite intercalation compounds (GICs) (CaC_6) have demonstrated high T_c (11.5 K) superconductivity.[32] However, charge transfer is needed for metals to intercalate into the space between two graphene layers in graphite.[17] Recently the Haddon research group has pursued the organometallic chemistry of the tricoordinate conjugated carbon allotropes[18-20] with particular emphasis on carbon nanotubes and has shown that the formation of covalent bis(η^6-SWNT)M bonds is an effective way to interconnect the junctions of the SWNTs in thin films leading to an enhanced electrical conductivity in the case of the some of the first row transition metals (Ti, V, Cr, Mn, Fe),[1] the group 6 metals (Cr, Mo, W),[21] and the lanthanides (La, Nd, Sm, Eu, Gd, Dy, Ho, Yb).[22, 23] It would be expected that the same chemistry could be applied to the insertion of transition metals between a pair of parallel graphene films to generate compounds analogous to the GICs in which the ionic bonds characteristic of the GICs are replaced by covalent bis-hexahapto bonds. Theorecal calculation[33] and TEM invesitgation[34] have shown that transition metal (TM) can migrate on the surface of graphene due to lower binding energy between TM and graphene surface. However, to the best of our knowledge, no thereotical calculations and experimental work have been done to interconnect two macroscopic graphene layers by group 6 transition metals as shown in Figure 3.4. In this work, we pursued a route to introduce chromium transition metals into the space between two SLCVD graphene and monitored the effect of the interaction of chromium atoms with two graphene surfaces on the conductivity of the samples.

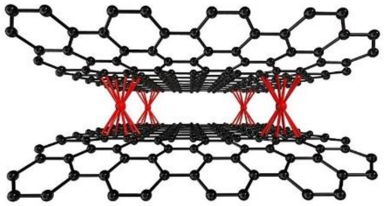

Figure 3.4. Schematic of the formation of a graphene-metal-graphene sandwich complex.

Experimental Section

Device fabrication The evenly spaced (1mm) electrodes (10nm Cr/ 100 nm Au) on glass substrates were fabricated with a shadow mask by E-beam evaporation. Graphene was transferred by the naphthalene-assisted method described in Chapter 2.3. Semiconducting (Sc-) SWNT thin films were prepared by vacuum filtration using aqueous suspensions of semiconducting nanotubes (Nanointegris Inc). A cellulose ester membrane (Millipore VCWP) was put on the vacuum filter and a specific volume [calculated based on the concentration of the SWNT dispersion and the film density - 1.2 g/mL] of the Sc-SWNT suspension was filtered through the membrane to prepare the corresponding Sc-SWNT random network thin film. All devices were annealed under high vacuum at 300 ℃ for 8 hours before conducting the experiments.

Results and discussion

In our previous work, we have shown that 0.6 nm Cr deposition on the clean surface of a single layer chemical vapor deposition (SLCVD) graphene film can reduce the graphene conductivity by a factor of ~ 2, which we assigned to scattering effects or dissociation of C-C bond catalyzed by chromium atoms.[15]. Density functional theory shows that the transition metal ad-atoms on pristine graphene should be mobile at room temperature due to low migration barriers.[33]. Although theoretical calculations on the interaction of chromium atoms with two graphene surfaces is needed, it is reasonable to expect that Cr adatoms will also be mobile between two graphene surfaces. We tested this assumption by preparing the graphene-SWNT-graphene devices as shown in Figure 3.5a.

In a typical device, one macroscopic SLCVD thin film was transferred by the clean naphthazarine-assisted graphene transfer method reported in Chapter 2.3. The graphene film covered all four evenly spaced electrodes on the glass substrate to yield a device with a channel length of 1 mm. Then a 8 nm Sc-SWNT thin film was placed next to the outer electrode at one end on top of the bottom layer graphene. Finally, another layer of SLCVD graphene thin film was placed on top with the edge aligned with the edge of the outer electrode next to the Sc-SWNT film (Figure 3.5a). The function of the Sc-SWNT film here is to act as a spacer and introduce Cr atoms into the space between the two graphene layers, as Sc-SWNT was sandwiched between the two graphene films. Due to the known mobility of the Cr atoms on graphitic surfaces, we anticipated that the Cr atoms could move through the nanotube network towards the space between the two graphene layers and bridge the top and bottom layers graphene. The devices were annealed in vacuum at 300 ℃ for 8 hours in order to remove the dopants. A mica thin film was used as a mask to block the direct deposition of chromium atoms on the top graphene layer. As shown in Figure 3.5a bottom right, only the Sc-SWNT thin film on the bottom graphene layer was exposed to Cr atoms. The resistance of three different zones of the devices was monitored in-situ during the deposition and the results are shown in Figure 3.5b. In contrast with SLCVD graphene, the conductivity of Gr-CNT-Gr device doubled in all three zones, which indicates that Cr atoms are highly mobile between two graphene films and have penetrated into the space between the pair of graphene films even in zone 3, which is further away from the metal deposition spot. The abrupt decrease of conductivity immediately after the Cr deposition started may be caused by thermal effect, as graphene is one of the best thermal conductors; the conductivity of graphene in zones 1-3 decreased simultaneously due to increase of the device temperature. Interestingly, as the Cr atoms start to migrate in the direction of the red arrow (Figure 3.5b), the conductivity of graphene in zone 1 starts to increase after

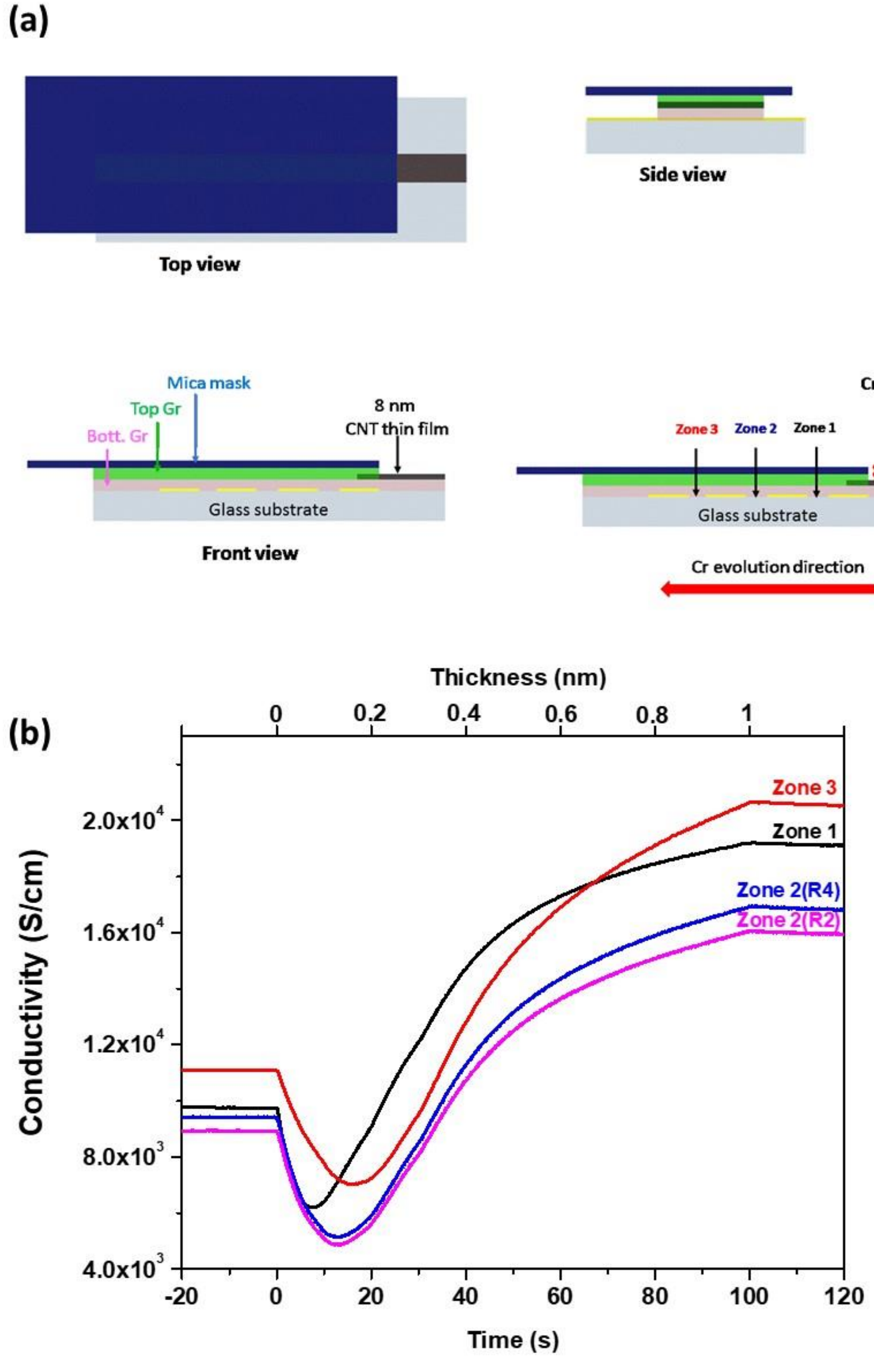

Figure 3.5. (a) Three views of a typical Gr-SWNT-Gr device employed in this study. (b) Evolution of on the in-plane conductivity of the device with e-beam deposition of Cr atoms between two graphene layers.

0.1 nm deposition of Cr at the right end of the device. Similarly, the conductivity of graphene in zone 2 and zone 3 starts to increase upon 0.17 nm and 0.19 nm Cr deposition, respectively. This shows a dynamic process of the evolution of Cr atoms between two macroscopic parallel graphene layers. Based on the data in Figure 3.5b the migration rate of Cr atoms between two SLCVDG is calculated to be (40~195) $\mathrm{\mu m}/s$.

In order to further investigate the mechanism of Cr migration and the conditions for Cr to reach such a high mobile rate, we conducted two reference experiments, in which we employed device configuration as shown in Figure 3.6a. In the first reference experiment, an 8 nm Sc-SWNT film (width: 2 mm) was transferred onto the evenly spaced pre-patterned electrodes (channel length: 1 mm) on glass substrate. In the second reference experiment, the bottom layer of SLCVD (width: 2 mm) and the top Sc-SWNT layer (width 2 mm) were transferred onto the substrate subsequently. Then a thin Kapton film with a hole (diameter: 80 $\mathbf{\mu m}$ was placed on top of the device so that the hole was located on top of zone 1. The edges of the Kapton film were further sealed with a Kapton tape. After annealing, the devices were loaded into the e-beam evaporator and exposed to Cr atoms (Cr film thickness up to 1.5 nm). The resistance of devices was monitored in-situ by a Keithley 2700 multimeter connected to the device by a feed hrough at the bottom of the e-beam chamber. As shown in Figure 3.6b, the conductivity of zone 1 increased only ~2 times as compared to enhancement of ~ 100 times achieved for

SWNT films fully exposed to 1 nm Cr atoms.[1] And there is almost no change of the device conductivity in zones 2 and 3, which may be due to the presence of oxygen groups on the surface of the glass substrate that can trap and oxidize the Cr adatoms, therefore inhibiting the atoms migration. This hypothesis can be further confirmed by the results of the second reference experiment as shown in Figure 3.6d.

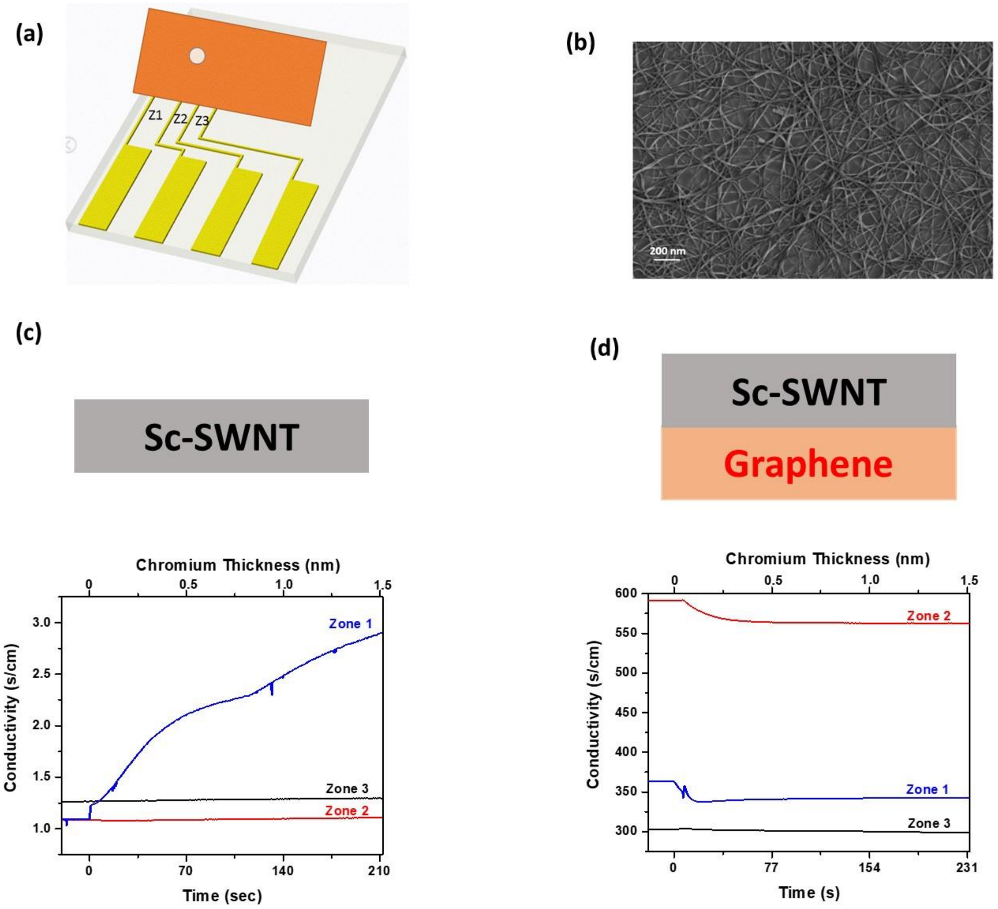

Figure 3.6 (a) Device configurations, carbon films were transferred to evenly-spaced pre-patterned electrodes on glass substrates. A Kapton thin film with a hole (d=80 um) in zone1 was used as a shadow mask for chromium deposition. The edges of the film were sealed with a Kapton tape. (b) SEM image of an 8 nm Sc-SWNT random network. (c) Conductivity evolution for the Sc-SWNT thin film only (top) upon chromium evaporation. (d) Conductivity evolution for a device of SLG (bottom) + Sc-SWNT thin film (top) upon chromium evaporation.

In this experiment, zones 1 and 2 exhibit a decrease of the film conductivity, with a larger decrease observed in zone 1 (~ 7% upon deposition of 0.1 nm Cr atoms), while the conductivity of zone 2 by ~ 4. Zone 3 did not show obvious change of conductivity.

Based on these results we obtain the following order of Cr migration rate in the different carbon systems: Gr-Gr > Gr + Sc-SWNT > Sc-SWNT. We assume that the higher migration rate observed in the configurations that contained graphene is that the bottom layer graphene can protect Cr from oxidation by oxygen groups of the substrate. Another possible reason is that Cr atom may be more mobile on flat graphene surfaces.

In order to further explore the reason for conductivity decrease after Cr deposition observed in Figure 3.6d, and better understand the underlying mechanism, we conducted another set of experiments as shown in Figure 3.7abc. Figure 3.7d shows a comparison of the conductivity change during Cr deposition on devices with different configurations. When Gr + 8 nm Sc-SWNT was fully exposed to 0.1 nm Cr, we observed a small increase of the conductivity, which is in contrast with the results in Figure 3.6d, and may indicate that the migration distance for Cr in configuration [SLCVD graphene + 8 nm Sc-SWNT] is not as large as in the configuration with SLCVD graphene only. Therefore, the Cr migration rate in different carbon system follows this order: Gr-Gr > Gr > Gr + Sc-SWNT> Sc-SWNT.

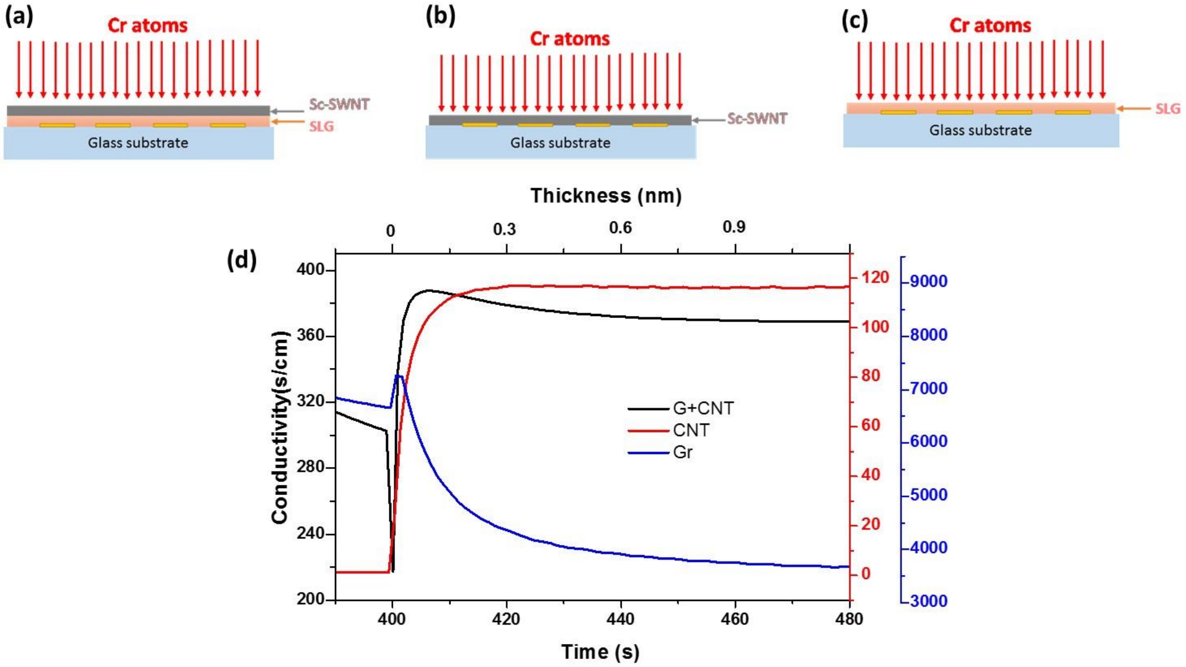

Figure 3.7 Device configurations of (a) SLG+Sc-SWNT (b) Sc-SWNT (c) SLG. (d) Evolution of conductivity for corresponding devices upon Cr evaporation.

We also used photochemical routes to prepare the chromium complexes with a pair of SLCVD graphene layers. As shown in Figure 3.8a, similar configuration with the device illustrated in Figure 3.5a, Sc-SWNT is used to introduce Cr reagent to the space between two graphene layers. The reaction is conducted inside a glovebox under argon atmosphere. As soon as we cast a drop of the chromium reagent onto the Sc-SWNT sandwiched between two SLCVD graphene layers, UV light [UVC for $Cr(CO)_6$ and UVA for $Cr(\eta^6\text{-benzene})(CO)_3$] was shed on the whole device. Interestingly, without casting reagent to the device between the two electrodes, the conductivity of our samples increased by ~ 1-1.5 times, which is consistent with results from metal vapor synthesis (MVS) as shown in Figure 3.5b, which supports the proposed mechanisms.

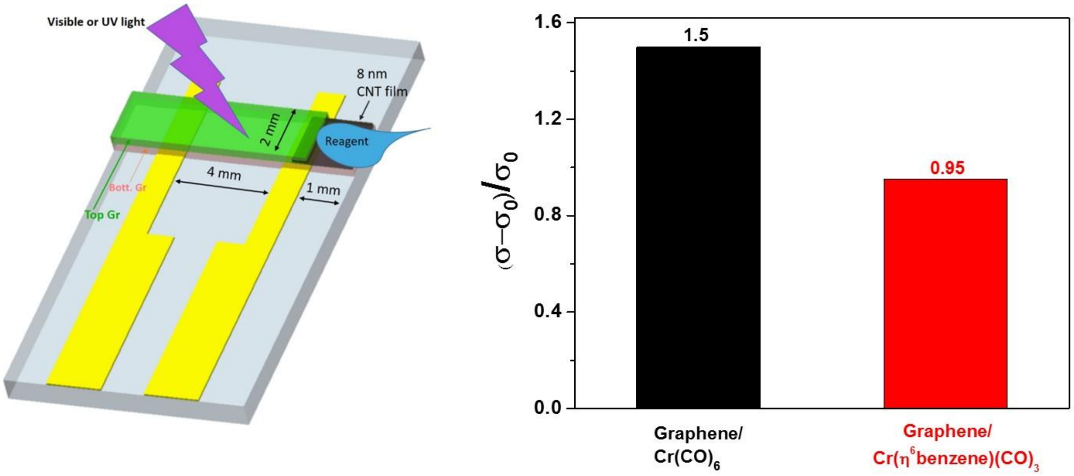

Figure 3.8. (a) Device configuration for the photochemical generation of graphene-Cr-graphene sandwich complexes. (b) Conductivity enhancement for two Cr reagents – $Cr(CO)_6$ and $Cr(Benzene)(CO)_3$.

Conclusion

In summary, we successfully synthesized Graphene-Cr-Graphene sandwich compounds using both metal vapor synthesis and photochemical methods, where the pair of graphene was interconnected with Cr atoms through the formation of covalent bishexahapto bonds. This new graphene sandwich complexes show increased of the in-plane conductivity, which indicates preserved conjugation of the π electrons. We also observed a fast migration rate [(40~195) $/s$] of the Cr atoms between two graphene surfaces. The Cr migration rate in different configurations follows the order: Gr-Gr > Gr> Gr + Sc-SWNT> Sc-SWNT. These compounds have potential applications in catalysis, electronics and spintronics. Moreover, these systems may exhibit superconductivity when the transition metal atoms are arranged in a specific order.

3.1.4 Application of organometallic chemistry to graphene nanoplatelets

Introduction

Graphene nanoplatelets (GNPs) are a particularly attractive material for a number of applications due to their large scale production, and the availability of simple routes to solution-based and film-based material forms.[35-38] The organometallic chemistry was previously attempted to enhance the conductivity of exfoliated GNPs by thermal processing under pressure, but this was not successful, perhaps due to the large particle sizes and the exposure of the samples to the atmosphere during the preparation.[37, 39] In the present section, we explore the organometallic chemistry of a new form of GNPs prepared by PPG Industries (http://corporate.ppg.com/Home.aspx) (PPG GNPs) in which the size of the GNPs is much smaller than that of the conventional exfoliated GNPs prepared from natural graphite. The PPG material possesses a crinkled morphology which should facilitate the interconnection of the graphene surfaces of different PPG GNPs and allow the formation of bis-hexahapto bonds between adjoining graphene surfaces within distorted individual PPG GNPs, thereby facilitating the formation of a novel 3D-connected material, as shown in Figure 3.9. Thus, it may be possible to conserve the extraordinary physical and chemical properties of graphene in the in-plane direction, while interconnecting and improving the interactions between adjacent GNP sheets by the formation of bis-hexahapto covalent bonds in the orthogonal directions, throughout the solid material (Figure 3.9). We make use of metal vapor synthesis (MVS)[1, 2] and photochemical[29] routes for the preparation of the transition metal complexes which are carried out in vacuum and in the atmosphere of a glove box, respectively, while the conductivities of the thin films of PPG GNPs are monitored in situ.

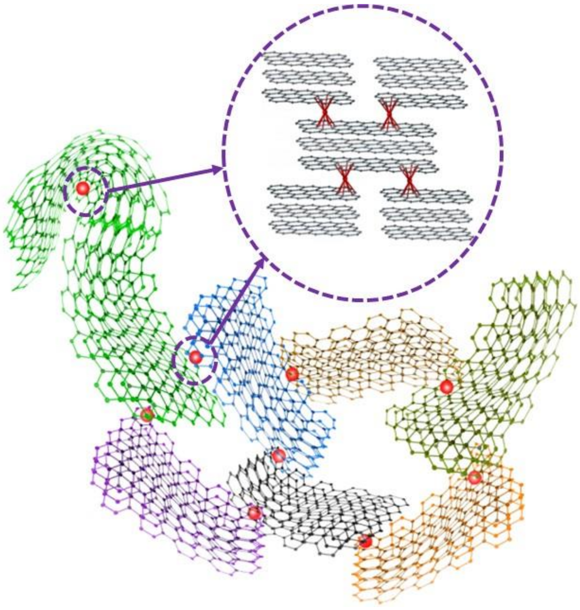

Figure 3.9. Schematic of the formation of metal complexes with the surface of PPG GNPs. Different colors of PPG GNPs represent different nanoparticles. Reprinted with permission from ref.58 (Copyright © 2016, American Chemical Society).

Experimental Section

Exfoliated graphene (XG). For the Raman spectroscopy, XG was exfoliated by the scotch tape method[40] from Highly Oriented Pyrolytic Graphite (HOPG) (Union Carbide Corporation, grade ZYH).

Epitaxial graphene (EG). For the Raman spectroscopy EG was grown on the C-face of a SiC substrate (Cree Inc, High purity) and was obtained from the de Heer group (Georgia Tech).

Single Layer Graphene transfer. Single layer graphene grown by chemical vapor synthesis on copper (Graphene Supermarket) was transferred onto glass substrates using literature methods.[41].

PPG GNP thin film preparation. PPG GNP powders (obtained from the PPG Industries) were dispersed in tetrahydrofuran (THF) at a concentration of 0.03 mg/mL; the dispersion was then sonicated for 1hr (VWR Ultrasonic Cleaner, Model No.75T). Then the solution was sprayed onto a glass substrate with pre-patterned electrodes at 70 ℃. For conductivity measurement, the samples were annealed in vacuum for 5 hours at 300 ℃ in order to remove atmospheric dopants.

Metal vapor synthesis (MVS). After vacuum annealing, the samples were transferred into a cryopumped Temescal BJD 1800 E-beam evaporator and the system pumped for 10 hours until the vacuum inside the chamber had reached 8×10^{-7} Torr.

Photochemistry. Same conditions as described in Chapter 3.1.2. Solutions of Mo(CO)6 (Sigma-Aldrich 98%) and W(CO)6 (Alfa Aesar 97%) were prepared in degassed acetonitrile inside a glovebox at a concentration of 1 × 10−3 M. The protocol for the chromium organometallics is described in a previous paper.35 We employed the following light sources: Cr(CO)6, Mo(CO)6 and W(CO)6 [UVC, 254 nm], Cr(η6-benzene) (CO)3 [UVA, 365 nm], Cr(η6-benzene)2 [room light].

Conductivity measurement. The samples were interfaced with a computer controlled Keithley 2700 Model 7708 Differential Multiplexer by use of feed troughs and wire harnesses.

SEM. PPG GNPs were dispersed in dimethylformamide (DMF) in sufficient concentration to make samples of areal density 5 μg/cm^2 after filtration through an Al_2O_3 membrane (Whatman 0.02 μm). Pt/Pd was sputtered on the surface of the sample before conducting the GeminiSEM study.

Raman spectroscopy. Raman spectra were acquired with a Nicolet Almega XR Dispersive Raman microscope using 532 nm laser excitation and 25% power source.

Optical Microscopy. Optical microscope images of sprayed PPG thin film samples were obtained with Olympus BX51W1 microscope.

Measurement of film thickness. Cross-sectional profiles for thin film samples were obtained with a Dektak Profilometer.

UV-Vis-NIR spectroscopy. Absorption spectra of 0.03 mg/mL THF dispersions of PPG graphene nanoparticles were collected utilizing a Varian Cary 5000 spectrophotometer. The absorption spectra were measured using cuvettes of 2 mm light path length. The dispersions were prepared by 1 hour sonication (VWR Ultrasonic Cleaner, Model No.75T).

AFM. PPG GNP powders were dispersed in ortho-dichlorobenzene by ultrasonication (VWR Aquasonic HT250 bath sonicator) for 20 min. A drop of the dispersion was placed on a mica substrate, allowed to dry and the images were collected in a tapping mode (Digital Instruments, MMAFM-2). For the PPG GNP thin films a Dimension 3100 Nanoman Veeco AFM was employed to characterize the morphology with a golden silicon probe (NT-MDT, NSG01), and the images were obtained in tapping mode.

Results and Discussion

PPG GNPs. The PPG GNPs material is synthesized from methane in a gas phase, continuous plasma process, [42] and below we report some of our characterization studies of this new material. We carried out Atomic Force Microscopy (AFM) measurements to characterize the lateral dimensions and thickness of the PPG GNPs. Figure 3.10 shows that the lateral size of the PPG GNPs varies from 50 to 500 nm, and the thickness is in the range of 2 nm to 50 nm, which corresponds to 6 to 150 layers of graphene.

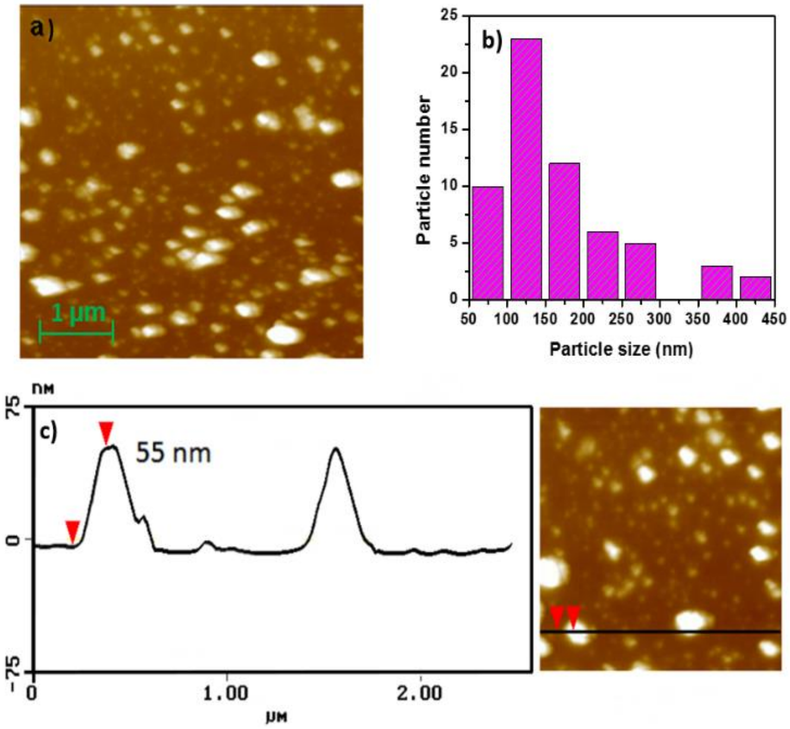

Figure 3.10. (a) AFM image of PPG GNPs previously dispersed in ortho-dichlorobenzene. (b) Distribution of the PPG GNPs by lateral size. (c) AFM analysis of nanoparticle thickness. Reprinted with permission from ref.58 (Copyright © 2016, American Chemical Society).

Scanning Electron Microscopy (SEM) was employed to study the morphology of PPG GNPs and the SEM image in Figure 3.11 indicates that the PPG GNPs have a crinkled morphology which distinguishes this material from traditional graphene nanoplatelets. Of particular importance in the present application is the relatively small size of the nanoplatelets in comparison to standard GNPs obtained from the exfoliation of natural graphite; furthermore the size distribution of the PPG GNPs is narrower than in the traditional materials.[37]

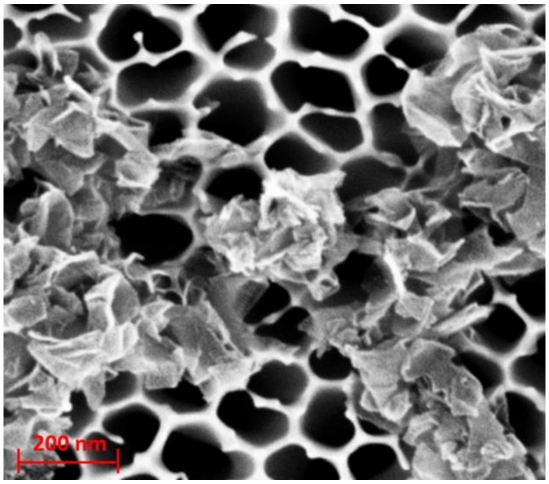

Figure 3.11 SEM image of PPG GNPs at an areal density of 5 mg/cm^2 on an Al_2O_3 filter membrane. Reprinted with permission from ref.58 (Copyright © 2016, American Chemical Society).

A representative Raman spectrum of the PPG GNPs is compared with other forms of graphene in Figure 3.12. The Raman spectrum shows a G-peak at ~1567 cm^{-1} and an intense 2D-peak at ~2678 cm^{-1}, which indicates a graphene-like electronic structure. The relatively strong D-peak in the PPG GNPs probably originates from the small flake size: based on literature analyses of the flake dimensions as a function of the Raman I_D/I_G ratio,[43, 44] we estimate a particle size for PPG GNPs of 0.5 μm which is a little larger than that obtained from the AFM measurements. The shape of the 2D-peak is a single Lorentzian and the intensity of G-peak is smaller than the 2D-peak, similar to single layer graphene, which suggests that the layers of the PPG GNPs sample are not Bernal-stacked , but are rotationally disordered much like in the case of epitaxial graphene.[45, 46] The disorder between graphene layers minimizes the electronic interaction between the sheets and preserves the single graphene sheet properties of the layers.

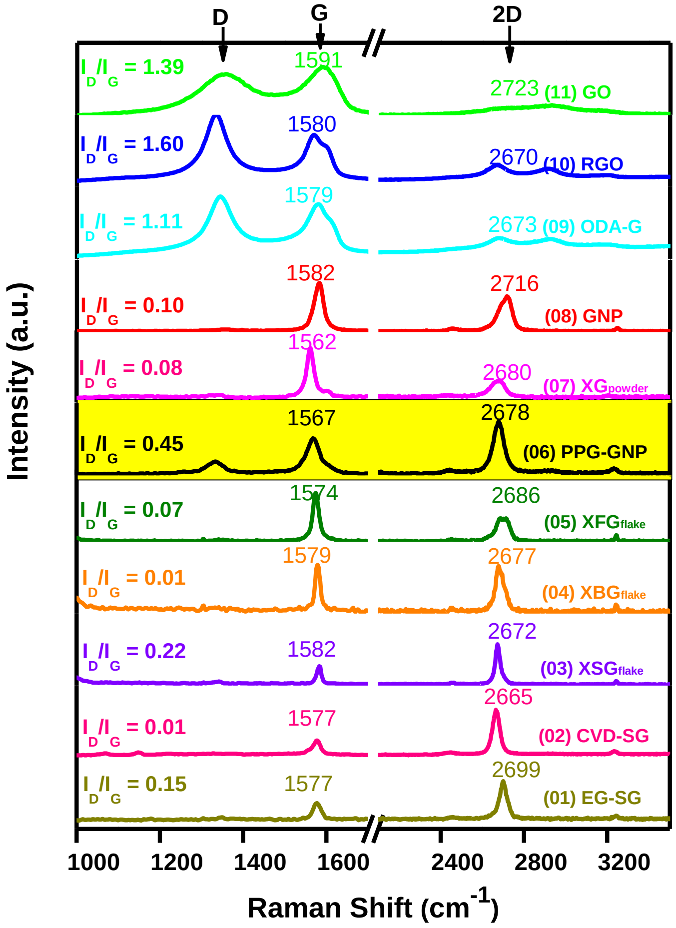

Figure 3.12. Raman spectra of PPG GNPs in comparison with other forms of graphene. Reprinted with permission from ref.58 (Copyright © 2016, American Chemical Society).

PPG GNP Film Formation. Thin films were prepared by spraying tetrahydrofuran (THF) dispersed PPG GNPs onto glass substrates with pre-patterned electrodes as shown in the microscope images of our pristine samples (Figure 3.13). There is some restacking of the PPG GNP particles on the substrate but in general the

PPG GNPs material does not seem to reaggregate to the same degree as other GNPs and reasonably uniform thin films can be obtained. Figure 3.13 shows the cross-sectional profile obtained by use of a Dektak Profilometer for a typical PPG GNP thin film used in our experiments (thickness ≈ 100 nm). These films are of comparable thickness to the particle dimensions and thus they retain characteristics of a percolating network which makes them sensitive to the quality of the inter-GNP junctions.[2]

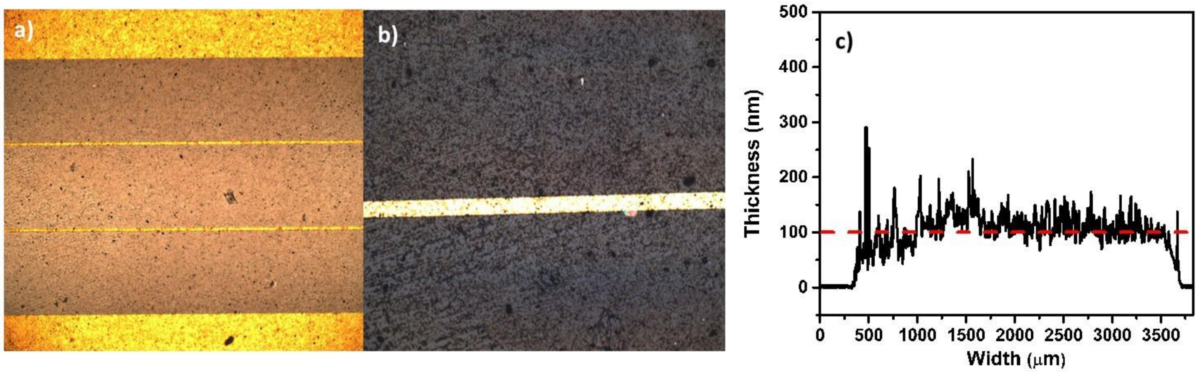

Figure 3.13 Microscope images of sprayed PPG GNP thin film at magnifications: (a) 100 X. (b) 500 X. (c) Dektak profilometer cross-sectional characterization of a typical PPG GNP thin film. Reprinted with permission from ref.58 (Copyright © 2016, American Chemical Society).

In order to better understand the properties of PPG GNP thin film, UV-Vis-NIR spectra were taken on our solid films on glass substrates (Figure 3.14). The spectra show well-defined slopes in the short wavelength region of the spectrum, which is characteristic of nanomaterials such as graphene or single-walled carbon nanotubes (SWNTs) that typically show a peak at ~270 nm, corresponding to the π→π* transitions within the graphene sheets. The extinction coefficient of PPG

GNPs dispersed in THF calculated from Figure 3.14a at 660 nm is $\varepsilon = 48$ L·g^{-1}·cm^{-1} and the absorbance coefficient of the PPG GNP thin film calculated from Figure 3.14b is $\alpha = 0.32 \times 10^5$ cm^{-1} (660 nm). Based on our previous analysis and the absorption characteristic of the materials,[47] we can calculate an effective density for the film of d = 0.29 g cm^{-3}; as expected, thicker films have higher densities (typically, d $\approx$ 0.77 g cm^{-3}).

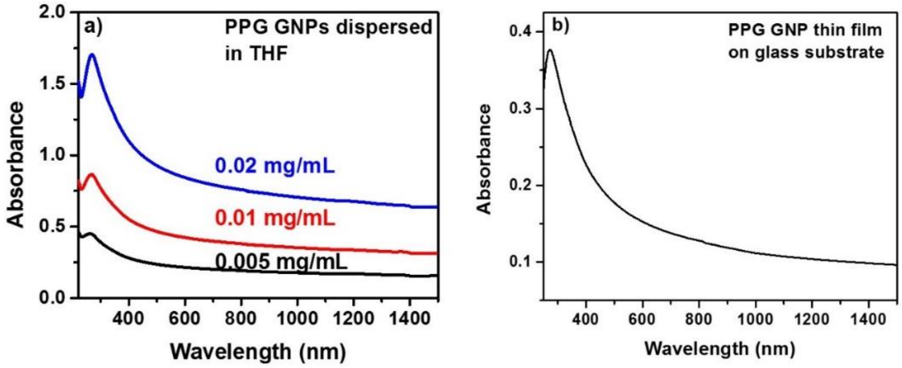

Figure 3.14 UV-Vis-NIR spectra of: (a) PPG GNPs dispersed in THF as a function of concentration. (b) PPG GNP film (100 nm) versus wavelength. Reprinted with permission from ref.58 (Copyright © 2016, American Chemical Society).

AFM image of the PPG GNP thin film is shown in Figure 3.15, which indicates that the PPG GNP particles flocculate during the spraying process thereby leading to a loosely packed structure.

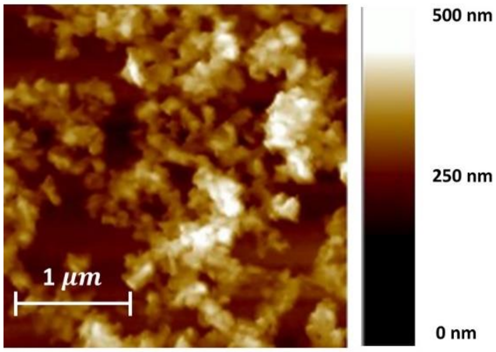

Figure 3.15 AFM image of sprayed PPG GNP thin film on glass substrate. Reprinted with permission from ref.58 (Copyright © 2016, American Chemical Society).

Response of the PPG GNP Thin Film Conductivities to Metal Deposition and Photochemical Reaction with Organometallic Precursors. Before exposure of the PPG GNP films to the metals and organometallic reagents, the pristine thin film samples were annealed at 300 ℃ in vacuum for 5 hours just before conducting the reaction in order to remove solvents and volatile dopants. Figure 3.16 shows schematics of the experimental setups employed in the MVS and photochemical experiments.

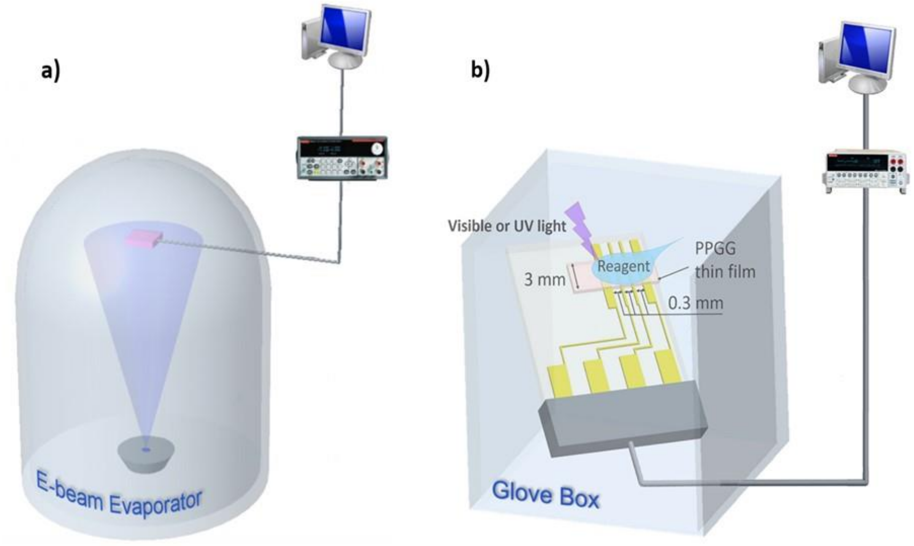

Figure 3.16 Schematics of the experimental organometallic conductivity configurations: (a) Metal Vapor Synthesis (MVS) conducted in a Temescal high vacuum E-beam evaporator. (b) Photochemical reaction conducted in a glove box. Reprinted with permission from ref.58 (Copyright © 2016, American Chemical Society).

For the MVS method,[1, 2] metal sources are loaded in the electron beam chamber and for the photochemical method, the various metal-derivatives are dissolved in acetonitrile.[29] In-situ measurements are conducted by use of pre-wired electrical harnesses connecting the samples inside the E-beam chamber or the glove box using feed throughs to interface with a computer controlled Keithley 2700 multi-channel meter. Single layer CVD graphene (SLG) was first used to benchmark the interaction between a graphene surface and the bare transition metal chromium (Cr). Figure 3.17a shows that after evaporating 0.6 nm Cr on the top surface of transferred SLG on a glass substrate, the conductivity of SLG decreased fromσ = 1.15×10^4 S/cm to $\sigma = 4 \times 10^3$ S/cm, which is probably due to electron scattering from the Cr atoms on the surface of graphene.

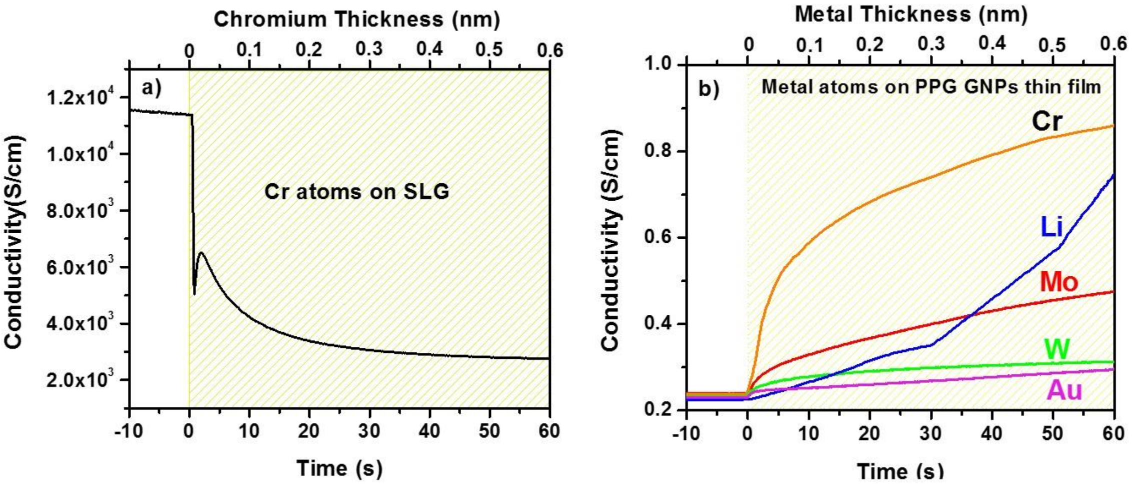

Figure 3.17 Conductivities of thin films on metal atom deposition from an E-beam evaporator: (a) Transferred single layer CVD Graphene as a function of metal thickness, (b) Conductivity of PPG GNP films as a function of metal deposition. Reprinted with permission from ref.58 (Copyright © 2016, American Chemical Society).

STM experiments indicate that Cr atoms are mobile on graphene surfaces and are attracted to defects and contaminants,[15] and the formation of clusters has been observed on graphitic surfaces[15] and carbon nanotubes.[21, 48, 49] In general, metals interact with graphitic surfaces in three distinct modalities: (a) physisorption in which there is minimal charge transfer or bonding, (b) chemisorption in which there are ionic bonding and charge transfer from the metal, and (c) covalent chemisorption in which there is appreciable rehybridization of the graphitic electronic structure. There is a fourth mode, which is less explores – mode (d) in which there is bis- hexahapto bonding to the graphitic surface with minimal rehybridization.[20] Thus for the present study we chose metals to represent the a, b and d classes: (a) Au, (b) Li, and (d) Cr, Mo, and W, in our studies of the PPG GNP films; the results of evaporating 0.6 nm of these metals on the surfaces of the PPG GNP films are shown in Figure 3.17b. The results for Au show a very weak effect, as expected for physisorption (a), in which there is the formation of a parallel conducting film. Previous studies indicate a very weak interaction between gold and graphitic surfaces.[1, 14-16] Lithium shows clear evidence of charge transfer with donation of electrons into the conduction band of the PPG GNPs and a strongly enhanced conductivity, providing clear evidence for mechanism (b), ionic chemisorption or doping. When 0.6 nm of Cr atoms was evaporated onto the PPG GNP thin films, the conductivity of the films increased from σ = 0.22 S/cm to 0.82 S/cm, which contrasts with the result obtained on evaporation of Cr on SLG sheets (Figure 3.17a). In the present instance it appears that the Cr atoms are able to bridge some of the nanoplatelets and to spontaneously form covalent bis(η^6-GNP)Cr bonds that enhance the conductivity. The observed conductivity enhancement amounts to about a factor of three to four which is very similar to the values observed on deposition of Cr on metallic (MT)-SWNT films.[2] The evaporation of the other group 6 metals, molybdenum (Mo) and tungsten (W) onto the PPG GNP films also enhances the conductivities, but the increases in conductivity are much more modest. Previously the same behavior was observed with SWNT films and the weaker effect of the larger group 6 metals was ascribed to the difficulty of inserting these atoms between the graphitic surfaces.[21] In Figure 3.18 we show the effect of irradiating the PPG GNP films after treatment with organometallic reagents; the lower traces of Figure 3.18a show the effect of the reagent alone and of a blank irradiation experiment. It is clear that the simultaneous application of the reagent together with UVC (254 nm) light is necessary to initiate the reaction.

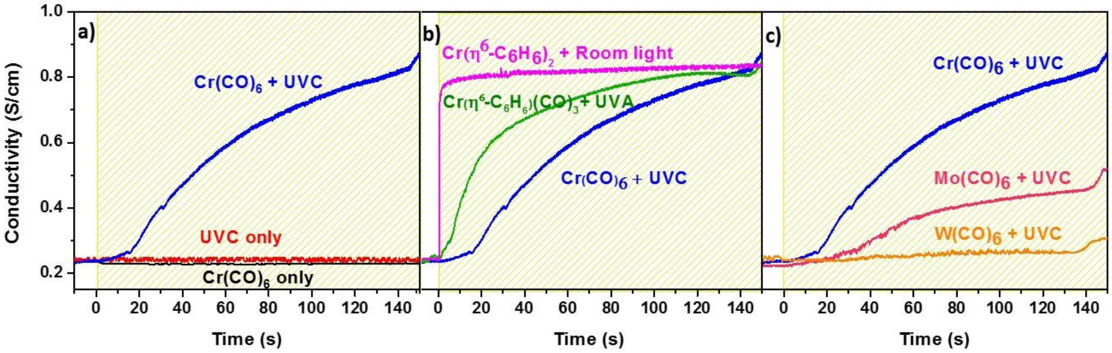

Figure 3.18 Evolution of PPG GNP thin film conductivities on photochemical reaction with organometallic reagents. Reprinted with permission from ref.58 (Copyright © 2016, American Chemical Society).

As may be seen in Figure 3.18a, irradiation with UVC light in the presence of $Cr(CO)_6$ leads to an increase in the conductivity of the PPG GNP thin film from $\sigma = 0.22$ S/cm to 0.9 S/cm, which is consistent with the MVS results (Figure 3.17). It is also clear that the same mechanism operates in the case of GNP and the SWNT films.[29]. Figure 3.18b compares the reactivity of the various chromium reagents with the PPG GNP films and it is apparent that the order of reactivity follows the sequence: $Cr(CO)_6$ < $Cr(\eta^6$-benzene$)(CO)_3$ < $Cr(\eta^6$-benzene$)_2$. Nevertheless the final conductivities are very close and it is apparent that the same final material composition is achieved irrespective of the organometallic reagent.

The $Mo(CO)_6$ and $W(CO)_6$ reagents also react with the PPG GNP thin films under UVC light but the final conductivities are less than in the case of the Cr compounds (Figure 3.18c).

The final conductivities of the new 3D cross-linked GNP materials synthesized by the photochemical route are fully consistent with those made by the MVS method (Figure 3.19), which adds further support to our proposed mechanism. To the best of our knowledge, this is the first report of new 3D graphene materials obtained from GNPs by constructive covalent bonding accompanied by an enhancement of the bulk electrical conductivity.

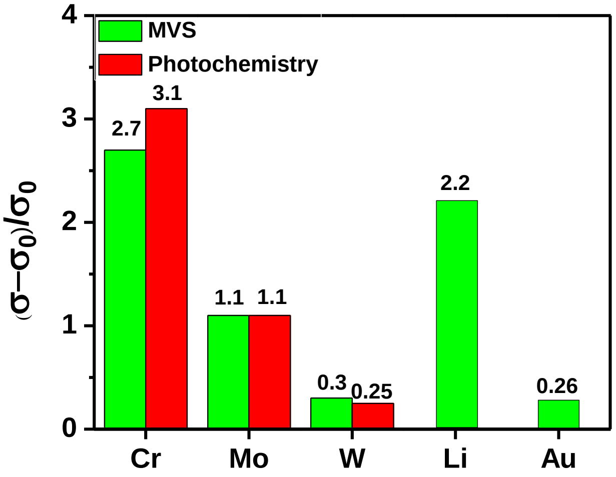

Figure 3.19 Conductivity enhancements of various metal complexes formed with PPG GNP thin films by MVS and by photochemistry of organometallic reagents. Reprinted with permission from ref.58 (Copyright © 2016, American Chemical Society).

3.2 Organometallic Chemistry of Aligned Carbon Nanotubes

3.2.1 Introduction

Single-walled carbon nanotubes are a promising material for advanced flexible electronics[50, 51] and wearable devices.[52] However, the performance of the SWNT thin film based devices has been restricted by the low density of SWNTs[53] and large junction resistance compared to individual SWNTs, especially for semiconducting SWNTs.[29, 54] Recent advances in the spontaneous alignment of SWNTs by filtrations provide a low cost tool for the preparation of densely packed and globally aligned SWNT films of arbitrary thickness on a large (wafer) scale,[55] which could reduce the number of junctions and improve the conductivity along the alignment direction at the expense of sacrificing the conductivity perpendicular to the SWNTs. We have shown that bishexahapto bonds formed between transition metal and SWNTs [(η^6-SWNT)-metal-(η^6-SWNT)] in the junction of random networks can increase the electrical conductivity of Sc-SWNT thin film dramatically due to a constructive rehybridization nature. In this work, we applied the same chemistry to interconnect sidewalls of parallel SWNTs (Figure 3.20a) and two ends of series SWNTs (Figure 3.20b), which preserves the unique electronic structure and thus the remarkable optical, electronic and mechanical properties of individual SWNTs while extend its dimensionality from 1D to 2D and 3D. Furthermore, for the first time, we experimentally realized bishexahapto bonds with aligned carbon surfaces, which may contribute to the fabrication of carbon based organometallic spintronic[25] and magnetic nanodevices.[56]

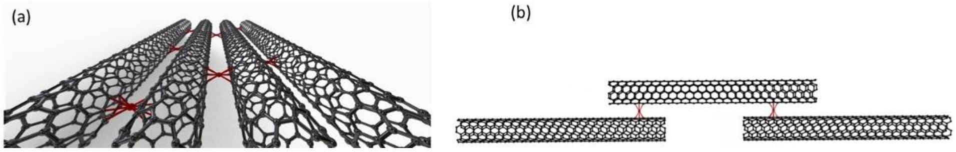

Figure 3.20 Schematic of the formation of chromium complexes with adjacent carbon nanotubes in perpendicular (a) and parallel (b) configurations.

3.2.2 Alignment of carbon nanotubes

The alignment of SWNTs was achieved using a process reported in the literature.[55] However, we used aqueous suspensions of semiconducting carbon nanotubes (Nanointegris Inc.-IsoNanotubes-S 99%) as the stock solution with a concentration of 10 ug/ml. The stock solution was diluted into 1.5 ug/ml with nanopure water and then we filtrated the diluted solution using a polycarbonate, track-etched screen filter (pore size 100 nm; Isopore™ Membrane Filters, EMD Millipore) at a filtration speed of one droplet per 40 s. Additional vacuum was applied overnight to dry the membrane after the end of the filtration. The film was taken out from the filtration system after the top of the membrane was completely dried.

3.2.3 Results and Discussions

The AFM image shown in Figure 3.21a demonstrates that the Sc-SWNTs are well aligned and comprised of small bundle size. The aligned Sc-SWNT thin film was transferred to an SiO_2/Si substrate with pre-patterned electrodes. Photolithography and plasma etching was used to patterned the aligned Sc-SWNT thin films. The substrates was designed with pre-patterned gold contacts that were positioned in various angles ($0^\circ \sim 90^\circ$, Figure 3.21b) in order to contact the aligned nanotubes in an array with $0^\circ \sim 90^\circ$angle between the contact surface and nanotube axis. In this work, we explored organometallic chemistry of Cr atoms with aligned perpendicularly and parallel Sc-SWNTs (Figure 3.21c) with regard to the direction of the current flow.

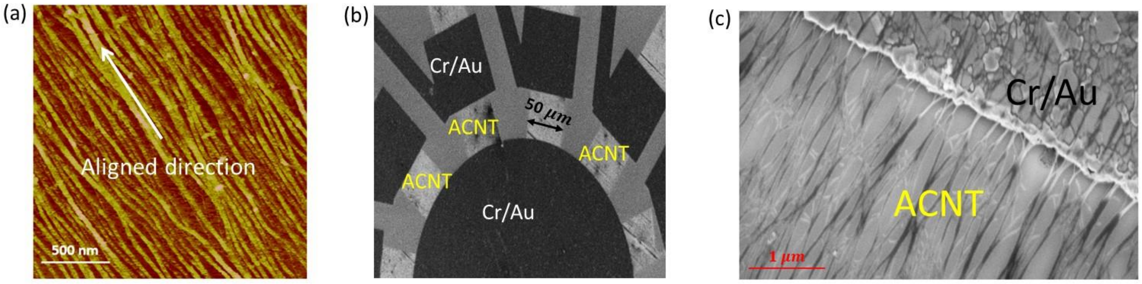

Figure 3.21 (a) AFM image of aligned semiconducting single-walled carbon nanotubes deposited on SiO_2/Si substrate (300 nm). (b) SEM image of devices with various current flow directions. (c) SEM image of a parallel Aligned Sc-SWNT device.

The alignment of the Sc-SWNT thin films (nominal film thickness - 2 nm) was further characterized by Raman spectroscopy. The G band shows two main peaks, G+ and G- (Figure 3.22a). Also the G-band shows a Lorentzian lineshape, characteristic of semiconducting SWNTs.[57] Moreover, the intensities of the D, G and 2D peaks show a prominent dependence on the angle between the laser light polarization direction and SWNT alignment: along the individual SWNT (θ), perpendicular to the individual SWNTs ($\theta + 90^\circ$). This dependence is illustrated in

Figure 3.22a and it indicates the high degree of alignment of our SWNT films.[55] The relationship between the intensity of the G peak and θ is shown in Figure 3.22b; the intensity of G peak follows a sinusoidal function of θ, which corresponds to the continuous change in the alignment of SWNTs.

The temperature dependence of these two types of devices also shows a strong anisotropy as shown in Figure 3.22c. At room temperature the ratio of the resistances of the perpendicular and parallel Sc-SWNT films is in the range of 5~10. The perpendicular configurations shows a more prominent temperature dependence, which is attributed to the high contact resistance between the sidewalls of adjacent parallel carbon nanotubes. Because of the large size of the device channel ($50\ \mu\text{m} \times 50\ \mu\text{m}$), even the films comprised of nanotubes aligned in the parallel configuration, contain junctions between the ends of two individual tubes as shown in Figure 3.20b. However, because of the high length to width ratio (~ 1,000,000 : 1) of SWNTs the contribution of the junctions in the parallel films to the overall film resistance is less dominant that in the films comprised of perpendicular SWNTs, where the carriers have to hop or tunnel between adjacent parallel SWNTs nearly every 2 nanometers.

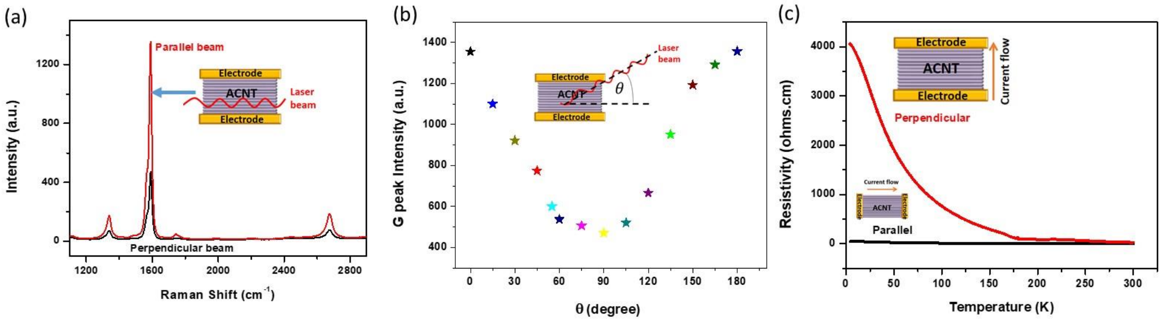

Figure 3.22 (a) Raman spectra of aligned semiconducting single-walled carbon nanotubes (Sc-SWNTs): incident laser beam is parallel (red) and perpendicular (black) to the nanotube alignment direction. (b) G peak intensity versus the angle θ between nanotube alignment direction and laser incident beam direction. (c) Temperature dependence of resistance of perpendicular (red) and parallel (black) aligned Sc-SWNTs.

The devices were annealed at 300 ℃ for 8 hours in vacuum before transfer to the chamber of e-beam evaporator. The resistances of the devices were monitored in-situ during the exposure of metals as reported in our previous work (see above).[58] As discussed above the interaction between metals and carbon materials are categorized into four types: (a) physisorption (Au), (b) doping (Li), (c) covalent chemisorptions (Ti) and (d) constructive covalent bis-hexahapto bonding (Cr). In this work, we focus on the interactions that can enhance the electrical transport properties of SWNT thin films: (b) and (d). The results of the conductivity change after deposition of 1 nm of the representative metals – Li and Cr, are shown in Figure 3.23. Lithium is a well- known electron donor, which is expected to donate electrons to the conduction band of SWNTs and thus increase the conductivity of the individual SWNTs with negligible effect on the contact resistance between adjacent carbon tubes.

As shown in Figure 3.23a, lithium increased the conductivity of the parallel Sc-SWNTs ($\sigma_{//}$) by a factor of 263, from 0.55 S/cm to 145 S/cm, while for the perpendicular configuration the conductivity ($\sigma\perp$) of the aligned SWNT device remains nearly unchanged ~ 0.06 S/cm. However, evaporation of Cr (1 nm) increased the perpendicular conductivity $\sigma\perp$ of the aligned SWNT device by a factor of 1036, and the parallel conductivity $\sigma_{//}$ by a factor of 73 (Figure 3.23b). This is a strong evidence for the formation of bishexahapto bonds between the sidewalls of adjacent aligned SWNTs (Figure 3.20a), which provide efficient electron pathways and increase the perpendicular conductivity $\sigma\perp$ dramatically.

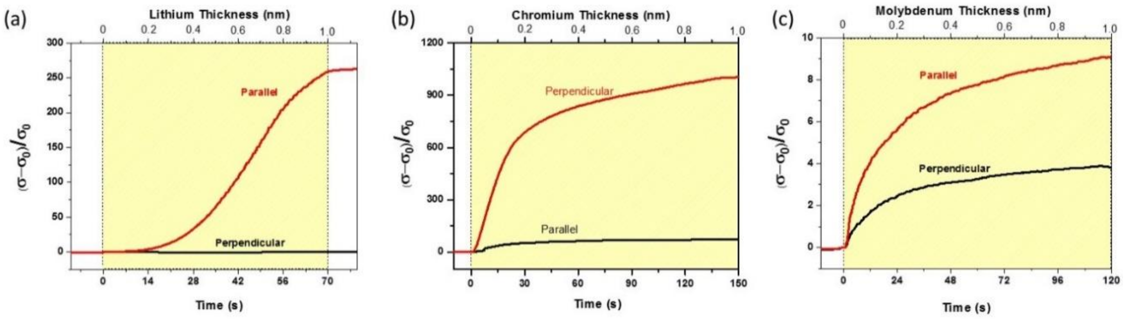

Figure 3.23 Effect of metal deposition on the electrical conductivity of aligned carbon nanotube thin film devices. (a) The parallel conductivity increased 260 times upon 1 nm deposition of Li in contrast with the flat perpendicular conductivity curve. (b) The perpendicular conductivity increased 1006 times upon 1 nm deposition of Cr in contrast with 77 times increase for parallel conductivity. (c) The parallel and perpendicular conductivities increased 9 times and 3.8 times, respectively, upon 1 nm deposition of Mo atoms inside E-beam Evaporator.

In the instance of parallel conductivity, the series of individual SWNTs can also be bridged together, however, due to the high length to diameter ratio of SWNTs, the available spots that can be fitted with Cr atoms are significantly less (Figure 3.20b), which results in some enhancement of the parallel conductivity. When we tried to evaporate another Group VI transition metals, such as Mo, both parallel and perpendicular conductivities were enhanced by only a factor of less than 10 (Figure 3.23c). This confirms previous results obtain with random SWNT networks, and it indicates that it is difficult to insert larger diameter transition atoms between graphitic surfaces restricted by the van der Waals distance. [1, 58].

3.2.4 Conclusion

In conclusion, we increased the dimensions of aligned carbon nanotubes from 1D to 3D by organometallic chemistry and demonstrated the effectiveness of constructive covalent bishexahapto bonds in improving the electrical properties of aligned carbon nanotubes, which is essential for accelerating the commercialization of SWNTs based electronics. Besides, macroscale aligned bishexahapto bonds were achieved by inserting Cr atoms between the sidewalls of aligned SWNTs, which will facilitate the development of novel magnetic devices, spintronics, and selective catalysts.

References

1. Wang, F.; Itkis, M. E.; Bekyarova, E.; Tian, X.; Sarkar, S.; Pekker, A.; Kalinina, I.; Moser, M.; Haddon, R. C., Effect of First Row Transition Metals on the Conductivity of Semiconducting Single-Walled Carbon Nanotube Networks. Appl. Phys. Lett. 2012, 100, 223111.

2. Tian, X.; Moser, M. L.; Pekker, A.; Sarkar, S.; Ramirez, J.; Bekyarova, E.; Itkis, M. E.; Haddon, R. C., Effect of Atomic Interconnects on Percolation in Single-Walled Carbon Nanotube Thin Film Networks. Nano Lett. 2014, 14, 3930-3937.

3. Geim, A. K.; Novoselov, K. S., The Rise of Graphene. Nat. Mater. 2007, 6, 183-191.

4. Sarkar, S.; Bekyarova, E.; Niyogi, S.; Haddon, R. C., Diels-Alder Chemistry of Graphite and Graphene: Graphene as Diene and Dienophile. J. Am. Chem. Soc. 2011, 133, 3324-3327.

5. Wang, Y.; Li, Z.; Wang, J.; Li, J.; Lin, Y., Graphene and Graphene Oxide: Biofunctionalization and Applications in Biotechnology. Trends in Biotechnology 2011, 29, 205-212.

6. Berger, C.; Song, Z.; Li, T.; Li, X.; Ogbazghi, A. Y.; Feng, R.; Dai, Z.; Marchenkov, A. N.; Conrad, E. H.; First, P. N.; de Heer, W. A., Ultrathin Epitaxial Graphite: 2d Electron Gas Properties and a Route toward Graphene-Based Nanoelectronics. J. Phys. Chem. B 2004, 108, 19912-19916.

7. Chen, Z. H.; Lin, Y. M.; Rooks, M. J.; Avouris, P., Graphene Nano-Ribbon Electronics. Physica E 2007, 40, 228-232.

8. Liu, C.-H.; Chang, Y.-C.; Norris, T. E.; Zhong, Z., Graphene Photodetectors with Ultra-Broadband and High Responsivity at Room Temperature. Nature Nanotech. 2014, 9, 273-278.

9. Torrisi, F.; Hasan, T.; Wu, W. P.; Sun, Z. P.; Lombardo, A.; Kulmala, T. S.; Hsieh, G. W.; Jung, S. J.; Bonaccorso, F.; Paul, P. J.; Chu, D. P.; Ferrari, A. C., Inkjet-Printed Graphene Electronics. ACS Nano 2012, 6, 2992-3006.

10. Nair, R. R.; Sepioni, M.; Tsai, I.-L.; Lehtinen, P. O.; Keinonen, J.; Krasheninnikov, A. V.; Thomson, T.; Geim, A. K.; Grigorieva, I. V., Spin-Half

Paramagnetism in Graphene Induced by Point Defects. Nature Phys. 2012, 8, 199-202.

11. Charlier, J. C.; Arnaud, L.; Avilov, I. V.; Delgado, M.; Demoisson, F.; Espinosa, E. H.; Ewels, C. P.; Felten, A.; Guillot, J.; Ionescu, R.; Leghrib, R.; Llobet, E.; Mansour, A.; Migeon, H. N.; Pireaux, J. J.; Reniers, F.; Suarez-Martinez, I.; Watson, G. E.; Zanolli, Z., Carbon Nanotubes Randomly Decorated with Gold Clusters: From Nano(2)Hybrid Atomic Structures to Gas Sensing Prototypes. Nanotechnology 2009, 20, 375501.

12. Sargolzaei, M.; Gudarzi, F., Magnetic Properties of Single 3d Transition Metals Adsorbed on Graphene and Benzene: A Density Functional Theory Study. J. App. Phys. 2011, 110, 064303.

13. Sevincli, H.; Topsakal, M.; Durgun, E.; Ciraci, S., Electronic and Magnetic Properties of 3d Transition-Metal Atom Adsorbed Graphene and Graphene Nanoribbons. Phys. Rev. B 2008, 77, 195434.

14. Chan, K. T.; Neaton, J. B.; Cohen, M. L., First-Principles Study of Adatom Adsorption on Graphene. Phys. Rev. B 2008, 77, 235430.

15. Zan, R.; Bangert, U.; Ramasse, Q.; Novoselov, K. S., Metal-Graphene Interaction Studied Via Atomic Resolution Scanning Transmission Electron Microscopy. Nano. Lett. 2011, 11, 1087-1092.

16. Liu, X.; Wang, C.-Z.; Hupalo, M.; Lin, H.-Q.; Ho, K.-M.; Tringides, M. C., Metals on Graphene: Interactions, Growth Morphology, and Thermal Stability. Crystals 2013, 3, 79-111.

17. Dresselhaus, M. S.; Dresselhaus, G., Intercalation Compounds of Graphite. In Advances in Physics, Martin, D. H., Ed. Taylor & Francis Ltd: London, 1981; Vol. 30, pp 139-326.

18. Sarkar, S.; Niyogi, S.; Bekyarova, E.; Haddon, R. C., Organometallic Chemistry of Extended Periodic P-Electron Systems: Hexahapto-Chromium Complexes of Graphene and Single-Walled Carbon Nanotubes. Chem. Sci. 2011, 2, 1326-1333.

19. Sarkar, S.; Moser, M. L.; Tian, X.; Zhang, X. J.; Al-Hadeethi, Y. F.; Haddon, R. C., Metals on Graphene and Carbon Nanotube Surfaces: From Mobile Atoms to Atomtronics to Bulk Metals to Clusters and Catalysts. Chem. Mater. 2014, 26, 184-195.

20. Bekyarova, E.; Sarkar, S.; Wang, F.; Itkis, M. E.; Kalinina, I.; Tian, X.; Haddon, R. C., Effect of Covalent Chemistry on the Electronic Structure and Properties of Carbon Nanotubes and Graphene. Acc. Chem. Res. 2013, 46, 65-76.

21. Kalinina, I.; Bekyarova, E.; Sarkar, S.; Wang, F.; Itkis, M. E.; Tian, X.; Niyogi, S.; Jha, N.; Haddon, R. C., Hexahapto-Metal Complexes of Single-Walled Carbon Nanotubes. Macromol. Chem. Phys. 2012, 213, 1001-1019.

22. Moser, M. L.; Tian, X.; Pekker, A.; Sarkar, S.; Bekyarova, E.; Itkis, M. E.; Haddon, R. C., Hexahapto-Lanthanide Interconnects between the Conjugated Surfaces of Single-Walled Carbon Nanotubes. Dalton Trans. 2014, 43, 7379-7382.

23. Moser, M. L.; Pekker, A.; Tian, X.; Bekyarova, E.; Itkis, M. E.; Haddon, R. C., Effect of Lanthanide Metal Complexation on the Properties and Electronic Structure of Single-Walled Carbon Nanotube Films. ACS Appl. Mat. & Interfaces 2015, 7, 28013-28018.

24. Li, E. Y.; Marzari, N., Improving the Electrical Conductivity of Carbon Nanotube Networks: A First-Principles Study. ACS Nano 2011, 5, 9726-9736.

25. Avdoshenko, S. M.; Ioffe, I. N.; Cuniberti, G.; Dunsch, L.; Popov, A. A., Organometallic Complexes of Graphene: Toward Atomic Spintronics Using a Graphene Web. ACS Nano 2011, 5, 9939-9949.

26. Dai, J.; Zhao, Y.; Wu, X.; Zeng, X. C.; Yang, J., Organometallic Hexahapto-Functionalized Graphene: Band Gap Engineering with Minute Distortion to the Planar Structure. J. Phys. Chem. C 2013, 117, 22156-22161.

27. Ketolainen, T.; Havu, V.; Puska, M. J., Enhancing Conductivity of Metallic Carbon Nanotube Networks by Transition Metal Adsorption. J. Chem. Phys. 2015, 142, 054705.

28. Gloriozov, I. P.; Marchal, R.; Saillard, J.-Y.; Oprunenko, Y. F., Chromium Tricarbonyl and Chromium Benzene Complexes of Graphene, Their Properties, Stabilities, and Inter-Ring Haptotropic Rearrangements - a Dft Investigation. Eur. J. Inorg. Chem. 2015, 2015, 250-257.

29. Pekker, A.; Chen, M.; Bekyarova, E.; Haddon, R. C., Photochemical Generation of Bis-Hexahapto Chromium Interconnects between the Graphene Surfaces of Single-Walled Carbon Nanotubes. Mater. Horiz. 2015, 2, 81-85.

30. Perutz, R. N.; Turner, J. J., Photochemistry of the Group 6 Hexacarbonyls in Low-Temperature Matrices. Iii. Interaction of the Pentacarbonyls with Noble Gas and Other Matrices. J. Am. Chem. Soc 1975, 97, 4791 - 4800.

31. Perutz, R. N.; Turner, J. J., Photochemistry of the Group 6 Hexacarbonyls in Low-Temperature Matrices. Iv. Tetracarbonylmolybdenum and Tricarbonylmolybdenum. J. Am. Chem. Soc 1975, 97, 4800 - 4804.

32. Csanyi, G.; Littlewood, P. B.; Nevidomskyy, A. H.; Pickard, C. J.; Simons, B. D., The Role of the Interlayer State in the Electronic Structure of Superconducting Graphite Intercalated Compounds. Nature Phys. 2005, 1, 42-45.

33. Krasheninnikov, A. V.; Lehtinen, P. O.; Foster, A. S.; Pyykko, P.; Nieminen, R. M., Embedding Transition-Metal Atoms in Graphene: Structure, Bonding, and Magnetism. Phys. Rev. Let. 2009, 102, 126807.

34. Zan, R.; Bangert, U.; Ramasse, Q.; Novoselov, K. S., Interaction of Metals with Suspended Graphene Observed by Transmission Electron Microscopy. J. Phys. Chem. Lett. 2012, 3, 953-958.

35. Biswas, S.; Drzal, L. T., A Novel Approach to Creat a Highly Ordered Monolayer Film of Graphene Nanosheets at the Liquid-Liquid Interface. Nano Lett. 2009, 9, 167-72.

36. Lotya, M.; Hernandez, Y.; King, P. J.; Smith, R. J.; Nicolosi, V.; Karlsson, L. S.; Blighe, F. M.; De, S.; Wang, Z. M.; McGovern, I. T.; Duesberg, G. S.; Coleman, J. N., Liquid Phase Production of Graphene by Exfoliation of Graphite in Surfactant/Water Solutions. J. Am. Chem. Soc 2009, 131, 3611-3620.

37. Sun, X.; Ramesh, P.; Itkis, M. E.; Bekyarova, E.; Haddon, R. C., Dependence of the Thermal Conductivity of Two-Dimensional Graphite Nanoplatelet-Based Composites on the Nanoparticle Size Distribution. J. Phys.: Condens. Matter 2010, 22, 334216.

38. Biswas, S.; Fukushima, H.; Drzal, L. T., Mechanical and Electrical Property Enhancement in Exfoliated Graphene Nanoplatelet/Liquid Crystalline Polymer Nanocomposites. Composites Part a-Applied Science and Manufacturing 2011, 42, 371-375.

39. Tian, X.; Sarkar, S.; Moser, M. L.; Wang, F.; Pekker, A.; Bekyarova, E.; Itkis, M. E.; Haddon, R. C., Effect of Group 6 Transition Metal Coordination on the Conductivity of Graphite Nanoplatelets. Mater. Lett. 2012, 80, 171-174.

40. Novoselov, K. S.; Geim, A. K.; Morozov, S. V.; Jiang, D.; Zhang, Y.; Dubonos, S. V.; Grigorieva, I. V.; Firsov, A. A., Electric Field Effect in Atomically Thin Carbon Films. Science 2004, 306, 666-669.

41. Lin, W. H.; Chen, T. H.; Chang, J. K.; Taur, J. I.; Lo, Y. Y.; Lee, W. L.; Chang, C. S.; Su, W. B.; Wu, C. I., A Direct and Polymer-Free Method for Transferring Graphene Grown by Chemical Vapor Deposition to Any Substrate. ACS Nano 2014, 8, 1784-1791.

42. Vanier, N. In Properties of Plasma Produced Graphene Nanonplatelets and Electrical Conductivity Applications, IDTechEx, Santa Clara, CA, 2014; Santa Clara, CA, 2014.

43. Khan, U.; O'Neill, A.; Lotya, M.; De, S.; Coleman, J. N., High-Concentration Solvent Exfoliation of Graphene. Small 2010, 6, 864-871.

44. Lotya, M.; King, P. J.; Khan, U.; De, S.; Coleman, J. N., High-Concentration, Surfactant-Stablized Graphene Dispersions. ACS Nano 2010, 4, 3155-3162.

45. Niyogi, S.; Bekyarova, E.; Itkis, M. E.; Zhang, H.; Shepperd, K.; Hick, J.; Sprinkle, M.; Berger, C.; Lau, C. N.; de Heer, W. A.; Conrad, E. H.; Haddon, R. C., Spectroscopy of Covalently Functionalized Graphene. Nano. Lett. 2010, 10, 4061–4066.

46. de Heer, W. A.; Berger, C.; Wu, X.; Sprinkle, M.; Hu, Y.; Ruan, M.; Stroscio, J.; First, P. N.; Haddon, R. C.; Piot, B.; Faugeras, C.; Potemski, M.; Moon, J.-S., Epitaxial Graphene Electronic Structure and Transport. J. Phys. D: Appl. Phys. 2010, 43, 374007.

47. Tian, X.; Sarkar, S.; Pekker, A.; Moser, M. L.; Kalinina, I.; Bekyarova, E.; Itkis, M. E.; Haddon, R. C., Optical and Electronic Properties of Thin Films and Solutions of Functionalized Forms of Graphene and Related Carbon Materials. Carbon 2014, 72, 82-88.

48. Kalinina, I.; Bekyarova, E.; Wang, Q.; Al-Hadeethi, Y. F.; Zhang, X. J.; Al-Agel, F.; Al-Marzouki, F.; Yaghmour, S.; Haddon, R. C., Formation of Transition Metal Cluster Adducts on the Surface of Single-Walled Carbon Nanotubes: Hrtem Studies. Fuller. Nanotub. Carb. N. 2014, 22, 47-53.

49. Kalinina, I.; Al-Hadeethi, Y. F.; Bekyarova, E.; Zhao, C.; Wang, Q.; Zhang, X.; Al-Zahrani, A.; Al-Agel, F.; Al-Marzouki, F.; Haddon, R. C., Solution-Phase Synthesis of Chromium-Functionalized Single-Walled Carbon Nanotubes. Mater. Lett. 2015, 142, 312-316.

50. Kumar, S.; Cola, B. A.; Jackson, R.; Graham, S., A Review of Carbon Nanotube Ensembles as Flexible Electronics and Advanced Packaging Materials. J Electron Pack 2011, 133, 020906.

51. Park, S.; Vosguerichian, M.; Bao, Z. N., A Review of Fabrication and Applications of Carbon Nanotube Film-Based Flexible Electronics. Nanoscale 2013, 5, 1727-1752.

52. Yamada, T.; Hayamizu, Y.; Yamamoto, Y.; Yomogida, Y.; Lzadi-Najafabadi, A.; Futaba, D. N.; Hata, K., A Stretchable Carbon Nanotube Strain Sensor for Human-Motion Detection. Nature Nanotech. 2011, 6, 296.

53. Park, S.; Pitner, G.; Giri, G.; Koo, J. H.; Park, J.; Kim, K.; Wang, H.; Sinclair, R.; Wong, H. S. P.; Bao, Z., Large-Area Assembly of Densely Aligned Single-Walled Carbon Nanotubes Using Solution Shearing and Their Application to Field-Effect Transistors. Adv. Mater. 2015, 27, 2656-2662.

54. Fuhrer, M. S.; Nygard, J.; Shih, L.; Forero, M.; Yoon, Y.-G.; Mazzoni, M. S. C.; Choi, H. J.; Ihm, J.; Louie, S. G.; Zettl, A.; McEuen, P. L., Crossed Nanotube Junctions. Science 2000, 288, 494-497.

55. He, X. W.; Gao, W. L.; Xie, L. J.; Li, B.; Zhang, Q.; Lei, S. D.; Robinson, J. M.; Haroz, E. H.; Doorn, S. K.; Wang, W. P.; Vajtai, R.; Ajayan, P. M.; Adams, W. W.; Hauge, R. H.; Kono, J., Wafer-Scale Monodomain Films of Spontaneously Aligned Single-Walled Carbon Nanotubes. Nature Nanotechnology 2016, 11, 633-638.

56. Samouhos, S.; McKinley, G., Carbon Nanotube-Magnetite Composites, with Applications to Developing Unique Magnetorheological Fluids. J. Fluids Eng. 2007, 129, 429-437.

57. Dresselhaus, M. S.; Dresselhaus, G.; Saito, R.; Jorio, A., Raman Spectroscopy of Carbon Nanotubes. Phys. Rep 2005, 409, 47-99.

58. Chen, M.; Tian, X.; Li, W.; Bekyarova, E.; Li, G.; Moser, M.; Haddon, R. C., Application of Organometallic Chemistry to the Electrical Interconnection of Graphene Nanoplatelets. Chem. Mater. 2016, 28, 2260-2266.

Chapter 4. Diels Alder Chemistry of Graphene

As discussed in Chapter 1.1, graphene is one of the most promising materials for the next generation electronics and spintronics due to its excellent transport properties. Because the conduction band touches the valence band in the momentum space, graphene does not have a band gap and this prevents its use as the building material for conventional transistors. However chemistry provides a way to controllably manipulate the electronic structure of graphene and potentially openes a bandgap by converting sp^2 carbon to sp^3 carbon. It has been reported that Diels Alder chemistry could be used to functionalize fullerenes[1, 2] and carbon nanotubes.[3-5]. However, graphene's basal plane is comprised of aromatic hydrocarbons with stabile and inert π conjugation without any curvature, which makes it thermodynamically stable and hard to be functionalized by chemical reactions.

4.1. Introduction

Our group has reported[6] and rationalized[7] the Diels-Alder chemistry of graphene based on the orbital symmetry and the frontier molecular orbital (FMO) theory. However, it is still not clear whether the Diels Alder chemistry of graphene occurs only at the graphene edges or the basal plane also takes part in the reaction.[8, 9] In this work, we characterize the properties of DA-graphene adduct with semi-quantitatively Raman spectroscopy, and measured the temperature dependence and magnetoresistance of product using Physical Properties Measurement System (PPMS).

4.2 Experimental Section

CVD Graphene Single layer CVD graphene grown on Cu foil was purchased from Graphene supermarket, and transferred onto 300 nm SiO2/Si substrate with the CAT method (Chapter 2.3.1).

Epigraphene Epigraphene grown on SiC (4.5 mm x 3.5 mm) on the C side with an average thickness of 9 layers was provided by Prof. Walt de Heer (Georgia Institute of Technology).

XG$_{\mathbf{flake}}$ Single layer graphene flakes were exfoliated from Kish graphite with scotch tape by the micromechanical exfoliation technique.

Raman spectroscopy

Raman spectra were recorded with a Nicolet Almega XR Dispersive Raman microscope using 532 nm laser excitation and 25% power source.

Temperature dependence of resistance and magnetoresistance measurements Four in-line gold contacts (10 nm Cr, 100 nm Au; evenly space with 3 gaps of 1 mm) were deposited by e-beam evaporation on the Epigraphene with a shadow mask. The devices were loaded into the chamber of Physical

Property Measurement System (PPMS, Quantum Design International, USA) before and after reaction. The temperature was decreased from 300 K to 2 K and the magnetic field swept from -9 T to 9 T at 300 K, 100 K, and 2 K respectively.

Reaction Conditions

In a typical reaction, 100 mg naphthazarin was dissolved in 50 mL p-xylene (~ 0.01 M), and then the solution was added to a 100 mL flask reactor where graphene devices were placed on the bottom. The reaction was performed in continuous argon flow for 2 days at room temperature. After 2 days, the devices were taken out and washed with acetone, isopropanol and methanol before characterization.

4.3 Results and Discussion

Our group demonstrated that graphene can function as both diene and dienophile.[6] In the current work, graphene functions as a diene that reacts with naphthazarin (dienophile) at room temperature (Figure4.1).

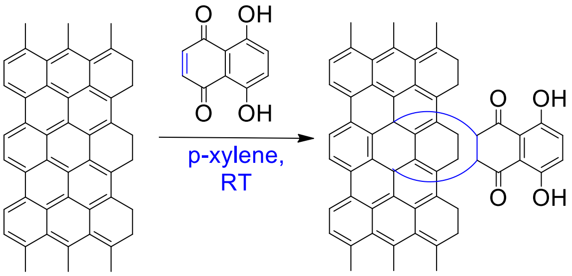

Figure 4.1. Schematic of the Diels Alder reaction between naphthazarin and graphene.

Graphene is only one-atomic thick and therefore its electronic structure can be easily affected by the substrate.[10-12] We compared the reactivity of a single layer graphene (SLG) on different substrates, namely, tape exfoliated graphene on SiO_2/Si substrate, CVD graphene on quartz and epitaxial graphene on SiC substrate. A reference experiment was conducted with a SLG device immersed in a reactor with solvent (*p*-xylene, 50 mL) under continuous argon flow for 2 days. As shown in Figure 4.2a, the Raman spectrum shows no change, indicating that the solvent *p*-xylene has no prominent effect on graphene under this experimental condition. In a typical experiment, naphthazarin (0.01 M dissolved in *p*-xylene) was added to the reactor that contained the graphene film deposited on a substrate. To evaluate the reaction progress we analyzed the graphene samples with Raman spectroscopy. Before reaction, the Raman spectra of pristine graphene (single layer Epigrahene, CVD graphene and XG_{flake}) shows small or no D peak as illustrated in Figure4.2b, suggesting an intact sp^2

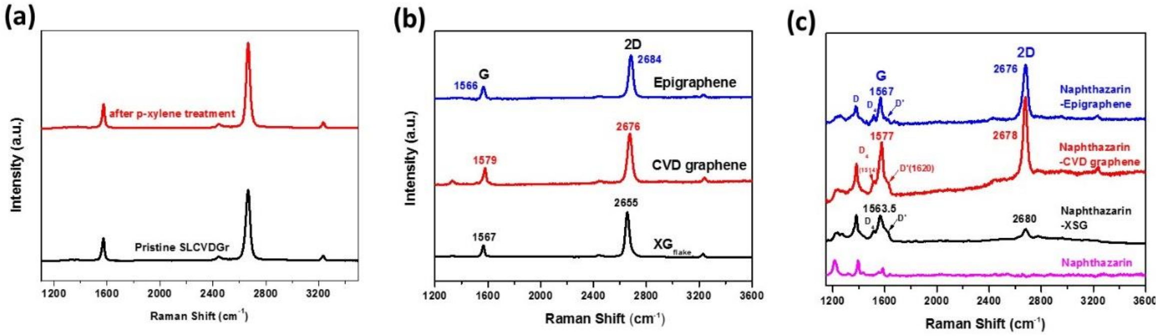

Figure 4.2. (a) Raman spectra of CVD single layer graphene before (black) and after immersion in p-xylene solvent for two days (red). Raman spectra of single layer Epigraphene, CVD graphene and scotch tape exfoliated graphene (b) before and (c) after Diels Alder reaction with naphthazarin.

conjugated carbon surface. After two days the reaction was stopped, the graphene sample was removed from the reaction mixture, washed with acetone and isopropanol, and characterized.

The degree of functionalization was followed with Raman spectroscopy as shown in Figure 4.2c. It was observed that the 2D- to G-band ratio has decreased after reaction; similar behavior has been observed in covalently functionalized graphene.[6, 13] Furthermore, the intensity of the D band increased, which is assigned to the break of symmetry of the six sp^2 carbon rings due to the introduction of defects by cycloaddition of naphthazarin molecules. From the reduced intensity of the 2D band, we estimate the reactivity of graphene on different substrates towards naphthazarin, which follows the order: XSG on SiO_2/Si > CVD graphene on quartz and Epigraphene on SiC. Interestingly, a new band at 1514 cm^{-1} (D_4 band)[14] was observed, which has been reported to be a consequence of geometrical constraints that occur at graphene functionalization in the range between ~0.5% and ~2%.[14].

The chemical modification modified the electronic properties of the functionalized graphene. Figure4.3 shows the four point resistance measurement of pristine single layer Epigraphene and the Naphthazarin-Epigraphene adduct. The resistance of the Naphtazarin-Epigrahene is ~2.2 times higher than that of pristine Epigraphene, which is due to defects introduced by the functionalization as discussed above. The temperature dependence of resistance of Epigraphene exhibits a weak nonmetallic behavior with a slight increase of the resistance as the temperature decreases.

The nonmetallic behavior in the transport properties of macroscopic pristine epigraphene samples have been observed previously and are due to a variety of factors including the inhomogeneity in the graphene growth over the macroscopic SiC wafers, that affects the point defects and the concentration of charge carriers especially at the ridges, due to misalignment of the π-orbitals.[15] All of these factors influence the scattering rate, as demonstrated by Hall measurements on large area EG wafers.[16]

The Naphthazarin-Epigraphene adduct shows a much stronger temperature dependence of the resistance over the whole temperature range, which may be associated with an increased tunneling between functionalized graphene regions. This type of behavior may also be a sign of a weak localization,[17-19] which suggests that the naphthazarin functionalization starts to transform the epigrahene from a semimetal to a semiconductor by changing more sp^2 carbons to sp^3 carbons.

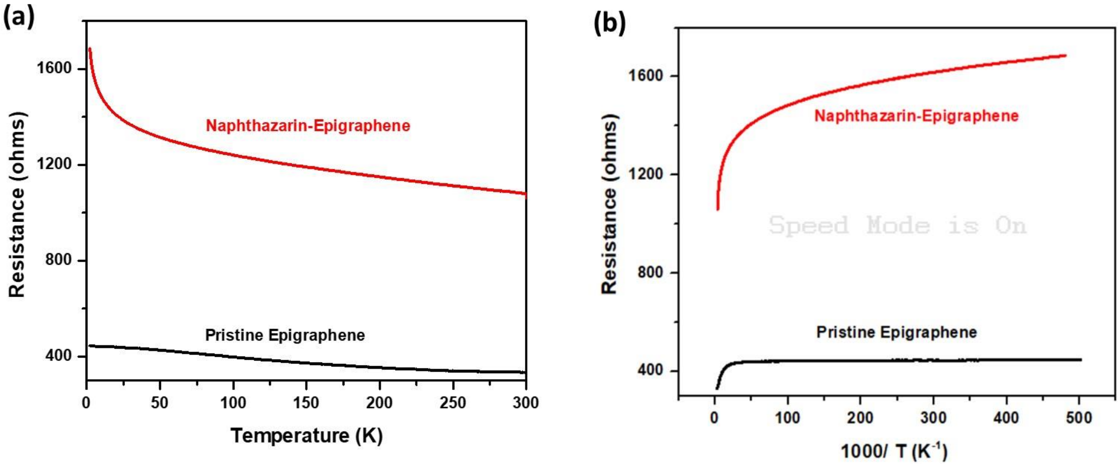

Figure 4.3. Temperature dependence of resistance of pristine Epigraphene and Naphthazarin-Epigraphene adduct presented as (a) linear (b) Arrhenius plot.

Weak localization (WL) of pristine Epigraphene (Figure 4.4b) at low temperature under small magnetic field has been reported in the literature.[20, 21] As the magnetic field increases beyond 100 Oe, a positive magnetoresistance over the temperature range from 2 K to 300 K (Figure 4.4a) has been observed due to the weak antilocalization effect (WAL). However, after functionalized by naphthazarin via Diels Alder chemistry, the device shows a large negative magnetoresistance at 2 K, a decent negative magnetoresistance at 100 K and a reduced positive magnetoresistance at 300 K as shown in Figure 4.4c. This behavior is similar to that observed in nitrophenyl functionalized epigraphene by radical addition chemistry.[21] This phenomenon has been ascribed to the quenching of WAL by functionalization process, which further supports the formation of covalent bonds between naphthazarin and the graphene lattice of Epigraphene.

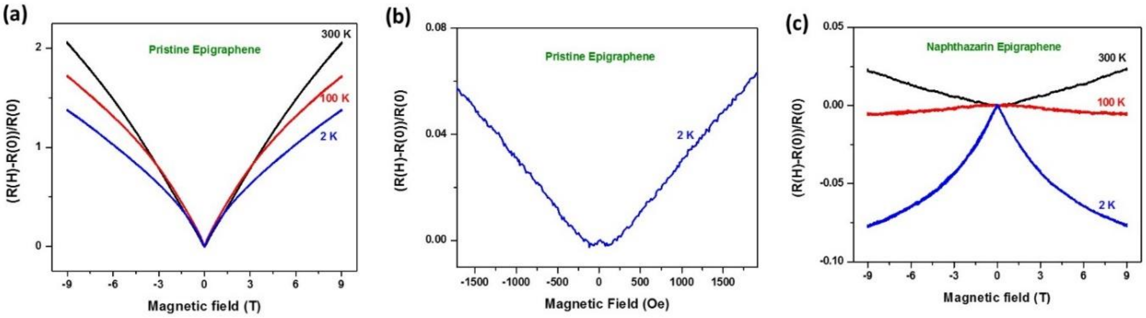

Figure 4.4. Magnetoresistance (magnetic field perpendicular to graphene surface) of (a) pristine Epigraphene at 300 K, 100 K and 2 K and (b) a magnified magnetoresistance curve of the pristine Epigraphene at 2K. (c) Naphthazarin-functionalized Epigraphene at 300 K (black), 100 K (red) and 2K (blue), respectively.

4.4 Conclusion

In conclusion, we demonstrated a room temperature, facile route to covalently functionalize graphene with naphathazarin. By comparing the Raman spectra, we found that graphene on SiO_2/Si substrate is more reactive than graphene on SiC or quartz. Furthermore, temperature dependence of resistance shows that the transport characteristics of graphene change towards non-metallic dominated behavior after the DA reaction. We also observed the effect of DA reaction on the magnetic behavior of Epigraphene, which shows that the WAL is quenched by the DA reaction to a larger extent at lower temperature, which could be potentially used to fabricate future electronics and magneto-electronic devices.[22]

References

1. Chuang, S. C.; Sander, M.; Jarrosson, T.; James, S.; Rozumov, E.; Khan, S. I.; Rubin, Y., Approaches to Open Fullerenes: Synthesis and Kinetic Stability of Diels-Alder Adducts of Substituted Isobenzofurans and C-60. *J. Org. Chem* **2007,** 72, 2716-2723.

2. Nebhani, L.; Barner-Kowollik, C., Functionalization of Fullerenes with Cyclopentadienyl and Anthracenyl Capped Polymeric Building Blocks Via Diels-Alder Chemistry. *Macromol. Rapid Commun.* **2010,** 31, 1298-1305.

3. Delgado, J. L.; de la Cruz, P.; Langa, F.; Urbina, A.; Casado, J.; Navarrete, J. T. L., Microwave Assisted Sidewall Functionalization of Single-Wall Carbon Nanotubes by Diels-Alder Cycloaddition. *Chem. Commun.* **2004,** 15, 1734-1735.

4. Menard-Moyon, C.; Dumas, F.; Doris, E.; Mioskowski, C., Functionalization of Single-Wall Carbon Nanotubes by Tandem High-Pressure/$Cr(Co)_6$ Activation of Diels-Alder Cycloaddition. *J. Am. Chem. Soc.* **2006,** 128, 14764-14765.

5. Sun, J. T.; Zhao, L. Y.; Hong, C. Y.; Pan, C. Y., Selective Diels-Alder Cycloaddition on Semiconducting Single-Walled Carbon Nanotubes for Potential Separation Application. *Chem. Commun.* **2011,** 47, 10704-10706.

6. Sarkar, S.; Bekyarova, E.; Niyogi, S.; Haddon, R. C., Diels-Alder Chemistry of Graphite and Graphene: Graphene as Diene and Dienophile. *J. Am. Chem. Soc.* **2011,** 133, 3324-3327.

7. Sarkar, S.; Bekyarova, E.; Haddon, R. C., Chemistry at the Dirac Point: Diels-Alder Reactivity of Graphene. *Acc. Chem. Res.* **2012,** 45, 673-682.

8. Bian, S.; Scott, A. M.; Cao, Y.; Liang, Y.; Osuna, S.; Houk, K. N.; Braunschweig, A. B., Covalently Patterned Graphene Surfaces by a Force-Accelerated Diels–Alder Reaction. *J. Am. Chem. Soc* **2013,** 135, 9240–9243.

9. Cao, Y.; Osuna, S.; Liang, Y.; Haddon, R. C.; Houk, K. N., Diels–Alder Reactions of Graphene: Computational Predictions of Products and Sites of Reaction. *J. Am. Chem. Soc* **2013,** 135, 17643-17649.

10. Dean, C. R.; Young, A. F.; Meric, I.; Lee, C.; Wang, L.; Sorgenfrei, S.; Watanabe, K.; Taniguchi, T.; Kim, P.; Shepard, K. L.; Hone, J., Boron Nitride Substrates for High-Quality Graphene Electronics. *Nat. Nanotech.* **2010,** 5, 722-726.

11. Fan, X.; Nouchi, R.; Tanigaki, K., Effect of Charge Puddles and Ripples on the Chemical Reactivity of Single Layer Graphene Supported on Sio_2/Si Substrate. *J. Phys. Chem. C* **2011,** 115, 12960-12964.

12. Wang, Q. H.; Jin, Z.; Kim, K. K.; Hilmer, A. J.; Paulus, G. L. C.; Shih, C. J.; Ham, M. H.; Sanchez-Yamagishi, J. D.; Watanabe, K.; Taniguchi, T.; Kong, J.; Jarillo-Herrero, P.; Strano, M. S., Understanding and Controlling the Substrate Effect on Graphene Electron-Transfer Chemistry Via Reactivity Imprint Lithography. *Nat. Chem.* **2012,** 4, 724-732.

13. Sarkar, S.; Bekyarova, E.; Haddon, R. C., Covalent Chemistry in Graphene Electronics. *Mater. Today* **2012,** 15, 276-285.

14. Vecera, P.; Chacon-Torres, J. C.; Pichler, T.; Reich, S.; Soni, H. R.; Gorling, A.; Edelthalhammer, K.; Peterlik, H.; Hauke, F.; Hirsch, A., The First Precise Determination of Graphene Functionalisation by in Situ Raman Spectroscopy. *arXiv preprint arXiv:1703.02498* **2017**.

15. Niyogi, S.; Hamon, M. A.; Hu, H.; Zhao, B.; Bhowmik, P.; Sen, R.; Itkis, M. E.; Haddon, R. C., Chemistry of Single-Walled Carbon Nanotubes. *Acc. Chem. Res.* **2002,** 35, 1105-1113.

16. Tedesco, J. L.; VanMil, B. L.; Myers-Ward, R. L.; McCrate, J. M.; Kitt, S. A.; Campbell, P. M.; Jernigan, G. G.; Culbertson, J. C.; Eddy, C. R.; Gaskill, D. K., Hall Effect Mobility of Epitaxial Graphene Grown on Silicon Carbide. *Applied Physics Letters* **2009,** 95, 122102.

17. Abrahams, E.; Anderson, P. W.; Licciardello, D. C.; Ramakrishnan, T. V., Scaling Theory of Localization: Absence of Quantum Diffusion in Two Dimensions. *Phys. Rev. Lett.* **1979,** 42, 673-676.

18. Hilke, M.; Massicotte, M.; Yu, V.; Whiteway, E., Weak Localization in Graphene: Experiments and the Localization Length. *The Physics of Semiconductors: Proceedings of the 31st International Conference on the Physics of Semiconductors (ICPS)* **2013,** 1566, 155-156.

19. Hilke, M.; Massicotte, M.; Whiteway, E.; Yu, V., Weak Localization in Graphene: Theory, Simulations, and Experiments. *Scientific World J.* **2014,** 2014.

20. Wu, X.; Li, X.; Song, Z.; Berger, C.; De Heer, W. A., Weak Antilocalization in Epitaxial Graphene: Evidence for Chiral Electrons. *Phys. Rev. Lett.* **2007,** 98, 136801.

21. Hong, J.; Niyogi, S.; Bekyarova, E.; Itkis, M. E.; Palanisamy, R.; Amos, N.; Litvinov, D.; Berger, C.; de Heer, W. A.; Khizroev, S.; Haddon, R. C., Effect of Nitrophenyl Functionalization on the Magnetic Properties of Epitaxial Graphene. *Small* **2011,** 7, 1175-1180.

22. Bai, J.; Cheng, R.; Xiu, F.; Liao, L.; Wang, M.; Shailos, A.; Wang, K. L.; Huang, Y.; Duan, X., Very Large Magnetoresistance in Graphene Nanoribbons. *Nature Nanotechnology* **2010,** 5, 655-659.

Chapter 5. Conclusions

Two novel clean graphene transfer methods have been introduced, which have solved the notorious PMMA residue problems, reduced the cost, improved the efficiency of graphene transfer, and thus expedited the commercialization of graphene based electronics, spintronics and magnetic devices. These novel graphene transfer methods facilitate the research on graphene chemistry as clean graphene surface is of paramount significance .

Organometallic chemistry of carbon nanomaterials have been explored extensively in this work. First, graphene half sandwich complexes were synthesized via a facile photochemical route at room temperature and the reactivities of different reagents with single layer graphene was found to follow the order: Cr(6-benzene)2 > Cr(6-benzene)(CO)3 > Cr(CO)6 > Mo(CO)6 > W(CO)6. Voltage gated reactions indicate that organometallic chemistry reach optimum condition at the Dirac point, which provides a way to control the graphene functionalization.

Second, we successfully “intercalated” two asembled single layer graphene with Cr and thus prepared the graphene-transition metal-graphene sandwich strucutre, which has the potential to be superconducting at low temperature. Intercalation of graphite with transition metals has not been achieved because of the absence of charge transfer from the transition metal complexes to the graphene sheets.

Morever, the organoemtallic chemistry was employed to interconnect graphene nanoplatelets by bridging adjacent nanosheets with bishexahapto bonds, which is the first report of 3D graphene materials obtained from GNPs by constructive covalent bonding. These new materials showed enhanced bulk electrical conductivity.

Engineers have strived to reduce the contact resistance of carbon nanotube thin films and pave the way to commercialization of this carbon nanomaterial for the next generation electronics. In this research, we prepared aligned single wall carbon nanotube (SWNT) thin films and applied organometallic chemistry to interconnect not only the two ends of series of SWNTs, but also the sidewalls of parallel SWNTs, which preserves the unique electronic structure and thus the remarkable optical, electronic and mechanical properties of individual SWNTs while extending the dimentionality from 1D to 2D and 3D. With this method, for the first time, we experimentally realized aligned bishexahapto bonds with carbon surfaces, which may contribute to the fabrication of carbon based organometallic spintronic devices.

Last but not least, a room temperature, a facile route to covalently functionalize graphene with naphathazarin was realized utilizing Diels-Alder chemistry. Raman spectroscopy was used to characterize the reaciton process, and the transport properties of the graphene product were measured.